REAL-TIME DETECTION OF TELOMERASE IN A MICROELECTROMECHANICAL SYSTEMS PLATFORM

by

JEREMY RYAN GILBERTSON, B.S.

A DISSERTATION

IN

BIOLOGY

Submitted to the Graduate Faculty
of Texas Tech University in
Partial Fulfillment of
the Requirements for
the Degree of

DOCTOR OF PHILOSOPHY

Approved

Lauren Gollahon
Chairperson of the Committee

John Zak

Lou Densmore

Jordan Berg

Richard Gale

Accepted

John Borrelli
Dean of the Graduate School

May, 2005

Report Documentation Page

Form Approved
OMB No. 0704-0188

1. REPORT DATE	2. REPORT TYPE	3. DATES COVERED
19 MAY 2005	**N/A**	**-**

4. TITLE AND SUBTITLE	5a. CONTRACT NUMBER
Real-Time Detection Of Telomerase In A Microelectromechanical Systems Platform	5b. GRANT NUMBER
	5c. PROGRAM ELEMENT NUMBER
6. AUTHOR(S)	5d. PROJECT NUMBER
	5e. TASK NUMBER
	5f. WORK UNIT NUMBER
7. PERFORMING ORGANIZATION NAME(S) AND ADDRESS(ES) **Texas Tech University**	8. PERFORMING ORGANIZATION REPORT NUMBER
9. SPONSORING/MONITORING AGENCY NAME(S) AND ADDRESS(ES)	10. SPONSOR/MONITOR'S ACRONYM(S)
	11. SPONSOR/MONITOR'S REPORT NUMBER(S)

12. DISTRIBUTION/AVAILABILITY STATEMENT
Approved for public release, distribution unlimited

13. SUPPLEMENTARY NOTES
The original document contains color images.

14. ABSTRACT

15. SUBJECT TERMS

16. SECURITY CLASSIFICATION OF:			17. LIMITATION OF ABSTRACT	18. NUMBER OF PAGES	19a. NAME OF RESPONSIBLE PERSON
a. REPORT	b. ABSTRACT	c. THIS PAGE			
unclassified	**unclassified**	**unclassified**	**UU**	**147**	

Standard Form 298 (Rev. 8-98)
Prescribed by ANSI Std Z39-18

This Dissertation is Dedicated in Loving Memory of
My Grandmother

Esther Roppel Gilbertson

One of the most dedicated prayer warriors I have ever known. Her love for God, her husband, Gudmund Gilbertson, and her family made her a spiritual knight whose sword was as sharp as a razor. She dedicated her life to a greater cause, one that only God could have given her. She instilled in her children and grandchildren a seed that would grow for eternity. I aspire to be as great a person and spiritual leader as she was. I know she is watching over me.

The views expressed in this article are those of the author and do not reflect the official policy or position of the United States Air Force, Department of Defense or the U.S. Government."

ACKNOWLEGEMENTS

I would like to thank the God who created Adam and Eve and the heavenly father of Jesus Christ my Lord and Savior. He has provided all I need to make this journey possible. He has given me the physical and mental attributes that make crossing the finish line obtainable. He has blessed me with a beautiful, dedicated, intelligent, loving, and God fearing wife. She was put here especially for me and I for her. She has been and always will be my better half. He has also blessed me with three loving children that make me strive to do what is right so that I may lead by example. The three “Js”, my cup overflows, you bring joy that only children can. That joy has given me the strength and will to be the best person I can. I would also like to thank my parents, and my parents by marriage, they have provided a support net that can only be given by loving family members.

Dr. Lauren Gollahon, advisor, mentor, friend, and colleague, you have brought me so far, and I thank you for your support, patience, encouragement, and guidance. I aspire to be a professor and scientist of your calibre. We have been through a marathon together and as I cross the finish line it is now that my hindsight shows me all the things you have done. Much thanks and I will always remember you.

I would like to thank my committee members: Dr. Jordan Berg, Dr. Richard Gale, Dr. Lou Densmore, and Dr. John Zak. They have supported me through this journey many times without their knowing. Their knowledge and scientific prowess has made me a better person and scientist.

I would like to thank Dr. Randy Allen and his lab members for allowing me to use his lab like it was my own. His equipment made my project possible. I would also like to thank Dr. Michael San Francisco, his lab members, Dr. Randell Jeter, and his lab members for all the technical support they provided.

I would also like to thank the United States Air Force for making this Ph.D. opportunity possible.

TABLE OF CONTENTS

ABSTRACT

The integration of biology with Microelectromechanical Systems and Nanotechnology could result in a synergism with tremendous benefits in both basic research and clinical assays. The development of a functionalized liquid core waveguide to detect a biological function or substance via fluorescence could have broad range applications. One such target of interest for developing such a system, is the ribonucleoprotein enzyme telomerase. It is a confirmed biomarker for cancer; having been associated with over 90% of cancers examined. Development of a MEMS-based detection system would allow for accurate detection of small numbers of target molecules in the sample volumes. In order to accomplish this I first developed a bench-top assay to identify key components of the reaction and optimize the detection scheme before incorporation into a MEMS device. This assay itself will have utility in basic research labs for telomerase detection.

My ongoing efforts to synthesize such a system has resulted in the modification of the inside surface of the capillary using rapid, straightforward chemistry in order to indirectly attach a molecular beacon. The molecular beacon, the key component of the functionalized capillary, is a strand of DNA that is folded into a specific structure corresponding to the capture sequence that also

contains a fluorophore and a quencher moiety. When the fluorophore and quencher molecules are in close proximity, fluorescence resonance energy transfer (FRET) takes place; effectively quenching the fluorescence emission. However, binding of the target DNA, RNA, or protein to the molecular beacon target capture sequence causes a conformational change that separates the fluorophore and the quencher at which point fluorescent signal can be detected. The incorporation of this functionalized liquid core waveguide with a PDMS chip will facilitate fluid control and optic fiber couplings for fluorescence detection.

In addition, the development of a bench-top assay will have great utility in basic research in addressing critical biological questions about telomerase. Such questions include: does telomerase remain bound to the telomeric DNA, or does it hop between the ends; what are the regulatory mechanisms that prevent binding of telomerase to an exposed strand of telomeric DNA; are there other associated proteins not yet identified. Furthermore, the successful protein capture using a molecular beacon demonstrates the utility of this methodology for other DNA-binding proteins.

LIST OF TABLES

LIST OF FIGURES

CHAPTER I

INTRODUCTION

1.1 Cancer Statistics

Cancer is a devastating and debilitating disease that is becoming more prevalent in the United States and worldwide. The American Cancer Society estimates that there will be 1,368,030 new cancer cases and 563,700 deaths from cancer this year in the United States (1). These estimates do not include carcinoma *in situ* of any site except urinary bladder, and they do not include basal and squamous cell skin cancers (1). In 2004, it is estimated that Texas will have 84,530 new cases of cancer and 34,830 deaths due to cancer (1). The 5-year survival rate for all cancers combined is 63%, with dramatic variations within individual cancer types (1). The National Institutes of Health estimates the nationwide cost for cancer in 2004 will be $189.5 billion in direct cost, $64.2 billion for direct medical cost, $16.3 billion for indirect morbidity costs, and $109 billion for indirect mortality costs (1). Although recent advances have helped diagnosis and improved prognosis, there is still an urgent need for more accurate, quantitative assays for cancer detection. In addition, there is a major incentive to promote adoption of novel assays by clinicians. These assays need to be convenient with as little sample manipulation as possible as well as cost effective.

1.2 Telomerase Function

In the mid 1990's the ribonucleic protein telomerase was shown to be present in more than 90% of all cancers (10). In addition, it was found to be present only in certain stem cell populations, germ cells, and not detectable in normal somatic cells (10). This marked telomerase as a potentially very important biomarker for cancer (5,7,19,20,41). Telomerase activity confers immortality to cells. It is considered the key component that allows immortal cells to transform, and ultimately become cancerous (20,24,42,57), not by causing mutations, but by allowing cells to be viable long enough to accumulate key mutations. This leads to the transformed or malignant, phenotype. Telomerase accomplishes this by alleviating the "end-replication problem" (6,10,14,23,33,43).

First described by Hayflick in 1965, the end-replication problem arises from the inability of DNA polymerases to fully replicate the chromosome ends (22,54). When DNA polymerases replicate the template DNA strands in a chromosome, each new "daughter" strand is ~50-200 bases shorter at the 5' end (36). The chromosome ends or "telomeres" are made up of a tandem repeats (TTAGGG in humans and its complementary sequence) (14-17). This region is non-coding and its sole purpose is to maintain genomic stability by keeping the chromosomes from sticking to one another and otherwise interacting in ways that threaten the chromosome's stability (33). The essential genetic information remains

unperturbed until this telomeric region becomes critically short. When the telomeric region is too short, the functional DNA is affected (15,17) (Figure 1). This telomeric shortening inhibits specific telomeric binding proteins from forming critical loop structures that allow for telomeric cap formation and chromosomal stabilization (15,23,33). The two critical loop formations that the telomeres provided are the t-loop and the d-loop. The t-loop is formed by the telomere's ability to integrate its 3' overhang into the double stranded DNA of the telomere. The d-loop is formed by the displaced DNA created by the insertion of the 3' overhang. Both of these formations are guided and bound in each respective state by specific proteins. These formations allow for telomere regulation and chromosomal stabilization (15).

Mammalian telomerase solves the end-replication problem in cancer cells (25), human stem cells, and reproductive cells (57) by adding TTAGGG repeats onto the telomeres using its intrinsic RNA as a template for reverse transcription (12). When telomerase is activated, a cell becomes immortal (unlimited cell proliferation). Telomerase activity has been found in almost all human tumors, but not in adjacent normal cells (25). The holoenzyme (telomerase) is composed of the RNA subunit hTR, and the protein subunit hTERT, along with many associated proteins. For a review of the holoenzyme complex components, see Cong YS et. al. 2002 (8). The most widely accepted hypothesis is that

1) DNA replication is initiated at the origin; the replication bubble grows as the two replication forks move in opposite directions

2) Finally only on primer (pink) remains on each daughter DNA molecule

3) The last primers are removed by a 5'→ 3' exonuclease, but no DNA polymerase can fill the resulting gaps because there is no 3'-OH available to which a nucleotide can be added

4) Each round of replication generates shorter and shorter DNA molecules

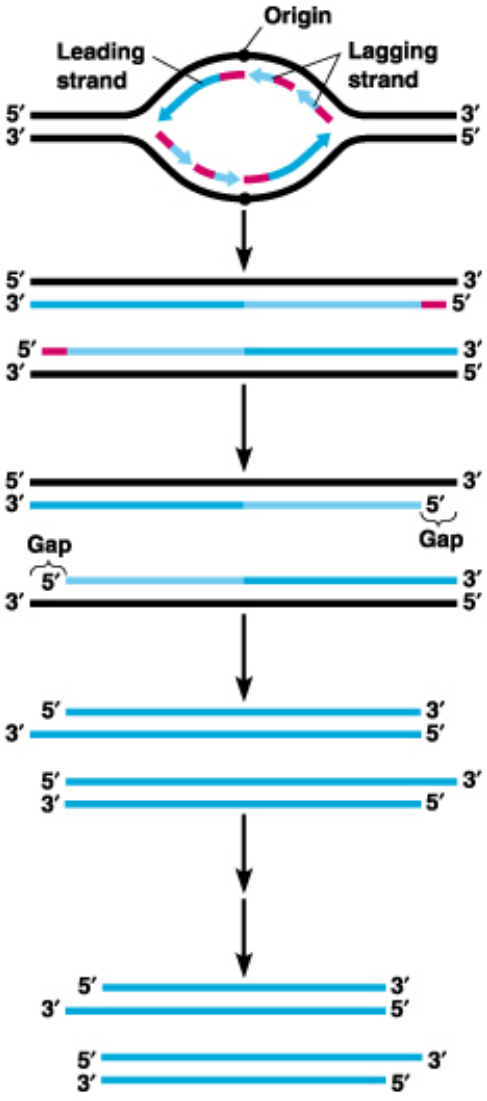

Figure 1. End-replication problem

maintenance of telomere stability is required for the long-term proliferation of tumors (42). Thus, escaping from cellular senescence and becoming immortal by telomerase activation constitutes an additional step in oncogenesis that most tumors require for their ongoing proliferation. Cellular senescence (replicative senescence) is the natural process of cell death, which happens when the cell cannot sustain normal DNA replication due to telomeres that have shortened to a critical length and begin to interfere with the normal activity of important genes (33). Alternatively, it is suspected that a decrease in the telomere heterochromatin begins to affect senescence by activating normally silenced genes that trigger a senescence cascade (33). The importance of the telomere in this aging process, the strong association between aging and cancer, and its association with cancer directly, makes telomerase a target not only for cancer diagnosis, but also for the development of novel anti-cancer therapeutic agents (7).

1.3 Telomerase detection

The current standards for many cancer diagnoses are morphologically based (cytology) (19). The empirical evaluation of the target cell's appearance or change in appearance compared to a typical cell of the same type, dictates morphological diagnosis. This diagnosis can vary depending on the preparation

of the specimen, the judgment of individual evaluators, and the criteria used to distinguish normal from cancerous or precancerous cells (5,7,19). This type of analysis does not have the capability to screen for telomerase activity. The ability to provide a molecular assay that is based on objective, quantifiable parameters could greatly enhance cancer diagnosis. The current detection methods for telomerase are based on its intrinsic polymerase characteristics. The addition of the telomeric repeat sequence to a DNA template is the basic action from which many different assays are derived (7,23,41). This fundamental telomerase activity is utilized in a plethora of detection methods, most in relation to polymerase chain reaction (PCR).

The most common test currently used for detecting cancer at the molecular level is the telomeric repeat amplification protocol (TRAP) assay. There are many different variants of the TRAP assay, but all utilize a telomeric substrate (G-rich oligonucleotide) upon which telomerase adds TTAGGG repeats. Then, polymerase chain reaction (PCR) amplification of the newly added repeats is performed. The PCR product can be labeled for detection using radioisotope incorporation, chemiluminescence, or fluorescence. The PCR product is confirmed using polyacrilamide gel electrophoresis. Although several of the methods are qualitative and/or semi-quantitative, (real time PCR), drawbacks still remain. The primary drawback is extensive sample preparation. The samples

need to be lysed and proteins extracted under sterile conditions to avoid contamination (7,23,41).

There are a number of techniques that can detect telomerase from whole cells (cytometry) (59), fixed tissue samples (38), or tissue lysates (39). However, these techniques generally require expensive instrumentation and extensive sample manipulation. There are also methods that involve antibodies, however their detection is not consistent enough to be useful as a clinical assay. Although the determination of telomerase activity could be an extremely powerful marker in cancer diagnosis, results of such assays are not consistent between techniques (7). Nor are many of these assays convenient to perform clinically (7).

There is also potential for using telomerase activity as a prognostic indicator of cancer survivorship. However to date, a quantitative assay with reproducible results that could lead to standard ranges of telomerase activity for a given stage of malignancy, has not yet been developed.

1.4 Relevance

The goal of my research project is to develop a bench top molecular based telomerase detection assay that would be quantitative, convenient, provide real-time results, require little sample manipulation, minimize testing time, and require minimal instrumentation. This combination would make cancer diagnosis and

prognosis much more affordable, less objective, and considerably more user friendly. The ability to further integrate this research into a nanobiotechnology biosensor would allow for great convenience and portability. In addition, successful detection of telomerase using a molecular beacon would demonstrate the potential application of this assay for capturing other DNA binding proteins.

CHAPTER II

METHODOLOGICAL BACKGROUND

2.1 Biological

2.11 Fluorescence Resonance Energy Transfer (FRET)

In order to measure molecules of telomerase proteins a reliable method of detection was needed. In reviewing the current detection techniques, one mechanism that fit the necessary criteria for detection was Fluorescence Resonance Energy Transfer (FRET). Regular non-fluorescence resonance energy transfer (non-FRET) fluorescence occurs when a fluorescent molecule (fluorophore) absorbs electromagnetic energy of one wavelength (the excitation frequency) and re-emits that energy at a different wavelength (the emission frequency) (2,11,40,47,51). Fluorophores have a two-peaked spectrum in which the first peak is the excitation, and the second is the emission (51). For the combined FRET effect, the emission peak of the fluorophore must overlap with the excitation peak of the quencher and the two molecules must be in close proximity (Figure 2) (11,47,52). In FRET, light energy is added at the excitation frequency for the fluorophore, which transfers some of this energy to the quencher, which then re-emits the light at its own emission wavelength (32,35,45). The net result is that the fluorophore emits significantly less energy

than it normally would in a non-FRET configuration (since some of the energy it would radiate as light gets transferred to the quencher instead). The amount of light emitted from the fluorophore is in direct relationship with the distance between the fluorophore and quencher (32,35,45). The principles of FRET were utilized to detect telomerase. This was accomplished by using the intrinsic thermodynamic properties of the molecular beacon.

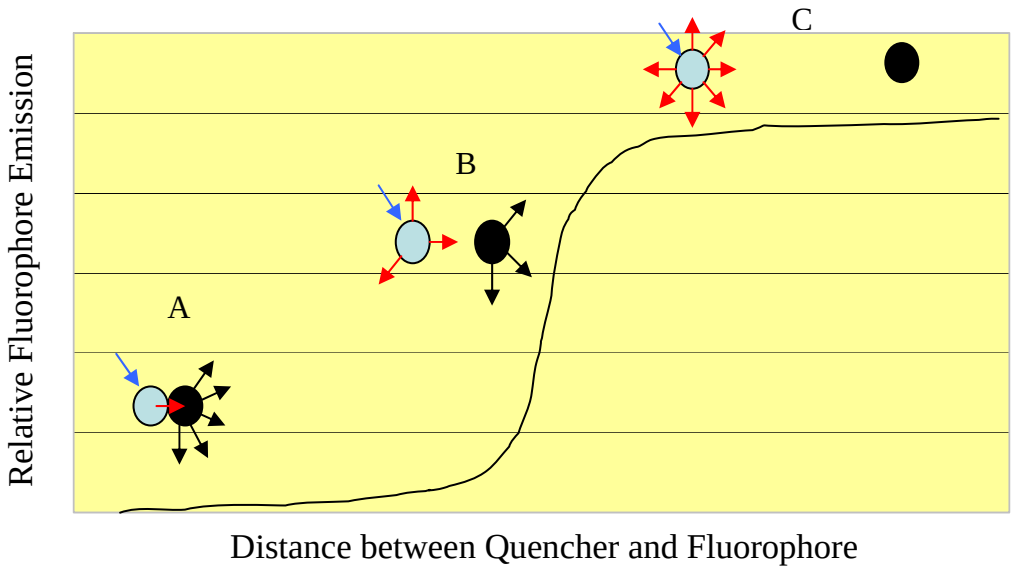

Figure 2. Fluorescence Resonance Energy Transfer (FRET)

Fluorophore Quencher Excitation wavelength Emission wavelength Quencher emission

(A) The close proximity of the fluorophore and the quencher allows the emitted light from the fluorophore to be absorbed by the quencher. The result is that no fluorescent emission is detected from the fluorophore. (B) As the distance between the fluorophore and the quencher increases the detectable emission from the fluorophore increases. (C) When the critical distance is achieved, 100% of its emission is detectable.

2.12 Molecular Beacon

The molecular beacon (Figure 3) (TriLink, Inc.) is one of the core components of this research. This molecular beacon (MB) can be broken down into several

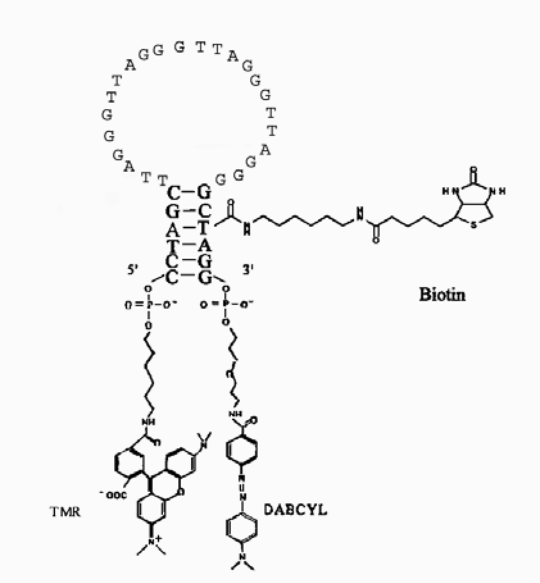

Figure 3. Modified molecular beacon
The hairpin loop sequence is modified for telomerase capture $(TTAGG)_4$ and a biotin moiety was added to the 3' stem. The fluorophore is TMR and the quencher is DABCYL. (27)

different moieties. These individual moiety characteristics give the entire MB unique molecular properties. The different moieties are the 3' end region, 5' end region, and hairpin loop. The 5' end region contains the fluorescent molecule, tetramethylrhodamine (TMR) and a sequence of nucleotide bases that form a stem structure with the 3' end region. TMR performs maximum excitation at 546 nm

(spectra 450 nm to 525 nm) and maximum emission at 576 nm (spectra 475 nm to 650 nm). The 3' end region contains a biotin, and quencher moiety. The biotin moiety will be used to attach the MB to the bovine serum albumin (BSA) - biotin and streptavidin modified surface. The quencher is (4-dimethylaminophenylazo) benzoyl (DABCYL), for which the maximum excitation is 453 nm (spectra 350 nm to 575 nm) with maximum emission in the IR range. The coupling of DABCYL with TMR for FRET purposes optimized the signal to noise ratio (32). The 5' and 3' flanking regions form a stem structure, which creates the hairpin loop. This loop contains a 24-mer sequence specific for telomerase binding $(TTAGGG)_4$. When the 5' and 3' ends are in close proximity to each other, under excitation conditions, there is effective (but not total) FRET from the fluorescent molecule to the quencher molecule (11,29,32,52). This energy transfer slowly digresses upon separation of the fluorophore and quencher either by stem splitting or random coil formation (increases in temperature from 70°-95°C or in high pH, see Figure 4).

Two different molecular beacons were utilized during my research. Each was specifically developed to study two different applications. The first MB, which is non-biotinylated, was used to develop a bench top assay. The fluorophore for this MB was FAM (6-carboxyfluorescein). The second MB, which was biotinylated for surface attachment, was used to study the surface preparation and for the

eventual transition from the bench top assay to a biosensor. These two molecular beacons were very similar, but have several significant differences. The most important similarity was the sequence and length of the hairpin loop. The differences were less significant in relation to target acquisition, but played a significant role in utilization and detection. The fluorophore attached to the 5' end was employed to allow for fluorescence detection utilizing an ABI Prism 7000 (detailed instrument description in Materials and Methods). The other major difference was the biotin moiety on the 3' end. This plays a critical role in surface attachment.

The interactions of the molecular beacon's with its sequence-specific target was governed by the laws of thermodynamics [binding constant 1.725e5 M^{-1}(27)]. The thermodynamic state of the molecular beacon/target complex dictated what the MB conformation, which directly correlated with the FRET state between the fluorophore and quencher. There were many variables that could influence the thermodynamic properties of this reaction, e.g. the concentrations within the solution could be manipulated so that the molecular beacon/target complex was formed more readily.

The MB alone has three critical functions that allowed the thermodynamic reaction to be optimized. The first was manipulation of the length of the stem (50). The longer the stem of the MB, the more energy it would take to break the

bonds formed between complementary bases (50). The second was to vary the energy needed to form a stable molecular beacon/ target complex. This was accomplished by varying the length of the hairpin loop. Increasing the number of bases in the loop also increased the amount of energy it would take to form a stable complex (50). Lastly, the specific sequence of the MB served the most important function. This sequence acted like a "lock" that only the correct "key" sequence would open. The target specificity was the key that was crucial to its function (2-4,11). The MB had the ability to discriminate between a complementary sequence and a sequence that had just one base mismatch (binding constant 3.8e4 M^{-1}) (27).

Molecular beacons have the ability to form three different conformations, depending upon the thermodynamic characteristics (Figure 4) (3,50). The first conformation is the stem loop structure and in this conformation, normal FRET takes place (normal state, Figure 4B). The second conformation is the random coil, which occurs at high temperatures or high pH (Figure 4C). Partial FRET takes place in this conformation due to the fact that the fluorophore and quencher are slightly separated (3,50). The final conformation is the molecular beacon/ target complex (Figure 4A) (3,50). This complex causes the fluorophore and quencher to completely separate, eliminating FRET.

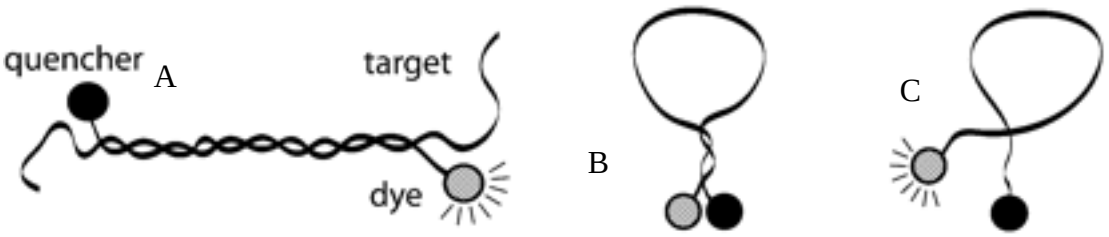

Figure 4. Molecular Beacon Conformations
A. Linear conformation (molecular beacon bound to target, non-FRET). B. Hairpin loop conformation (FRET). C. Random coil conformation (partial FRET) (3,50).

2.13 DNA Binding Proteins

Proteins are composed of amino acids, which were translated from an mRNA. The amino acid sequence folds into a specific shape that dictates its function. The shape (conformation) of any protein can change depending upon specific post translational modifications (methylation, phosphorylation, etc.). DNA-binding proteins directly interact with DNA. Some of these proteins bind DNA in a nonspecific fashion and others recognize and bind to a specific sequence of DNA (55).

DNA-binding proteins regulate many processes in biological systems. These proteins play a critical role in controlling gene regulation, chromosomal protection and repair, gene expression, and many other functions (55). These proteins interact with DNA through ionic or hydrogen bonds provided by the phosphate backbone or through intercalation of bulky ring-shaped side chains

between the bases. The binding kinetics of these proteins are governed by thermodynamic principles. Since, DNA is inherently negatively charged and DNA binding proteins are inherently positively charge there is constant interaction between the two species (55).

For some proteins these simple interactions are enough to form relatively stable protein-DNA hybrids. These types of proteins are nonspecific and usually have stable, albeit weak interaction with their DNA counterparts. Other DNA binding proteins must produce a relatively strong DNA binding hybrid (along with other protein interactions) for activation. This type of DNA binding protein recognizes a specific DNA sequence and forms a hybrid in which the decrease in free energy is more significant. This reaction forms a strong DNA-protein hybrid that is very stable. Theoretically in a MB, a DNA binding protein should be able to bind to the specific sequence in the hairpin loop, open the MB, and cause signal emission when excited.

An example of protein binding to a DNA sequence of a MB was described by Jianwei Jeffery Li at the University of Florida (28). His results indicated that a single-stranded DNA binding protein (SSB) bound to the hairpin loop of a MB forming a linear hybrid (and thus separating the stem causing fluorescence). The DNA-protein binding kinetics of the MB were much quicker (MB and SSB, binding constant 2.0e7 M^{-1}) than the DNA-DNA binding kinetics (1.725e5 M^{-1}).

Extrapolations from these experiments showed that the thermodynamics of the DNA-protein binding and the DNA-DNA binding were similar in that they both linearize the MB causing fluorescence. Li also showed that a 1:1 ratio of SSBs to molecular beacons in solution gave approximately the same fluorescent results as a 4:1 ratio (SSB:MB). Li was able to detect SSBs at a concentration of 0.2nM using a mercury excitation source. If a laser excitation source was utilized, detection was enhanced by three orders of magnitude down to ~0.2pM (58). Since there are no standardized detection systems for this type of assay, my project will utilize the ABI Prism 7000 real time PCR machine as a detector of fluorescence. The excitation source was a tungsten-halogen lamp.

2.14 Purified hTERT and hTR production

Telomerase has multiple components (as described in section 1.2, pg. 2), but hTERT and hTR have been shown to be the two critical components of telomerase activity both *in vivo* and *in vitro* (21,26,48,56). The hTERT protein acts as the catalytic portion of the telomerase holoenzyme and the hTR RNA acts as the synthesizing template (21,26,48,56). These two components along with rabbit reticulocyte lysate (RRL) produce telomerase activity *in vitro* (21,56).

The cDNAs for the transcription and translation reactions were made available via modified plasmids. There were two different plasmids utilized in the

production of these components. The hTR component was produced using pGRN83 plasmid (Geron Corp.). The pGRN83 plasmid was constructed by PCR of the exact 5' and approximate 3' end of the RNA component of human telomerase from the genomic clone of hTR. This PCR product was blunted with Klenow and cloned into the ECL36II site of pGEM5Zf+ (26). The production of hTERT was accomplished using the pXhTRTE plasmid. This plasmid contained the hTERT sequence cloned into the EcoR I splice site of the pcDNA3.1/his C plasmid (Invitrogen Corp). The two plasmids were obtained from Geron Corp, (Menlo, CA) and the laboratory of Dr. Shawn Holt (Medical College of Virginia, Virginia Commonwealth University), respectively.

These plasmids were inserted into competent bacterial cells (DH5α, Gibco). These cells were specifically engineered to readily take up target plasmids. This plasmid uptake transformed the cell, opening pores in the cell membrane when heated. These pores closed when cooled on ice. The new plasmid containing bacteria were placed in general growth broth for recovery and given time to express the plasmid-borne antibiotic resistance gene. Then a portion of the culture was placed into an antibiotic-selective media so that only the cells that were transformed would survive. The transformed cells retained the plasmid, which contained the antibiotic resistance gene specific to the antibiotic in the media, as well as the gene for the target protein or RNA. The cells were grown in

the selective media until the peak of the log phase and then the plasmids were extracted. The extracted plasmids were then used in the transcription/ translation reaction. This reaction provided purified hTERT and hTR in RRL.

2.2 Use of the ABI Prism 7000 for Molecular Beacon Signal Detection

Since this novel assay had no standard detection mechanism, I followed the literature and utilized a real-time PCR machine as the detection source. The ABI Prism 7000 (Applied BioSystems Inc., Foster City, CA) was the instrument available for my use. The ABI Prism 7000 device allows for temperature control of the sample, and is capable of providing fluorescent data on 96 different samples during one run. This device utilizes a tungsten-halogen lamp as a broad range excitation source. The excitation light passes through an excitation filter and then through the top of the sample container exciting the fluorophores. The emission from each sample well is then reflected through a dichroic mirror, emission filter and collected by a charge-coupled device (CCD) camera (Figure 5).

2.21 ABI Prism 7000 Operation

Before conducting any experiments using the ABI Prism 7000, a background assay was performed so that the machine calibrated background fluorescent levels

for each individual well. In this manner, the instrument had the capacity to extract the background fluorescence from each well during the sample run (following manufacturer's instructions). The extracted background was used by the machine to determine relative sample fluorescence during experimental runs. Secondly, this machine was built to perform real-time PCR and optimized to detect the characteristics of a real-time PCR reaction.

The operation of this machine as a fluorescence reader required several program variations. Since, normal PCR is a three stage temperature-dependent process, with fluorescence detection in the final stage, several of these stages had to be removed or manipulated with software supplied by the manufacture. Two of the thermal stages were removed and the other one was placed one degree lower than the temperature of data collection. The sample would be at one degree below testing temperature for one second and then the program would move into the second stage where the fluorescence could be read and held at this stage for 1:36 minutes (this is the minimum time require for this field). This thermal cycle was run three times. After the temperature data were collected, a new experiment had to be setup in the software so that a different temperature could be tested. The experiment was completed upon finishing the temperature cycle (80°C to 10°C to 80°C, in increments of 5°). All data were exported into Microsoft EXCEL.

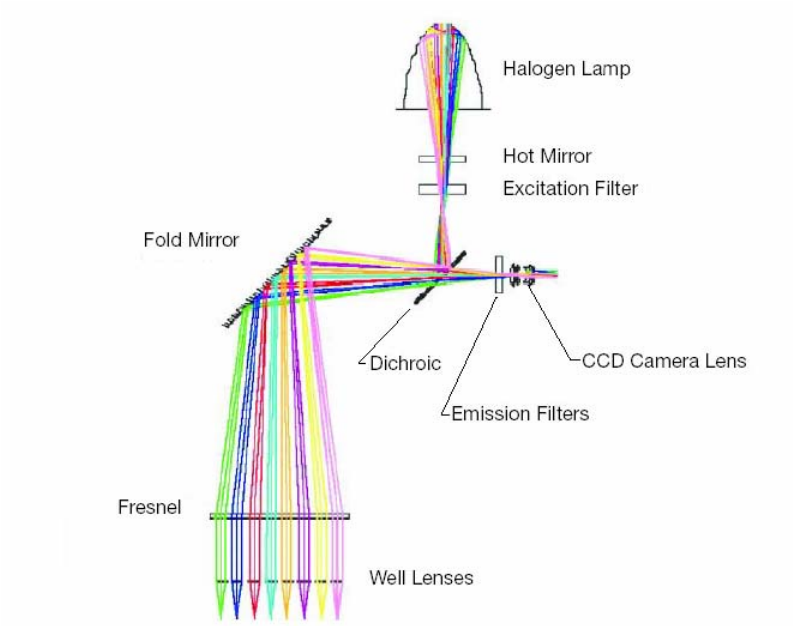

Figure 5. Illustration of Light Path in the ABI Prism 7000
The picture illustrates the path from the excitation lamp to the sample and the emission from the sample to the CCD camera lens. This figure is reproduced with permission from Applied BioSystems Inc.

2.3 Olympus FV300/IX80 Confocal Microscope

Detection of the biotinylated-MB and interactions with fluorescently-labeled avidin coated polystyrene beads had to be performed using microscopy. This was important in showing proof-of-concept for a MEMS-based device. To that end, the Olympus FV300/IX80 confocal microscope was utilized. The Olympus FV300/IX confocal microscope, utilizes several unique functions to optimize sample viewing; incoming laser light sources, a beam collimator, laser adjustment neutral density filter turret, dichroic mirrors, pinhole turret, photomultiplier tubes

(PMT), beam splitters, fluorescence filters, transmitted-light differential interference contrast (DIC) imaging, bright light, and UV (mercury lamp) capabilities. Additional information is available at http://www.olympusfluoview.com/theory /confocalintro.html.

The two laser sources available for confocal microscopy were the Helium-Neon (Green HeNe) and a multi-Argon laser. The most frequently utilized laser was the green HeNe; optimized to emit light at the 543 nm wavelength. The Multi-Argon (blue) laser emits light at the 488nm wavelength. There are two dichroic mirrors in the platform, which allowed the sample to be adjusted for optimal viewing and photomultiplier tube selection. The two photomultiplier channels allowed for multiple fluorescent views of the sample. The photomultiplier tubes were adjusted via the operating voltage to increase or decrease the sensitivity of the light detected from the sample being viewed. This type of microscope utilized a pinhole turret that allowed the user to view different planes of the sample or the entire sample depending on sample thickness. The depth of the plane depended upon the pinhole size. There were five different aperture sizes from which to select, with each aperture having individual visual characteristics relative to the sample area. The confocal microscope discussed here and used for these studies was equipped with multiple emission filters, which were easily interchangeable, and regulated the emission wavelengths from the

sample that passed through to the PMT. The culmination of these characteristics made this microscope well suited to optimize and view fluorescent samples with great accuracy and precision (Figure 6).

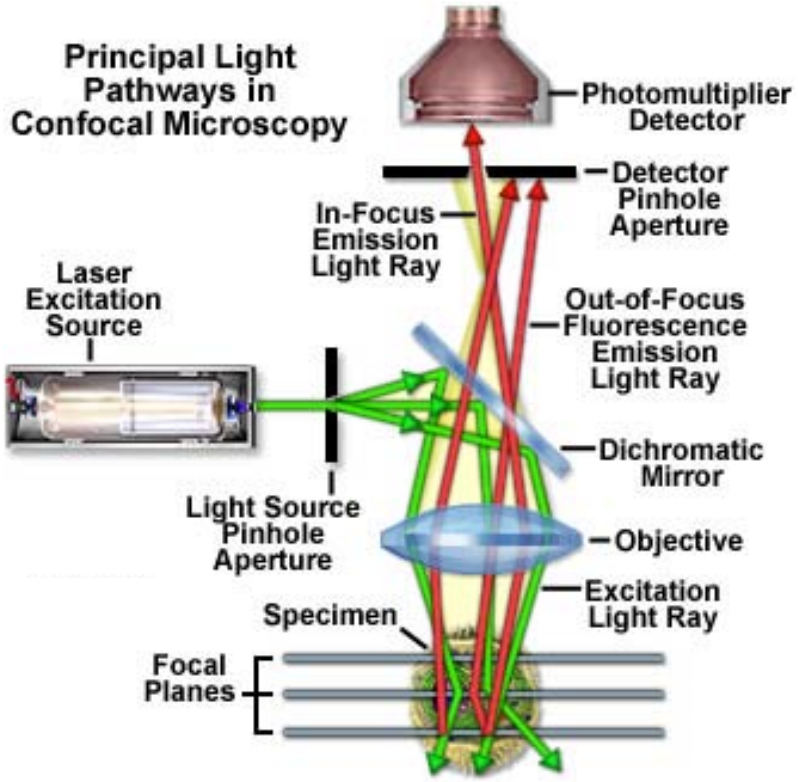

Figure 6. Illustration of Light Path in Basic Confocal Microscope Configuration The picture depicts the excitation from the laser to the sample and the emission from the sample to the photomultiplier tube. Figure source: http://www.microscopyu.com/articles/confocal/confocalintrobasics.html

2.4 Electrical Engineering Principles Applied to Device Development

2.41 Overview

The capacity to integrate a molecular assay into the lumen of a capillary tube (attached indirectly to the inner lumen), which has the ability to direct the emission from the MB down the capillary to a detection source while eliminating the excitation source, would be ideal for developing a biological assay in a microchip. The electrical engineering principles from which these capabilities are derived are as follows: defining a liquid core waveguide (LCWG), Snell's Law, total internal reflection (TIR), and transverse excitation/axial detection. These principles are described below.

2.42 Liquid core waveguide (LCWG)

A liquid core waveguide is defined by the relationships of the refractive indices of the materials used to produce the capillary or surround the capillary after production (18). These relationships are governed by many laws, but Snell's law governs how light is reflected or refracted when it passes from one media into another media with a different refractive index (18). I anticipate that the inner lumen of the LCWG will be filled with water, (refractive index of 1.33) and the material surrounding the water must have a lower refractive index than the water for a portion of the light to be total internally reflected. The lower the refractive

index of the surrounding material, the more light will be internally reflected down the LCWG. There are several key qualities that make a glass liquid core waveguide a useful platform for fluorescence detection. These qualities are based on the ability to integrate it into a fluidic system, modify the surface chemistry for functionalization, decrease signal to noise and channel fluorescence emission (Appendices A-B). The TIR properties of the LCWG can be predicted using Snell's Law. This prediction should correlate directly with the percentage of light captured down the LCWG and thus, address the sensitivity of detection.

2.43 Snell's Law

$$n_1 \sin \theta_1 = n_2 \sin \theta_2$$

One of the functions of this law is controlling the interactions of light when passing from one media into another with differing indices of refraction (18). Calculations based on this law will determine the amount of fluorescence that is totally internally reflected (TIR), passing to the fiber optic cable (Appendices A-B). This law does not take into account the quality of the glass or smoothness of the surface, both of which could enhance or detract from signal detection.

2.44 Total Internal Reflection (TIR)

When light interfaces with a boundary (with an angle ≤ the critical angle, as defined by Snell's law), at which the medium it is exiting has a significantly higher index of refraction than the medium it is entering, the light is reflected and remains inside the first medium (18). This reflected light will continue in the first medium unless it encounters imperfection in the glass or the angle of incidence changes exceeding the critical angle (Appendix B). When the light traveling in a glass capillary encounters these types of problems, the signal can be significantly diminished or lost. I predict that the most efficient method of excitation and signal detection will be transverse excitation/ axial detection based on Snell's law.

2.45 Transverse Excitation/Axial Detection

To optimize the transverse excitation/ axial detection a functionalized capillary will slide into a fitted sleeve, around which will be a cushion of air. The excitation wavelength from a line source most probably light emitting diodes (LEDs), will pass through the outer cladding and into the water exciting the fluorophores attached to the inner lumen of a functionalized capillary, while the unused portion of the excitation beam passes directly through the LCWG (based on Snell's Law). A percentage of the emission from the excited fluorophore transmits down the LCWG and will enter a fiber optic cable (Figure 7). The

signal to noise ratio should be greatly enhanced due to the LCWG's ability to significantly reduce the amount of excitation wavelength that is TIR. The enhancement effect of the signal is predicated on the glass quality and the turbidity of the solution inside the LCWG.

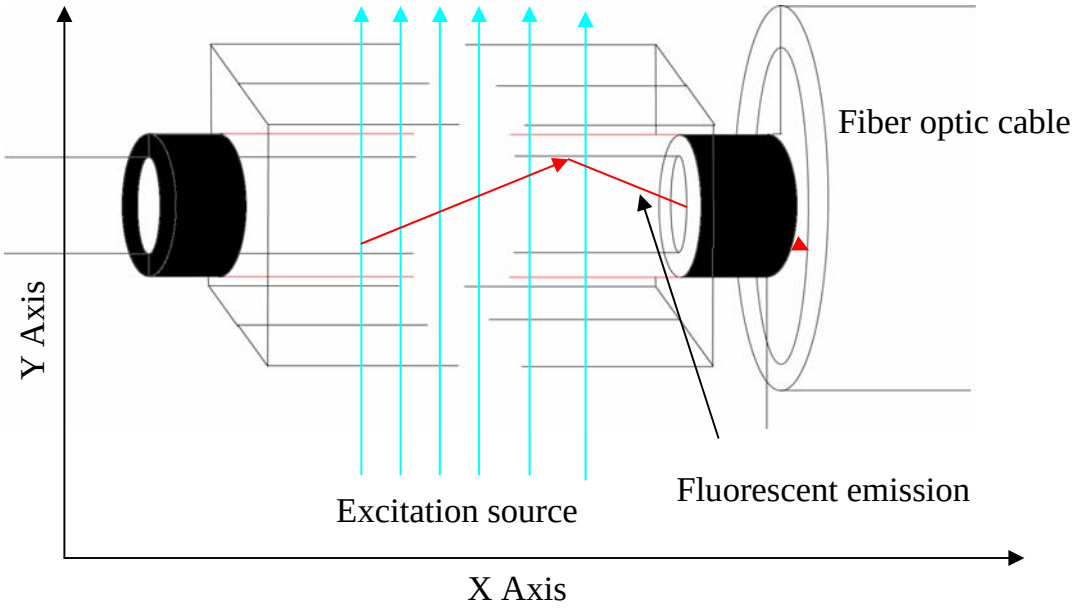

Figure 7. Illustration of Transverse Excitation/ Axial Detection
This picture illustrates the LCWG placement in the PDMS chip and the cushion of air that would surround the LCWG. The excitation source would emit from the Y axis and the fluorescent emission for the MB would be detected on the X axis.

2.5 Mechanical Engineering Principles Applied to Device Development

2.51 Overview

The mechanical engineering principles of chip fabrication and micromachining would be use to produce a PDMS chip that would house the LCWG, and modification to the LCWG that would optimize fluorescence detection.

2.52 Photolithography

In order to fabricate this PDMS chip, the design pattern must first be transferred using photolithography. Photolithography is the use of light to transfer a two-dimensional pattern (mask) onto a surface that has been uniformly covered with a photoresist (30). The mask is produced using a computer drawing program (Adobe Illustrator) and printed onto a transparency using a laser printer. The laser printer's resolution directly correlates to the mask's precision. Therefore, greater resolution yields higher quality masks. The mask will determine the area of the photoresist that will remain after developing. The thickness of the photoresist determines the third dimension. Thickness is determined by the type of photoresist used and the revolutions per minute (RPM) at which the photoresist is applied.

The photoresist is centered on the surface of the substrate and then the substrate is spun at a designated RPM to uniformly spread the photoresist to specified uniform thickness. The higher the RPM (correlates to more centrifugal forces acting on the photoresist) the thinner the photoresist layer. There are two categories of photoresist, negative and positive. When exposed to UV light, negative photoresist (e.g. S-1813) will crosslink the main chains or pendant side chains thus making the exposed area insoluble in the developing solution (30)(Figure 8). When exposed to UV light positive photoresist (e.g. SU-8) will weaken the polymer by rupture or scission of the main and side polymer chains, thus making the exposed area soluble in developing solution (30)(Figure 8). By varying mask design, photoresist type and thickness, and multiple applications, photoresist structures produced can be complex.

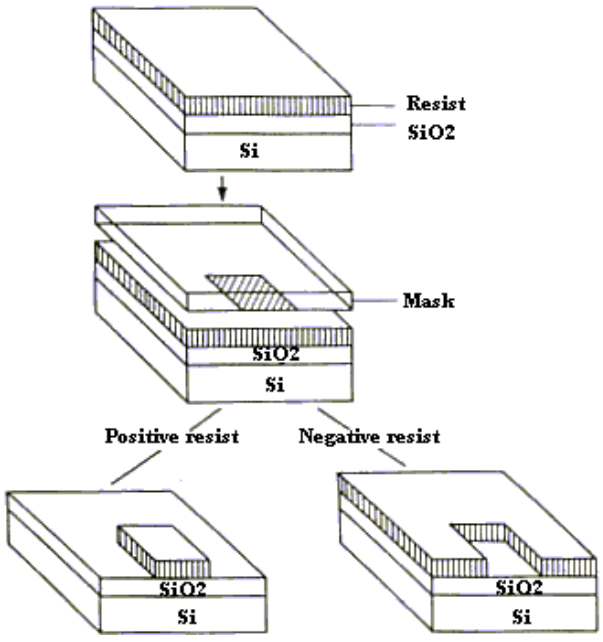

Figure 8. Illustration of Photolithography for Negative and Positive Photoresist. This illustration shows with the same mask (after UV exposure) two different results based on the type of photoresist utilized. For the positive photoresist the portion not exposed to the UV remains intact. For the negative photoresist the portion exposed to the UV remains intact. (Picture created by http://www.ece.gatech.edu/research/labs/vc/theory/photolith.html)

2.53 Poly(dimethylsiloxane) (PDMS)

Poly(dimethylsiloxane), also known as PDMS, is a polymer that is frequently used in the fabrication of micro-fluidic systems. PDMS is a low cost material that has many advantages, as it is easy to bond (PDMS:PDMS, PDMS:Glass), optically transparent (230 to 700 nm wavelength), and permeable to some gases (31,34,44,53). Compared to traditional etching and bonding approaches, PDMS micro-molding is simple and rapid.

The PDMS polymer was mixed with a hardener and then placed on top of the mold which was produced by photolithography. The PDMS hardens and is removed leaving the pattern imprinted on the PDMS surface. This PDMS structure can then be bonded to a glass surface or to a PDMS surface for fabrication of micro-fluidic device. This was the most readily used technique for adhering the PDMS to the surface is called plasma bonding.

2.54 Plasma Bonding

Plasma bonding is the process of etching the bonding surface of PDMS or glass with oxygen plasma so that the surface is covered with hydroxyl groups (30). This surface chemistry allowed for covalent bonds to form when it came into contact with other hydroxyl surface groups. This reaction (with other hydroxyl groups) produced water and a covalent bond utilizing one of the oxygen

molecules. This bond between PDMS and PDMS, or PDMS and glass is very strong and can withstand significant internal pressures. Once, the PDMS has been bonded to the glass surface, the capillary needs to be modified for insertion into the PDMS. Deposition of a metal coat on the proximal and distal ends of the capillary will be necessary so that minimal signal is lost at the glass PDMS interface.

2.55 E-beam Evaporation/ Metal Deposition

Metal deposition is a process whereby a surface is coated with a specific metal while regulating the thickness. The metal is heated to its evaporating point under a vacuum so that the metal atoms diffuse uniformly, coating everything in their

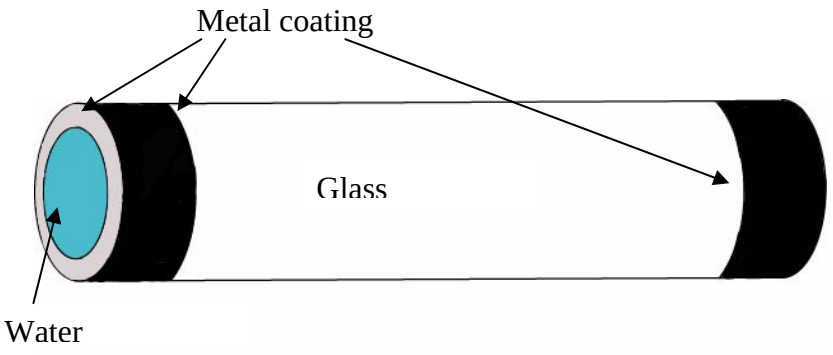

Figure 9. Illustration of Metal Deposition onto a Capillary. The extreme ends of the capillary and the exposed glass cladding (only one end) are coated with metal.

path. The thickness of the metal is monitored via a quartz crystal. The crystal's vibration or change in vibration measures the amount of the metal on the surface of the substrate. The metal can be deposited onto a glass surface with photoresist so that after deposition the photoresist can be removed and the metal coating will now retain the pattern that the photoresist did not cover. This deposition on the proximal and distal ends of the capillary is important because it is at these points that the capillary interfaces with the PDMS inner lumen. If the capillary makes direct contact with the PDMS, then signal is lost. The addition of the modified ends will allow for more fluorescence to be TIR down the LCWG to the fiber optic cable (Figure 9).

CHAPTER III

Experimental Materials and Methods

3.01 Overview

The material and methods section follows the chronological order of the research project. The first step was the characterization of the FAM labeled MB in the ABI Prism 7000 with a synthesized oligonucleotide target. The rationale was to provide a snapshot of the molecular beacon's behavior at different temperatures using this optical fluorescent detection device. Using an oligo target for the first step of optimization was critical for setting base line conditions from which the protein capture assay could be derived. During this step, a series of target oligonucleotide solutions were produced to determine the minimum detection limit of the ABI Prism 7000 as an optical fluorescent detection device. In addition, I wanted to recapitulate the behavior of the MB as described in the literature in order to familiarize myself with it under different conditions.

The second step was to modify a glass cover slip and attach non-fluorescent streptavidin-polystyrene particles on which the modified MB could be attached and analyzed. The rationale for this step was to show stable binding of the biotinylated MB to the streptavidin surface of the beads. In addition, this biotin arm did not impede target-MB binding. Finally, the streptavidin coated beads

provided a quality controlled environment for analyzing MB-target binding that was immobilized to a surface. The third step was to modify a glass cover and attach streptavidin to it. Onto this prepared surface the modified MB could be attached and analyzed. This was done to demonstrate that glass surface modification would result in an environment conducive to MB-binding, therefore providing preliminary evidence for glass capillary functionalization. The fourth step involved preparing competent bacteria cells for transformation.

Steps 5-8 were performed to produce translated hTERT product and transcribed hTR product. Both of these purified components should allow for specificity and binding to the MB without exogenous unknown factors from total protein extracts. The fifth step was transformation of the competent bacterial cells with the selected plasmids. Step six involved plasmid extraction, validation, and transcription reaction mix preparation. The seventh step was the transcription and translation of the selected plasmids. Step eight was reconstitution of telomerase *in vitro* via transcription of hTERT and hTR cDNA and translation of hTERT mRNA. The ninth step was testing the reconstituted telomerase with the MB bench-top assay, and comparing results with the more conventional TRAP assay (since the TRAP assay analyzes telomerase activity). The rationale for this step was to observe whether there was a direct correlation between telomerase molecules captured and signal intensity indicated by telomerase activity. The

tenth step was to test protein extracts from both telomerase-positive and telomerase-negative cell lines. Detection and subsequent measurements of the FAM labeled MB were done using the ABI Prism 7000.

3.02 Fluorescent Characterization of the FAM Labeled Molecular Beacon

Throughout development of the bench-top assay, the focus in regards to the MB and the target oligos, was not molarity, but molecular copies per micro liter. This approach was chosen because the goal of this project was to determine the molecules of telomerase that may be detected in a sample solution.

Several parameters were tested during these experiments. The first parameter was finding the optimal molarity of the MB in the assay reaction. The second parameter was determining the minimum detection limits of the assay utilizing the ABI Prism 7000. The third parameter involved determining the thermal characteristics of the MB from 80°C - 10°C - 80°C (3,4,50). Each of these parameters could be evaluated in a single 96 sample experiment. Four separate master mix solutions were prepared with the only variant being MB molarity. The molarities of Tris-HCl pH 8.0, KCl, and $MgCl_2$ were held constant to the manufacture's recommendations (20mM, 50mM, 5mM, respectively). The reference dye ROX (5-carboxy-X-rhodamine, Invitrogen, 25μM) was added at the

same concentration (125nM) to each master mix for normalization of the experiment.

These four solutions, 1.2e11 MB copies/µL (200nM), 9.04e10 MB copies/µL (150nM), 6.02e10 MB copies/µL (100nM), 3.01e10 MB copies/µL (50nM), were each compiled to make 16 different 50µL reactions. Of the 16 samples, two were used as controls, and the other 14 samples had varying concentrations of target oligonucleotide ranging from 2.0e11 copies/µL (332nM) to 0.2 copies/µL (0.332aM), decreasing in log increments. The master mix protocol for the 1.2e11 MB copies/µL (200nM) MB experiment is as follows (one sample volume was added to compensate for pipette error, all other master mix compilations can be extrapolated):

1. 12.5µL 200mM KCl/sample x 17 samples = 212.5µL KCl
2. 5µL 200mM Tris-HCl pH 8.0/sample x 17 samples = 85µL Tris-HCl
3. 1.25µL 200mM $MgCl_2$/sample x 17 samples = 21.25µL $MgCl_2$
4. 0.25µL 25µM ROX/sample x 17 samples = 4.25µL ROX
5. Vortex master mix and spin down
6. Add 31.05µL DDH_2O to the solution sample
7. Add 21.05µL DDH_2O to the blank sample
8. Add 18.95µL of Master mix to the solution sample (completed)
9. 10µL 1µM MB/sample x 16 samples (-1 for solution) = 160µL MB

10. Vortex master mix briefly and quick spin
11. Add 28.95µL of Master mix to the blank (completed)
12. 20.05µL DDH_2O/sample X 15 (-1 for blank) = 300.75µL DDH_2O
13. Vortex Master mix briefly and quick spin
14. Aliquot 49µL into each sample well
15. Add 2µL of target oligo into each sample well (pipette mixed)

    Starting with 1e13 oligo copies/µL (16.6 µM) and ending with 10 oligo copies/µL (0.0166fM)

The samples were loaded into optical tubes (Applied BioSystems Inc., Part No. 4316567) and the optical caps (Applied BioSystems Inc., Part No. 4323032) placed on top. The optical portion of the caps should not be touched at any time. The large end of a medium pipette tip was used to firmly secure the optical caps on the optical tubes. Also, powder-free gloves were used, as powder may interfere with the optics. Make sure there are no bubbles in the sample solutions. If bubbles are present, the samples must be spun down.

3.03 Preparation of the Target Solution

The lyophilized target oligonucleotide (oligo) was produced by Texas Tech University Center for Biotechnology and Genomics. The 24mer target oligonucleotide, with a sequence of 5'-CCCTAACCCTAACCCTAACCCTAA-

3', was complementary to the hairpin loop in sequence and length. This oligo was resuspended in 100µL of double distilled water (1.65e14 copies/µL, 273.5µM,). The molecular weight was given on the production sheet supplied by the synthesizer and calculations were made to produce a solution with an oligo count of 1e13 oligo copies/µL. This solution was then used to produce serial dilution, down to 1e1 oligo copies/ µL.

3.04 Molecular Beacon Attachment to Avidin-Polystyrene Particles on a Glass Cover

This first step may not have been the most logical step in project development, but the ability to locate, identify, and fluorescently characterize a bound particle that was 6.7µm in diameter was thought to be more effective and less problematic than one that was ~5nm (37). The first step was to clean the glass cover surface (FISHERfinest, Premium cover glass, 24mm x 60mm). The first wash sequence began with two washes; each with 5mL of acetone followed by three 5mL washes of ethanol (70%) and then washed with 10mL of double distilled water. The second wash sequence consists of a 5mL wash of 2 M ammonia hydroxide followed by a 10mL wash of double distilled water. The second wash sequence was repeated three times. After completing the last sequence of the second wash, compressed air was used to remove any residual water. Next, a 5µL drop of

biotinylated bovine serum albumin (BSA-biotin, Sigma, 1mg/mL, resuspended in 20mM phosphate buffered saline pH=7.0) was pipetted onto the glass surface. The sample was left at room temperature until the liquid evaporated. This time duration was dependent upon the humidity and temperature in the preparation area. After the liquid evaporated from the glass surface there was a transparent circle outline where the BSA-biotin was placed. This area was washed with 10mL of double distilled water to remove unattached BSA-biotin. The area of BSA-biotin was very hydrophilic and retained some of the water. Then avidin-coated polystyrene particles (2µLs) (Spherotech, SVP-69-5, 0.5% w/v, 6.7µm) was added to the biotinylated area of the glass cover. The sample was incubated at room temperature for 1 hour, then washed with 10mL of double distilled water to remove the unbound avidin-coated polystyrene particles. The last step in the attachment process was the addition of the biotin modified MB (Trilink, 1µM). The sequence and molecular configuration of the MB obtained from Trilink is 5'-(TAMRA)(C6NH)CCTAGCTTAGGGTTAGGGTTAGGGTTAGGGGC (Biotin-dT)AGG (DABCYL) -3'. The MB (3µLs) was added to the BSA-biotin/streptavidin surface and incubated at room temperature for 1 hour. The final wash consisted of 10mL of double distilled water. The sample was then ready for testing. Unused samples were stored in 10mM PBS at 4°C for future use.

3.05 Molecular Beacon Attachment to Avidin-Polystyrene Particles on a Glass Cover Analysis

The attachment process was monitored at each step. To accomplish this, four different glass covers were produced per batch utilizing the process described in section 3.04. Glass cover #1 contained only BSA-biotin. Glass cover #2 contained BSA-biotin with the non-fluorescent streptavidin coated polystyrene beads. Glass cover #3 contained BSA-biotin with the non-fluorescent streptavidin coated polystyrene beads and the attached MB*. Glass cover #4 contained BSA-biotin with the non-fluorescent streptavidin coated polystyrene beads with the MB attached, and 3μLs of the 1e13 oligos per μL target solution**. The target solution contained the aforementioned oligo concentration with 5 mM $MgCl_2$. The target solution selected was the highest concentration available outside the master solution. This concentration would assure maximum binding to yield maximum fluorescence. The concentration of $MgCl_2$ utilized was selected based on past experimental data and what was reported in the literature (49-51).

*This cover glass should show the background fluorescence of the MB while FRET is taking place, since FRET is not complete. **This cover glass should show the total fluorescence of the MB (non-FRET) when complexed with the target oligo.

The microscopy and fluorescent analysis of these samples was done using the Olympus IX80 confocal microscope with FV300 analysis software. A non-treated glass cover was placed on top of the damp (DDH_2O) treated glass cover, without inverting the sample. The sample was analyzed under a 60x oil immersion lens. Once the sample area was identified, laser excitation was employed. The fifth setting (300μm diameter) was selected for the aperture. The dichroic mirror in the control box was set to send the entire emission fluorescence to channel 1. The 605 band pass emission filter was utilized. This filters extraneous light emissions, only allowing light with the wavelengths of 575 to 630 nm passage to the PMT. The screen view size was set to 512 x 512 with three different views selected (channel 1 – sample emission, channel 2 – DIC, view of overlay) and the fastest scan rate selected. The scan rate directly correlated to picture resolution (e.g. a slower rate yields higher resolution). When all the filters were in place and the view was digitized, the PMT voltage was set so that the MB in the FRET state showed very slight emission. Once this PMT voltage (476v) was set, all other samples were viewed with the same parameters. Maintaining the same parameters allowed comparisons to be made of the fluorescent emissions between each sample. The only variable between samples was the focus depth of each sample. Digitized images were analyzed using the

Flow View software, which showed comparable quantitative fluorescence intensities.

3.06 Molecular Beacon Attachment to Streptavidin on a Glass Cover

Cleaning the glass cover (FISHERfinest, Premium cover glass, 24mm x 60mm) was the first step in the attachment process. The glass surface needed to be cleaned to expose its hydrophilic nature. The first wash sequence began with two washes; each with 5mL of acetone followed by three 5mL washes of ethanol (70%) and then washed with 10mL of double distilled water. The second wash sequence began with a 5mL wash of 2 M ammonia hydroxide followed by a 10mL of double distilled water. The second wash sequence was repeated three times. After completing the last sequence of the second wash compressed air was used to remove the visible water. Next, a 5µL drop of biotinylated bovine serum albumin (BSA-biotin, Sigma, 1mg/mL, resuspended in 20mM phosphate buffered saline pH=7.0) was pipetted onto the glass surface. The sample was left at room temperature until the liquid had evaporated. This time duration was dependent on the humidity and temperature in the preparation area. After the liquid had evaporated there was a transparent circle where the BSA-biotin was placed. The area was washed with 10mL of double distilled water so that all the unattached BSA-biotin was removed. The area of BSA-biotin was very hydrophilic and

retained some of the water with which it was washed. Two µLs of streptavidin was added (Sigma, 1mg/mL, resuspended in 20mM phosphate buffered saline pH=7.0) to the biotinylated area of the glass cover. The sample was incubated at room temperature for 1 hour. After incubation, the sample was washed with 10mL of double distilled water to remove the unbound streptavidin. The last step for the attachment process was the addition of the biotin modified MB (see materials and methods section 4). Three µLs of the MB was added to the BSA-biotin/streptavidin surface and incubated at room temperature for 1 hour. The final wash consisted of 10mL of double distilled water. The sample was then ready for testing. The unused samples can also be stored in 10mM PBS at 4°C for future use.

Strictly for a reference, during the attachment process fluorescent avidin coated polystyrene beads (SPHERO avidin coated fluorescent particles, nile red, 0.7-0.9µm, Spherotech Inc.) were added concurrently to the BSA-biotin glass surface when the purified streptavidin was add, Since the BSA-biotin is virtually impossible to see under the microscope and purified streptavidin is problematic, this reference proved very necessary. These beads acted as a confirmation marker and BSA-biotin reference point for each step of the process: BSA-biotin, Streptavidin, and MB.

3.07 Molecular Beacon Attachment to Streptavidin on a Glass Cover Analysis

The attachment process was monitored at each step. To accomplish this, four different glass covers were produced per batch, utilizing the process described in section 5 of material and methods (pg. 41). Glass cover #1 contained only BSA-biotin with the reference fluorescent avidin coated polystyrene beads. Glass cover #2 contained BSA-biotin with the reference fluorescent avidin coated polystyrene beads and purified streptavidin. Glass cover #3 contained BSA-biotin with the reference fluorescent streptavidin coated polystyrene beads, purified streptavidin and the attached MB*. Glass cover #4 contained BSA-biotin with the reference fluorescent avidin coated polystyrene beads, purified streptavidin, the attached MB, and 3µLs of the $1x10^{13}$ oligos per µL target solution**. The target solution contains the aforementioned oligo concentration with 5mM $MgCl_2$. The target solution selected was the highest concentration available outside the master solution. This concentration was used to obtain maximum binding corresponding to maximum fluorescence. The concentration of $MgCl_2$ utilized was selected partially on past experimental data described in the literature (49-51).

*This glass cover showed the background fluorescence of the MB while FRET was occurring, since FRET is not complete. **This glass cover showed the total fluorescence of the MB (non-FRET) when complexed to the target oligo.

The visual and fluorescent analysis of this sample was done using the Olympus IX80 confocal microscope with FV300 analysis software. A non-treated cover slide was placed on top of the damp (DDH_2O) treated glass cover. The sample was not inverted. This sample analysis setup directly correlated to the analysis of the fused silica capillary analysis. The sample was analyzed under 60x oil immersion lens. Using the bright light source, a field of interest was found by targeting the reference beads. Once the sample area was identified, laser excitation was employed. The aperture was set to the third setting (150µm diameter). The dichroic mirror in the control box was set to send the entire emission fluorescence to channel 1. The 605 band pass emission filter was utilized. This filtered extraneous light emissions only allowing light with the wavelength of 575 to 630 nm passage to the PMT. The screen view size is set to 512 x 512 with three different views selected (channel 1 – sample emission, channel 2 – DIC, view of overlay) and the fastest scan rate was selected. The scan rate correlated directly to the picture resolution. When all the filters were in place and the view digitized, the PMT voltage was set so that the MB in the FRET state showed very slight emission. Once this PMT voltage (466v) was set, all other samples were viewed with the same parameters. Maintaining the same parameters allowed for comparison of the fluorescent emission between samples. The only variable between samples was the depth of focus for each sample.

Depth of focus was partially controlled by manipulating the plane of focus for the reference beads. The other variable was the relative smoothness of the glass and the varying thickness of the BSA-biotin layer which could also affect signal emission.

Digitized images were analyzed using the Flow View software. This analysis showed comparable quantitative fluorescence intensities.

3.08 Preparing Competent Cells

Preparation of competent bacterial cells was done using a procedure provided by Dr. Michael San Francisco (Department of Biological Sciences, Texas Tech University, Lubbock, TX). Healthy DH5α *Escherichia coli* cells (Gibco) were streaked onto a Luria-Bertani (LB) (DIFCO, Luria - Bertani Agar, Miller base) agar plate with one loop of the original cell culture. The manufacturer's directions were strictly followed for making LB agar. Agar was autoclaved, cooled, and poured into petri dishes. The plates were allowed to dry for 24 hours and then placed at 4° C for storage. Aseptic technique was used throughout the entire process to maintain a pure culture. The streaked plates were grown overnight at 37° C. A single colony was extracted and inoculated into 2.0mL of LB broth (DIFCO, Luria - Bertani broth, Miller base) in a culture tube. The sample was incubated at 37° C overnight with aeration and shaking. Following incubation 50μLs, of the 2.0mL culture, was inoculated into 5.0mL of LB in a

culture tube. This culture was incubated at 37° C for approximately 2 hours with aeration and shaking. After this incubation the cells were pelleted at 5000 rpm for 30 minutes at 4° C. The supernatant was discarded and the pellet resuspended in 1.0mL of ice cold 50 mM $CaCl_2$. The resuspended cells were then placed on ice for forty five minutes. The cells were transferred into a cold 1.5mL tube and then centrifuged at 13,000g for 1 minute at 4° C. Next, the supernatant was discarded and the pellet resuspended in 0.2mL ice cold 50mM $CaCl_2$. The sample was placed on ice for 30 minutes. At this point the cells were competent, but the efficiency of transformation increases with extended incubation on ice. The samples that were not used immediately were stored at -70° C. To prepare the cell for storage 1-2 drops of Dimethyl sulfoxide (DMSO) was added to the cell culture and vortexed briefly at a medium speed.

3.09 Transformation of Competent DH5α *E. coli*

The procedure for transforming cells was provided by Dr. Michael San Francisco (Department of Biological Sciences, Texas Tech University, Lubbock, TX). The pGRN83 (10-20ng, in 10-25µL volume) and pcDNA3.1 His C plasmid was added to separate 0.1mL of ice cold competent cell cultures. The cell solutions were placed on ice for 40 minutes. The cells were then heat shocked in a 42° C water bath for 2 minutes and placed on ice for 5 minutes. Next 2.0mL of

LB broth (without selectable antibiotic) was added to the cell suspension and incubated for 1 hour at 37° C with aeration and shaking. The LB broth was made following the manufacturer's instructions, autoclaved, and stored at 4° C. This allowed the transformed cell to recover and express the plasmid-borne antibiotic resistance gene. Once the recovery took place the cells were aliquoted into an ampicillin-antibiotic media. The media composition consisted of LB broth with 100ug/mL of ampicillin. This media selected for the cells that were both transformed and had plasmid production.

3.1 Plasmid Extraction and Plasmid Transcription Preparation

The QIAprep miniprep plasmid extraction kit was used for the plasmid extraction procedure (Qiagen, QIAprep miniprep kit, 27104). The QIAprep spin miniprep kit protocol using a microcentrifuge was followed with no modifications.

Once the plasmids were extracted, each sample was analyzed for DNA quantity and purity using a NanoDrop 1000 spectrophotometer (NanoDrop Inc. Delaware, MA). After determining DNA quantity, each sample was placed in a restriction enzyme reaction mix to verify proper plasmid extraction. The pGRN83 plasmid [cccDNA (covalently closed, circular DNA), which contains hTR cDNA] is 3558bp in length and when digested with Bstx 1 (Fisher

BioReagents, BP3340-1) is linearized. The pcDNA3.1 His C plasmid (cccDNA, which contains hTERT cDNA) is 9565bp in length and when digested with ECOR I (Promega, R6011) forms two fragments, 4065bp and 5500bp. These digested plasmids along with the uncut cccDNA were run on a 1.2% agarose gel (BIORAD, 161-301) with ethidium bromide (Sigma-Aldrich, E7637, 800ng/µL) in 0.5X Tris-Borate-EDTA running buffer (Sigma, T-6400, 5X TBE) to determine proper plasmid extraction. These samples were run in conjunction with a 1Kb DNA ladder (Invitrogen, 15615-016) to verify plasmid products.

After confirmation and quantity assessments, a larger quantity of pGRN83 plasmid was cut with Bstx 1 to provide a proper stopping point during the transcription assay. This would supply the hTR mRNA at the proper length for integration into hTERT and allow for correct telomerase activity. The restriction enzyme assay was scaled up so that 4µg of pGRN83 plasmid would be digested in one reaction, according to manufacturer's instructions. After the cleavage, DNA was extracted using 2 volumes 95% ethanol and 0.1 volumes 3M sodium acetate. The solution was "finger thumped" several times, placed at -20°C for 30 minutes to promote DNA precipitation, and then centrifuged at 13,000 rpm for 30 minutes. The supernatant was removed and the DNA pellet was washed with 70% ethanol and left to dry for 5 minutes. The DNA was resuspended using 8 µL of the EB (10mM Tris-Cl, pH 8.5) buffer provided in the Qiagen plasmid

extraction kit. The pcDNA3.1 His C had a stop sequence at the terminal end of the transcript for correct transcript length. The plasmids were then ready for the transcription and translation reaction.

3.11 Transcription and Translation of Telomerase and Sample Preparation

The transcription - translation reaction for the pcDNA 3.1 His C plasmid was achieved using Ambion's PROTEINscripII T7 promoter (Ambion, 1280-127). Similarly, transcription of the pGRN83 was achieved using Ambion's PROTEINscripII T7 promoter (Ambion, 1280-127). Manufacturer's instructions were followed, except that translation was not performed.

A separate transcription - translation reaction was performed in which both plasmids were included, otherwise following the manufacturer's protocol. Since both products were co-produced, telomerase was reconstituted in this reaction and no additional reaction had to be performed to reconstitute telomerase. The end product was diluted 1:40 with CHAPS lysis buffer and stored at -20°C.

3.12 Reconstitution of Telomerase and Sample Preparation

Since, hTR and hTERT were produced in two separate transcription and translation reactions, they must be reconstituted in a separate reaction. The *in vitro* reconstitution of telomerase brings the two independently made components

(hTERT, hTR) together to form telomerase. This reaction was performed as previously described (21,56). Briefly, 0.2µL hTERT translation reaction, 0.5µL hTR transcription reaction, 0.4µL 10x buffer (200mM HEPES pH 7.6, 500mM KCl, 0.1% NP40, 10mM $MgCl_2$, 10mM EGTA, DEPC treated water), 2µL fresh RRL, and 0.9µL DEPC treated water were mixed. The reaction was incubated at 30°C for 90 minutes and stored at -20°C for future use. After incubation, 36µLs of CHAPS {3-[(3-Cholamidopropyl)dimethylammonio]-1-propanesulfonate} lysis buffer was added to dilute the PCR inhibitors (21,56). The hTERT translation reaction was then prepared for sample analysis. This sample preparation followed the same dilution as the reconstituted telomerase. The only difference was the addition of 0.5µL hTR transcription reaction, which was substituted for CHAPS lysis buffer. The hTR transcription reaction sample was prepared in the same manner as the hTERT sample, but the hTERT volume was substituted with CHAPS lysis buffer.

3.13 Telomerase Sample Analysis using the TRAPeze Kit

Analysis of telomerase activity (Chemicon International, Temecula, CA, S7700, TRAPeze Telomerase Detection Kit) followed the manufacturer's directions with the additional utilization of the hot start protocol located in the troubleshooting portion of the user manual (pg. 23). The single modification

performed, involved the process used to label the polymerase chain reaction (PCR) product with radio isotopic [α-^{32}P]-Deoxycytidine 5'-triphosphate (PerkinElmer, BLU513H250UC). Incorporation, not end-labeling the TS primer, was applied as suggested by the manufacturer's. Two microliters of each sample were utilized to determine telomerase activity. The PCR products were analyzed on a 12.5% acrylamide [40% acrylamide/bis solution (29:1), BIORAD, 161-0144] PAGE gel. The acrylamide gel was run at 300v for two hours, and fixed in a solution consisting of 5M NaCl, 2M NaOAc, 95% ethanol, in water, for thirty minutes. After the gel was fixed, it was incubated in DDH_2O for five minutes to remove residual NaOAc. The gel was then dried on a BIORAD gel air drying system (cat#165-1771). The dried gel was exposed to a BIORAD imaging screen (cat# 170-7320) and incubated overnight. The plate was removed from the incubator and analyzed using Molecular Analysis software version 2.0.

3.14 Molecular Beacon Bench-Top Assay Analysis of Reconstituted and Co-Transcription/ Translation Telomerase

The reconstituted telomerase along with the co-transcription and translation products and the separate components were analyzed using the MB bench-top assay. The controls during this experiment were: solution, blank, and 51mM RRL. In the reconstituted telomerase, co-transcribed telomerase and hTERT

samples, 51mM was the concentration calculated for RRL. This concentration was added back into a test sample in order to delineate the protein binding background from true signal. The hTR transcript sample never went through translation, therefore RRL was never added to the reaction mix. The 51mM RRL sample showed the protein binding background relevant to the test samples. The assay components utilized for this experiment were as follows: 20mM Tris-HCl pH 8.3, 63mM KCl, 1.5mM $MgCl_2$, 125nM Rox Dye, 200nM MB, and DDH_2O, for a total volume of 48µLs. The sample volume was 2µLs. These samples were analyzed in the 80°C - 10°C - 80°C scheme, in 5 degree increments by the ABI Prism 7000.

3.15 Molecular Beacon Telomerase Bench-Top Assay Analysis of Cell Protein Extracts

Total protein extracts from various cell lines were analyzed using the MB (MB) bench-top assay. The assay components for this analysis were as follows: 20mM Tris-HCl pH 8.3, 63mM KCl, 1.5mM $MgCl_2$, 125nM Rox Dye, 200nM MB, and DDH_2O, for a total volume of 46µL (in the case of a cell protein extract sample) or 48µL (for control samples). There were four controls for this experiment: solution, blank, DNA control, and RRL control. The solution sample contained all the components except the MB, and therefore provided a base

reading of the Rox reference dye and FAM fluorophore since none were present in the sample. The blank contained all the components with water added in place of an experimental sample volume. This control should show the molecular beacon's natural change in its thermodynamic state when cycled through the temperature range utilized in this experiment. The DNA control contains a specific target oligo at a concentration of 4e10 copies/µL, all other components remained the same. This control showed two specific criteria essential for this experiment. The first criterion demonstrated that the MB was functioning properly as described in the literature. The second criterion involved the molecular beacon's thermodynamic nature, in the presence of a substance. The MB changed into its linear confirmation (non-FRET). The RRL control contained all the components; however, 2µLs of 1mM RRL was also added to determine the baseline of the protein reaction that would take place in the cell protein extract samples.

The protein extracts utilized in this analysis were obtained from samples assayed using TRAP by Dr. Lauren Gollahon in 1995. These samples were stored at -80°C for ~10 years. Two microliters of each extract were utilized in the bench-top analysis. These samples were accompanied by 2µL 1mM RRL to complete the sample preparation.

The samples were “finger thumped” and briefly centrifuged to collect all the solution at the bottom of the sample tube. Each sample was then transferred by pipette to the optical tubes and optical caps were put in place. The optical tubes were then centrifuged to make sure no bubbles remained in the sample solutions and that all the solutions were at the bottom of the tubes. Then the samples were analyzed with the ABI Prism 7000.

3.16 Cell Lines Used for Testing the Efficacy and Sensitivity of Telomerase Capture Using a MB Strategy

All cell lines consisted of primary cultures established in affiliation with Dr. Gollahon’s postdoctoral research at UT Southwestern Medical Center, Dallas, TX. The cell lines utilized were as follows:

Telomerase Negative Cell Lines

Patient #	Sample #	Description
HME 50	#86	Mammary epithelial cell line established from tissue obtained from a patient with Li-Fraumeni Syndrome (germline p53 mutation). This cell line later spontaneously immortalized (13).

HME 50-8 #96 – A clone from the parent culture HME 50. This clone never spontaneously immortalized. It remained telomerase negative.

HME 31 #100 – Primary cell culture established from a patient undergoing radical mastectomy for breast cancer. Normal tissue was taken outside the area of resection.

HME 52-7 #103 – Clonol outgrowth of a primary cell culture obtained from a patient with a heritable mutation in BrCa II.

Telomerase Positive Cell Lines

Patient #	Sample #	Description

HME 31 E6/E7 #81 – This cell line was established by introducing a defective retrovirus containing Human Papillomavirus type 16 early genes (E6 and E7) to the HME 31 cells previously described (#100). This infection resulted in re-expression of telomerase and immortalization.

HME 32 (273)-1 #104 – Human mammary epithelia cell line derived from a patient who underwent reduction mammoplasty. The normal diploid cell line was transfected with a

construct containing p53 mutated at exon 273. This construct conferred immortality (9).

EC-2 #144 – Clone of HT 1299 a non-small cell lung carcinoma obtained from a patient with lung cancer.

EC-2 37°C #147 - Clone derived from HT 1299 transfected with p53 mutant 143 which retains the mutant phenotype when placed at 37°C. Cells were collected at 37°C, tested strongly for telomerase, but the exogenous p53 retained the mutant conformation. This cell line demonstrated more intense telomerase signal than the 32°C as determined by the semi-quantitative TRAP assay (Dr. Gollahon unpublished results).

EC-2 32°C #149 – Clone derived from HT 1299 transfected with p53 mutant 143 which confers a wild t ype phenotype when placed at 32°C. Cells were collected at 32°C, tested strongly for telomerase, but had some wild type p53 expression, determined by immunopercipitation (Dr. Gollahon, unpublished data).

CHAPTER IV

RESULTS

4.1 Fluorescent Characterization of the FAM Labeled Molecular Beacon

The fluorescent and thermodynamic characteristics of the MB in a known chemical solution, at a given temperature, being analyzed by a specific fluorescent reader, are all vital to assay development. These characteristics along with MB concentrations were tested in an ABI Prism 7000. The concentrations that were tested were 1.2e11 MB copies/µL (200nM), 9.04e10 MB copies/µL (150nM), 6.02e10 MB copies/µL (100nM), 3.01e10 MB copies/µL (50nM). This range of concentrations helped determine the optimal concentration at which the assay would be developed. The different concentrations would be tested with serial dilutions of target oligo to determine the detection limits for each and relative sensitivity within those limits.

The indicated concentrations show a wide range of detection limits from 4e8 oligos/µL (0.332nM) to 4e11 oligos/µL (332.0nM) (Figures 10-13). Concentrations below 4e8 oligos/µL were undetectable and above 4e11 oligos/µL were not tested due to concentration constraints of the master oligo solution. Each molarity showed unique individual fluorescent activity for the indicated temperature range. These individual responses to the target oligo concentration

were similar for each concentration, but different in direct correlation to the increase in MB concentration (Figure 10-13).

The overall MB pattern during these experiments was constant. When the solution was held at higher temperatures the random coil conformation was present (partial FRET). When the temperature decreased the MB random coil confirmation was reconfigured into the linear conformation (MB/target oligo, non-FRET). When the temperature of the solution reached the optimal annealing temperature ~25°C the maximum fluorescent value was obtained. When the temperature decreased below the optimal annealing temperature the MB changed its conformation back to the stem-loop formation (FRET).

The 1.2e11 MB copies/µL (200nM) solution was selected to continue assay development, because this concentration showed the greatest range of detection with limited effects from increased background due to increased numbers of molecular beacons. It also had the best workable detection range of the four different MB concentrations.

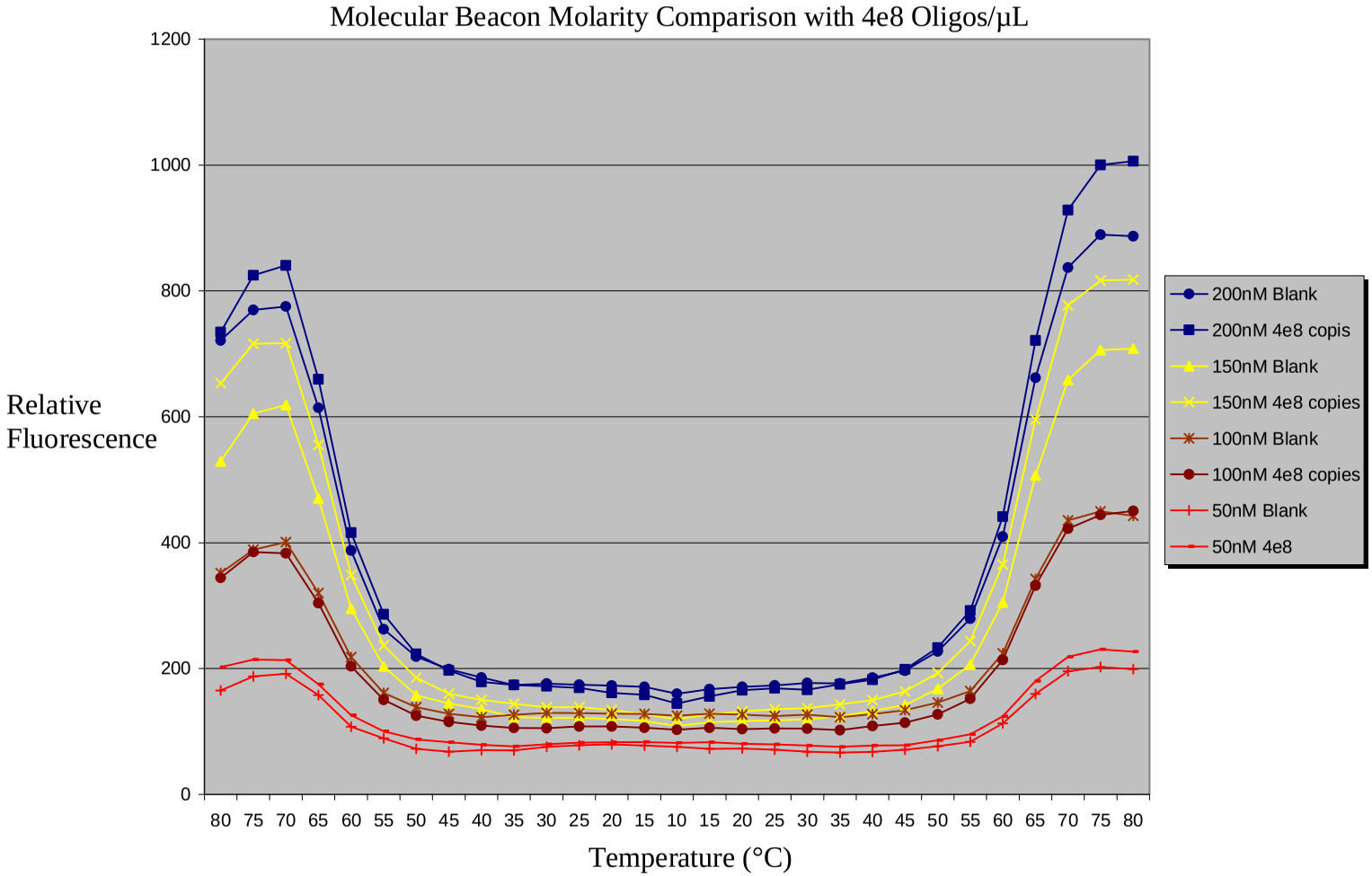

Figure 10. Molecular Beacon Molarity Comparison with 4e8 Oligos/µL.
The X axis is temperature in °C and the Y axis is relative fluorescence. The graph depicts four different MB molarities with each molarity having two test samples. The first sample for each molarity is a blank which only contains the MB and shows the thermodynamic nature of the molecular beacon with no target present. The second sample for each molarity has the target oligo added and shows the linear confirmation of the molecular beacon for that target concentration.

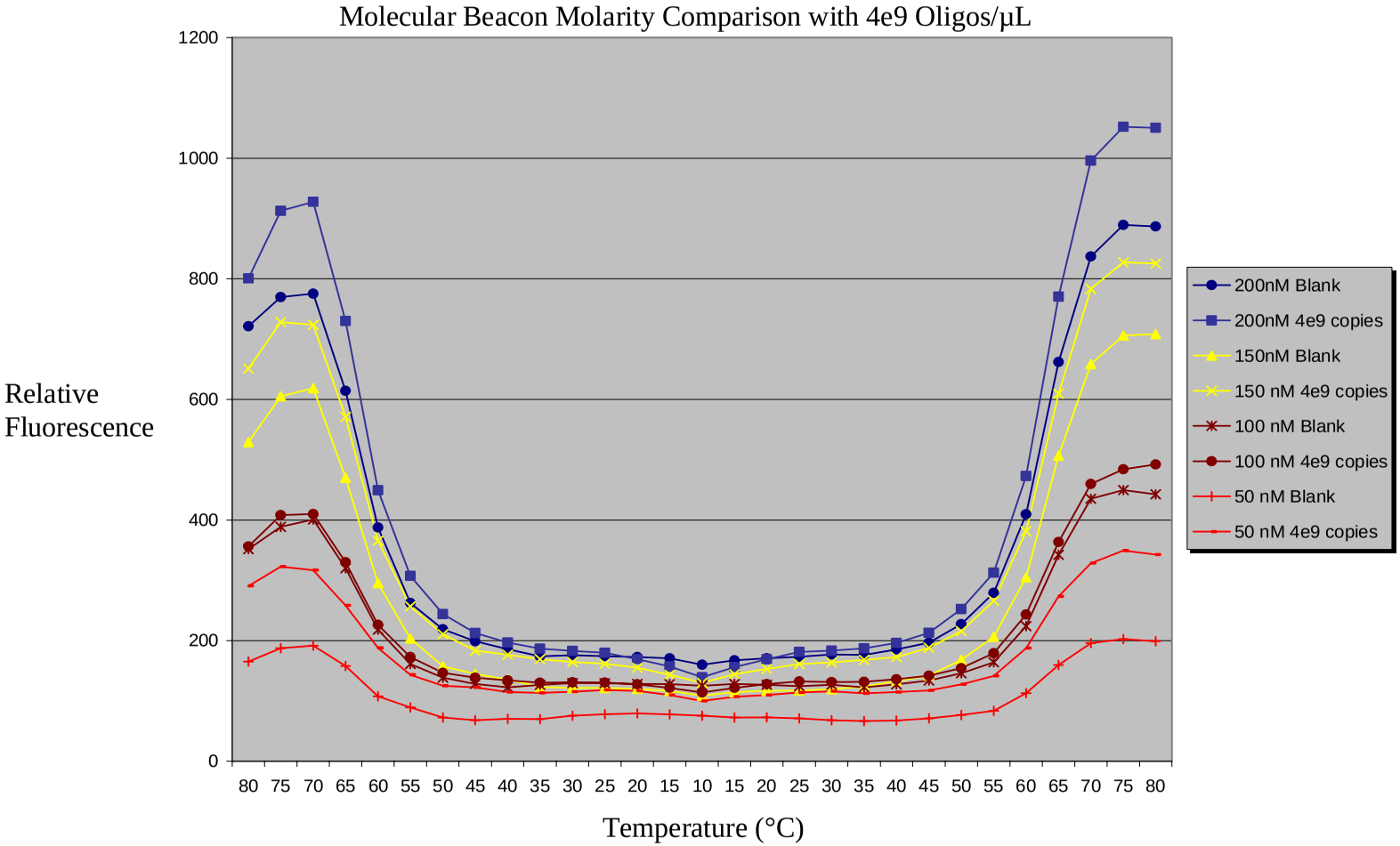

Figure 11. Molecular Beacon Molarity Comparison with 4e9 Oligos/µL.
The X axis is temperature in °C and the Y axis is relative fluorescence. The graph depicts four different MB molarities with each molarity having two test samples. The first sample for each molarity is a blank which only contains the MB and shows the thermodynamic nature of the molecular beacon with no target present. The second sample for each molarity has the target oligo added and shows the linear confirmation of the molecular beacon for that target concentration.

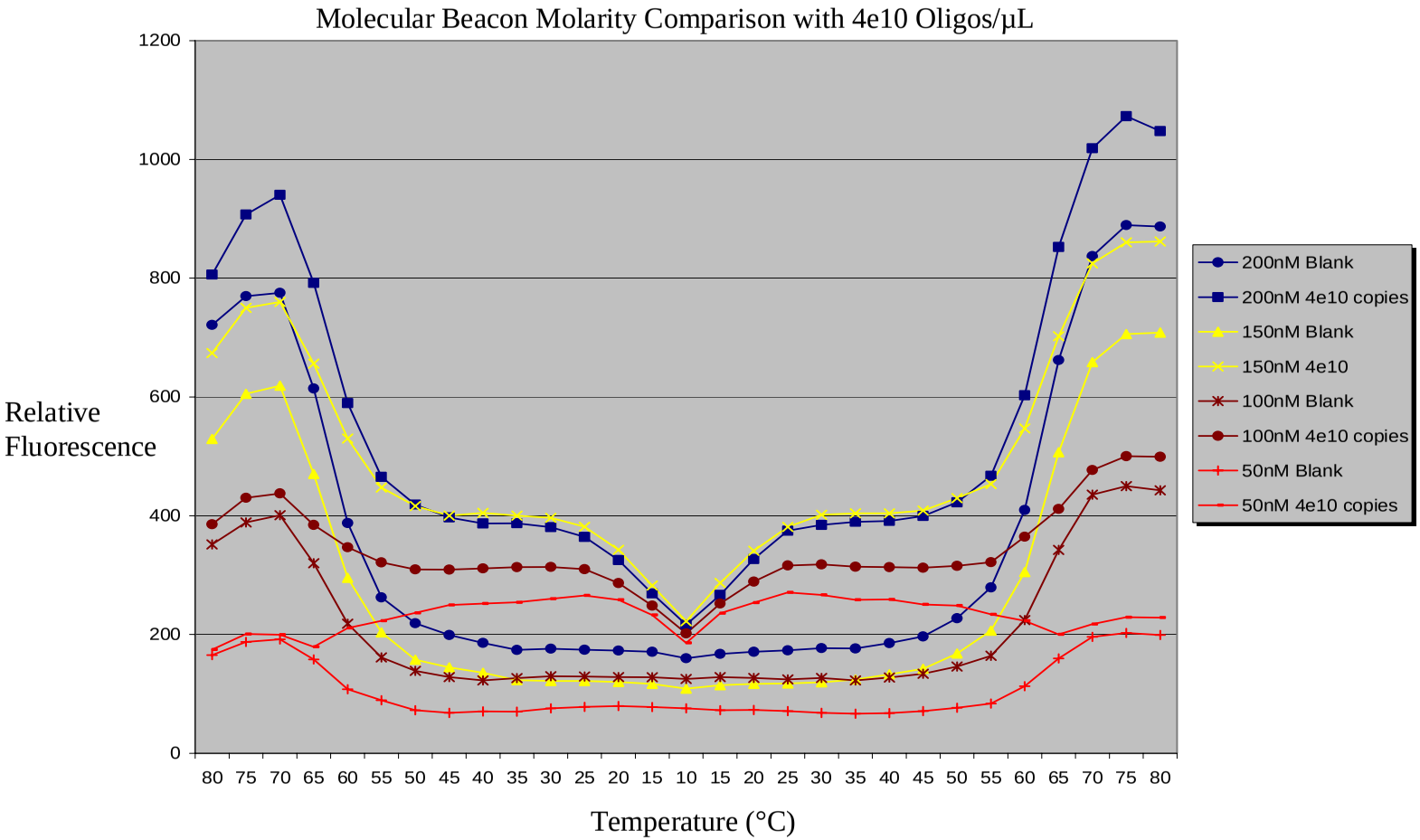

Figure 12. Molecular Beacon Molarity Comparison with 4e10 oligos/µL.
The X axis is temperature in °C and the Y axis is relative fluorescence. The graph depicts four different MB molarities each molarity having two test samples. The first sample for each molarity is a blank which only contains the MB and shows the thermodynamic nature of the molecular beacon with no target present. The second sample for each molarity has the target oligo added (2e12 copies) and shows the linear confirmation of the molecular beacon for that target concentration.

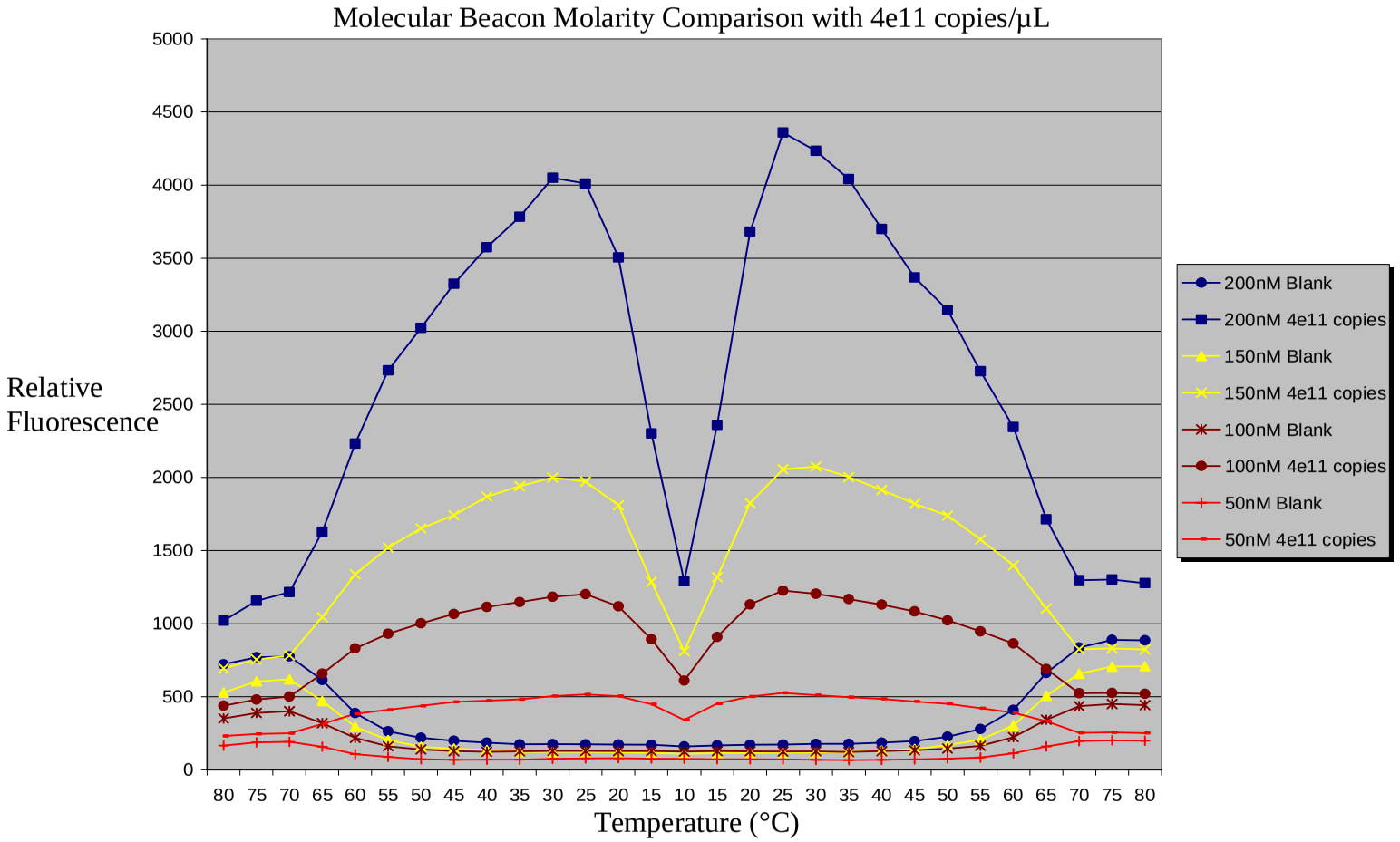

Figure 13. Molecular Beacon Molarity Comparison with 4e11 Oligos/µL.
The X axis is temperature in °C and the Y axis is relative fluorescence. The graph depicts four different MB molarities each molarity having two test samples. The first sample for each molarity is a blank which only contains the MB and shows the thermodynamic nature of the molecular beacon with no target present. The second sample for each molarity has the target oligo added and shows the linear confirmation of the molecular beacon for that target concentration.

4.2 Molecular Beacon Attachment to Avidin Coated Polystyrene Particles on a Glass Cover

The utilization of larger particles to propagate the molecular attachment process of the MB allows for ease of visual characterization, preliminary fluorescent characteristics, and attachment protocol familiarity. The attachment protocol required several steps, but the only step that did not involve biotin-streptavidin interactions [binding constant 1.0e15 M^{-1} (27)] was the BSA-biotin binding to the glass surface. The BSA-biotin binding is dependent on the glass surface's chemistry. The greater the number of hydroxyl groups present on the surface of the glass, the stronger the binding of the BSA-biotin or the greater number of BSA-biotin bonds. Data were collected during the entire attachment process when visual characteristics could be evaluated. The attachment of the BSA-biotin alone could not be detected by confocal microscopy because there were no fluorescent characteristics. However, with the human eye a small transparent circle could be seen. This circle of BSA-biotin also interacted differently with water than did the glass surface. After washing the cover slip with water to rinse off any unattached BSA-biotin, the water would bead up on the BSA-biotin deposited circle. The attachment of the non-fluorescent avidin coated polystyrene particles could be visualized by confocal microscopy and normal bright field microscopy. These particles have no fluorescent

characteristics (Figure 14A), but the differential interference contrast (DIC) channel of the confocal could be used to detect them (Figure 14B). The overlay of the fluorescent image and the DIC image co-localizes the fluorescent properties of the particles with the particles themselves (Figure 14C). The linear fluorescent analysis of a particle using FlowView 300 software was used to determine its relative fluorescence and DIC intensity (Figure 15). The pictures' color does not represent the actual emission by the specimen. The color utilized in the confocal pictures is superimposed by the FlowView 300 software and can be changed to any color.

The next step of the attachment protocol was the addition of the MB to the avidin coated beads. This sample showed background fluorescence attributed to incomplete FRET of the fluorophore by the quencher (Figure 16A). The ability to visualize the beads using DIC (Figure 16B) and co-localize the fluorescence with individual beads using the overlay (Figure 16C) showed the fluorescent characteristics of the MB (in the FRET configuration) when attached to the beads. The linear fluorescent analysis of a particle using FlowView 300 software determined its relative fluorescence and DIC intensity (Figure 17). The DIC intensity of this sample correlated with the DIC intensity of the previous sample. The fluorescent intensity of this sample (MB, FRET) is significantly higher than

the previous sample with the avidin coated beads without the MB attached (Figure 14).

The attachment protocol was completed at this point, but the analysis of the MB in the linear conformation still needs to be examined. The target solution was added to the MB coated polystyrene beads attached to the glass surface for analysis. The analysis showed a significant increase in fluorescence (Figure 18A) which co-localized (Figure 18C) to the MB coated polystyrene beads utilizing the DIC image (Figure 18B). The linear fluorescent analysis of a particle using FlowView 300 software determined its relative fluorescence and DIC intensity (Figure 19). The DIC intensity of this sample correlate to the DIC intensity of the previous two samples. The fluorescent intensity of this sample (MB, non-FRET, linear confirmation) was significantly higher than the previous sample with the avidin coated beads with the MB attached (FRET, Stem-loop confirmation).

The analysis of the MB attached to the non-fluorescent avidin coated polystyrene beads bound to a glass surface via BSA-biotin, builds a strong foundation for further experiments replacing the beads with molecular streptavidin, and ultimately the target oligonucleotide with the target protein – telomerase.

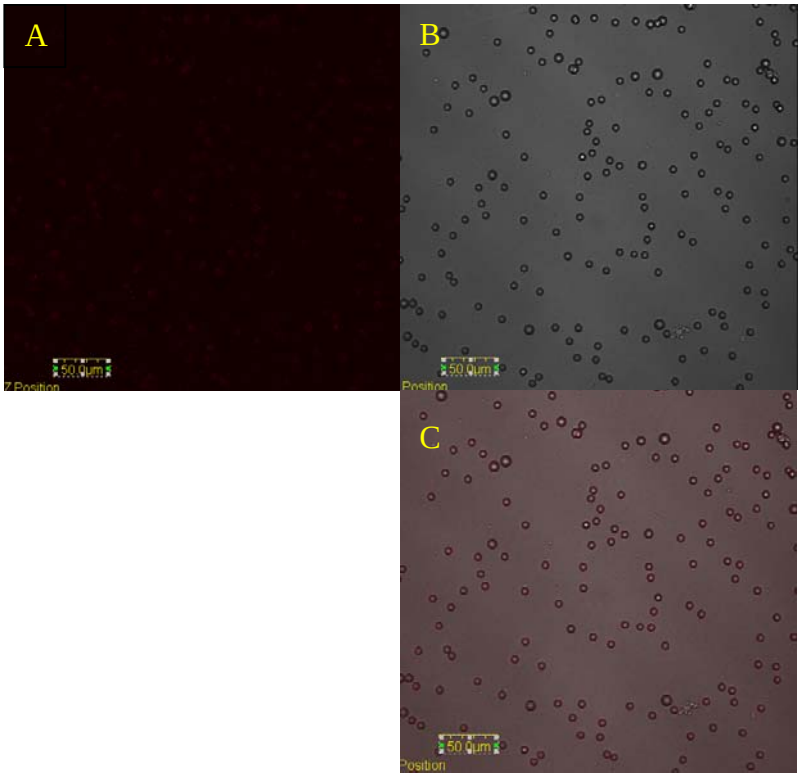

Figure 14. Representative digitized confocal picture of non-fluorescent avidin coated polystyrene beads. (A) Fluorescent channel, (B) DIC channel, (C) Overlay of channels A and B. Magnification is 60x, bead size is 6.7µm.

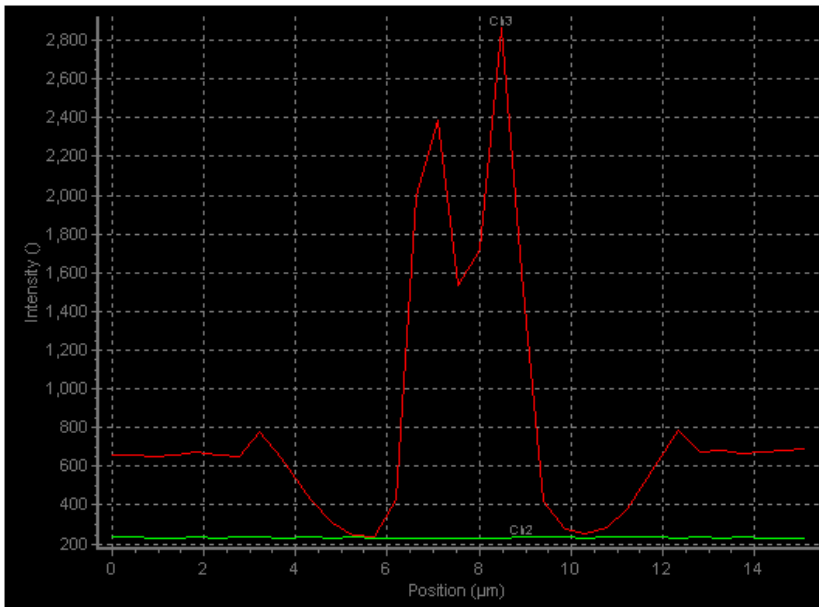

Figure 15. Linear fluorescent analysis of representative non-fluorescent avidin coated polystyrene beads (Figure 14). X axis is position in micrometers and Y axis is measured fluorescence intensity. Green line – relative fluorescent intensity. Red line - relative intensity of the differential interference contrast (DIC) .

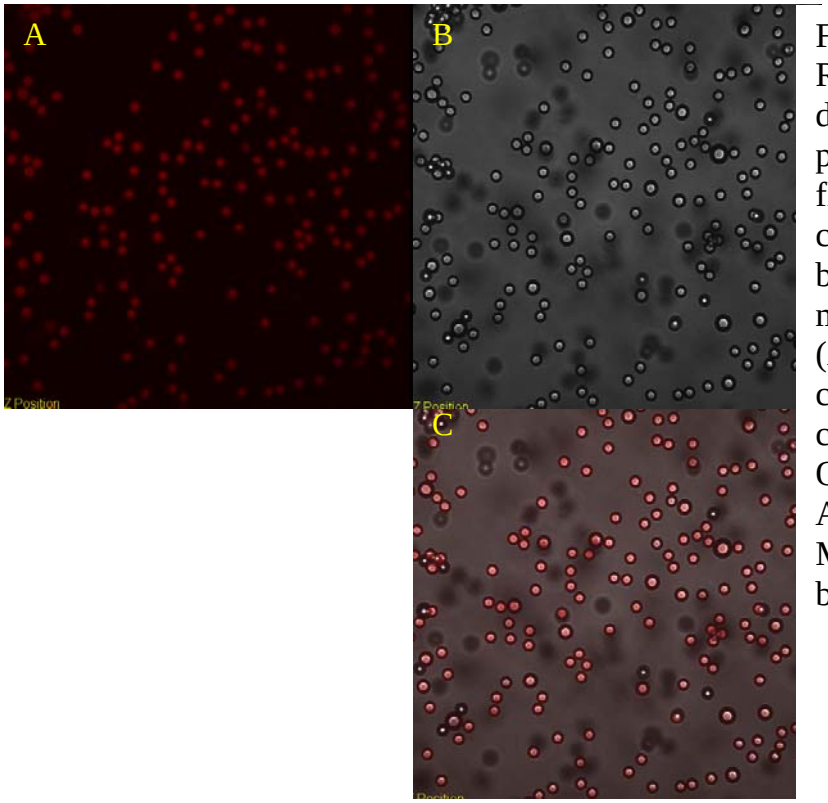

Figure 16. Representative digitized confocal picture of non-fluorescent avidin coated polystyrene beads and attached molecular beacon. (A) Fluorescent channel, (B) DIC channel, (C) Overlay of channels A and B. Magnification is 60x, bead size is 6.7µm.

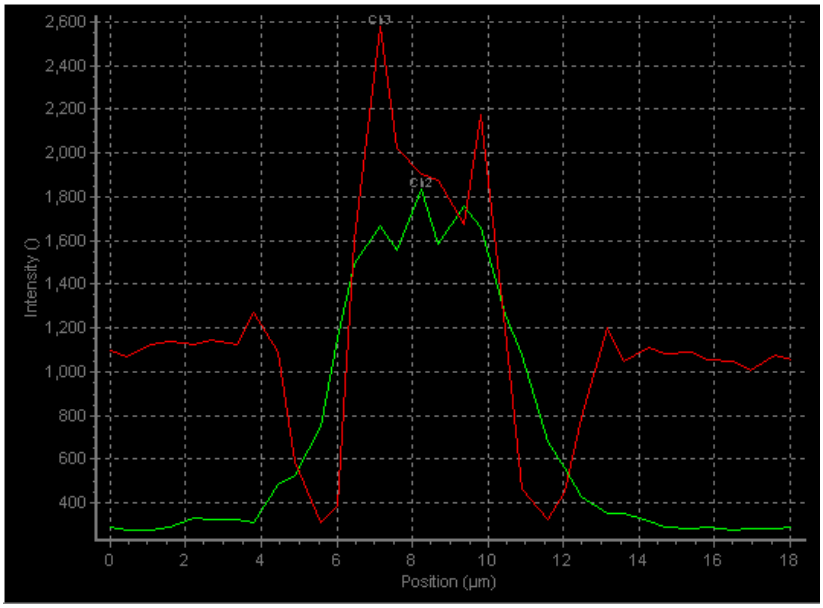

Figure 17. Linear fluorescent analysis of the representative non-fluorescent avidin coated polystyrene beads and attached molecular beacon (Figure 16). X axis is position in micrometers and Y axis is measured fluorescence intensity. Green line – relative fluorescent intensity. Red line - relative intensity of the differential interference contrast

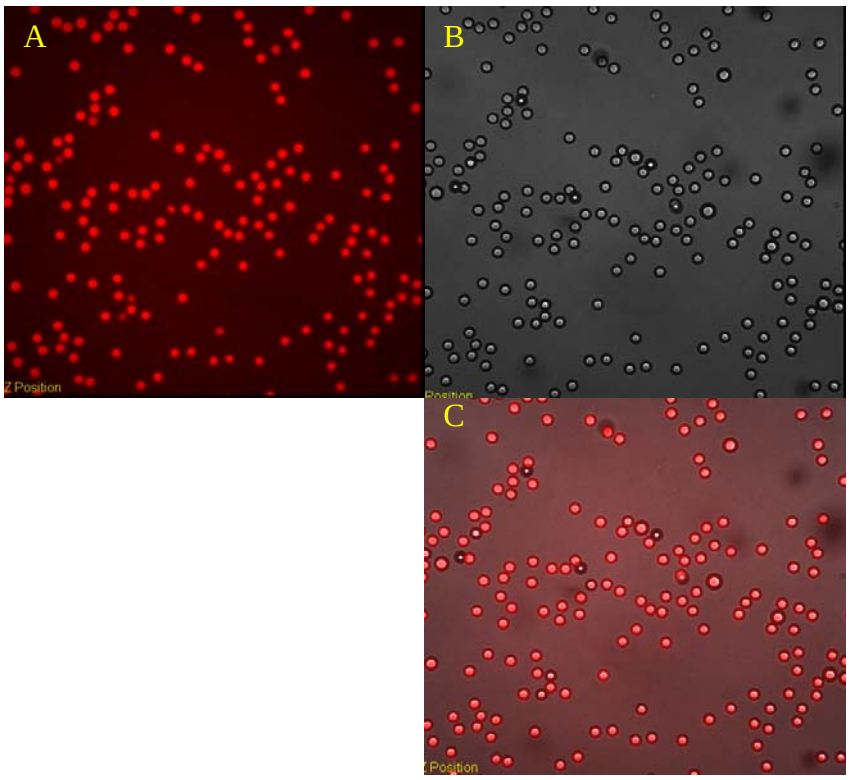

Figure 18. Representative digitized confocal picture of non-fluorescent avidin coated polystyrene beads, attached molecular beacon, and target oligo added. (A) Fluorescent channel, (B) DIC channel, (C) Overlay of channels A and B. Magnification is 60x, bead size is 6.7µm.

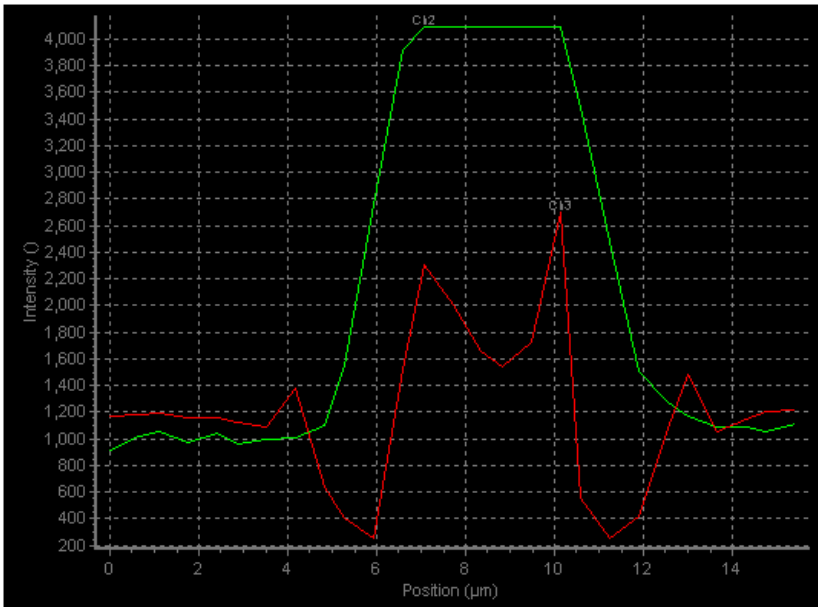

Figure 19. Linear fluorescent analysis of the representative non-fluorescent avidin coated polystyrene beads, attached molecular beacon, and target oligo added (Figure 18). X axis is position in micrometers and Y axis is measured fluorescence intensity. Green line – relative fluorescent intensity. Red line - relative intensity of the differential interference contrast (DIC)

4.3 Molecular Beacon Attachment to Molecular Streptavidin on a Glass Cover

To gain a better understanding of the visual characteristics of the attached MB, its fluorescent characteristics, and success of attachment protocol that were performed in the previous set of experiments, a more in-depth study of the process utilizing molecular streptavidin was needed. The utilization of streptavidin increased the number of MB bound to the surface of the glass while decreasing the likelihood of washing the molecules away during preparation and sample analysis. Data were collected during the entire attachment process when visual and fluorescent characteristics could be evaluated. The attachment of the BSA-biotin by itself is undetectable by confocal microscopy because it had no fluorescent characteristics. To detect the BSA-biotin, fluorescently labeled avidin coated polystyrene beads (0.6μm) were attached as a visual reference only. The conjugated fluorophore was nile red (excitation 550nm, emission 650nm). These fluorescent particles were detected using the same fluorescent channel that was used to detect the MB (Figure 20A). These particles were also detected by the differential interference contrast (DIC) channel of the confocal microscope (Figure 20B). The overlay of the fluorescent image and the DIC image co-localized the fluorescent properties of the particles with the particles themselves (Figure 20C).

The next step in the attachment protocol was the addition of the streptavidin to the BSA-biotin coated surface. This sample showed that the streptavidin has no fluorescent characteristics within the wavelengths that were being examined (Figure 21A) and no detectable DIC image (Figure 21B).

Following this step, the modified MB was incubated with the streptavidin coated glass cover. This sample showed background fluorescence attributable to incomplete FRET of the fluorophore by the quencher (Figure 22A). The linear fluorescent analysis of a particle using FlowView 300 software determined its relative fluorescence and DIC intensity (Figure 23). The fluorescent color observed in the figures does not represent the actual emission by the specimen. The color utilized in the confocal pictures is superimposed by the FlowView 300 software and can be changed to any color.

The attachment protocol was completed at this point, but the analysis of the MB in the linear conformation still needed to be examined. The target solution was added to the MB-streptavidin bridge attached to the glass surface for analysis. The analysis showed a significant increase in fluorescence intensity (Figure 24A). The linear fluorescent analysis of a particle using FlowView 300 software determined its relative fluorescence and DIC intensity (Figure 25). The fluorescent intensity of this sample (MB, non-FRET, linear conformation) was

significantly higher than the previous sample with the molecular streptavidin with the MB attached (FRET, Stem-loop conformation).

During the analysis of these samples it was noted that photobleaching was taking place when the laser was continually focused on smaller fields of view for closer analysis (Figure 26). This photo bleaching further confirms the presence of a fluorophore and that fluorophore was attached to the surface of the glass.

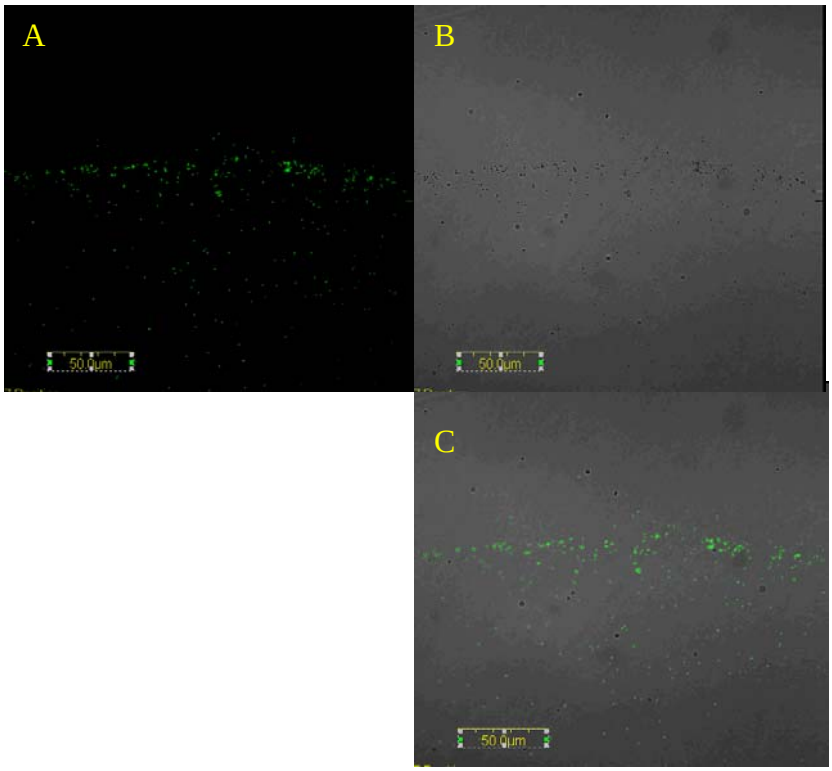

Figure 20. Representative digitized microscopy image of BSA-Biotin bound to the glass surface. Fluorescent avidin coated polystyrene beads were used as a visual reference. (A) Fluorescent channel, (B) DIC channel, (C) Overlay of channels A and B. Magnification 60x, bead size 0.6µm

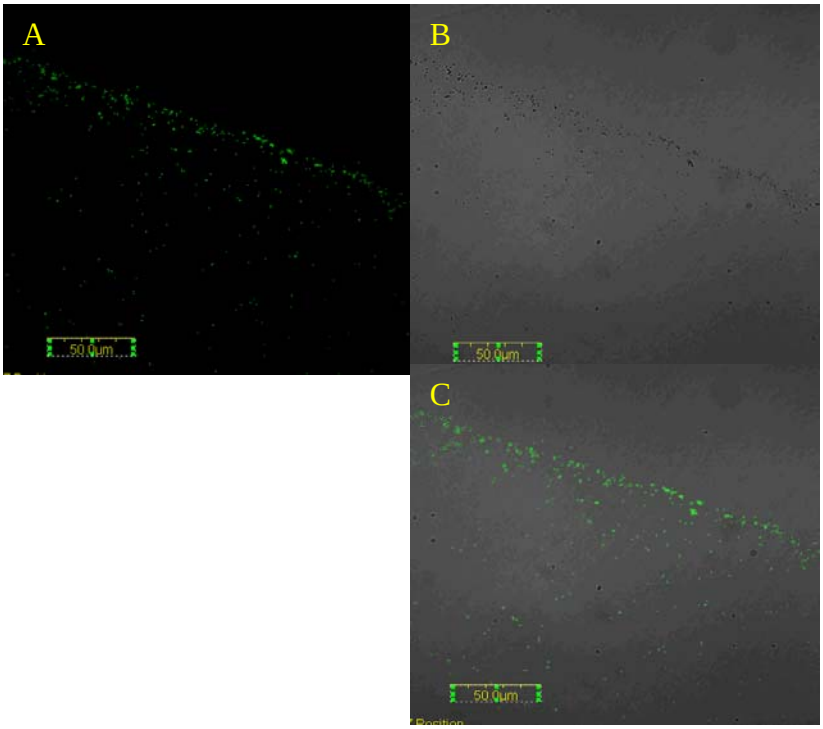

Figure 21. Representative digitized micrograph image of molecular streptavidin bound to the BSA-Biotin modified glass surface. Fluorescent avidin coated polystyrene beads were used as a visual reference. (A) Fluorescent channel, (B) DIC channel, (C) Overlay of channels A and B. Magnification 60x, bead size 0.6µm

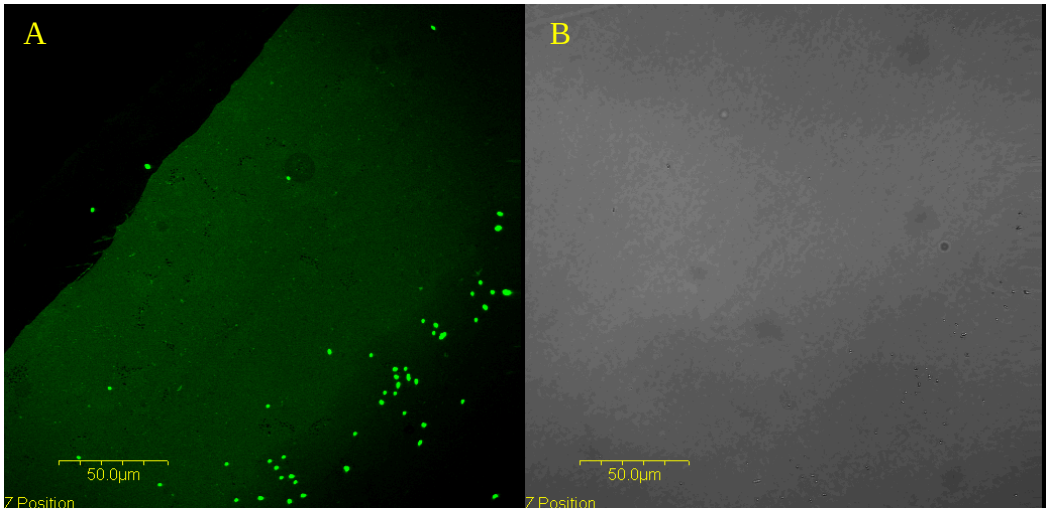

Figure 22. Representative digitized microscopy image of the molecular beacon (FRET) attached to the streptavidin on the glass surface. Fluorescent avidin coated polystyrene beads were used as a visual reference. (A) Fluorescent channel, (B) DIC channel. Magnification 60x, bead size 0.6µm

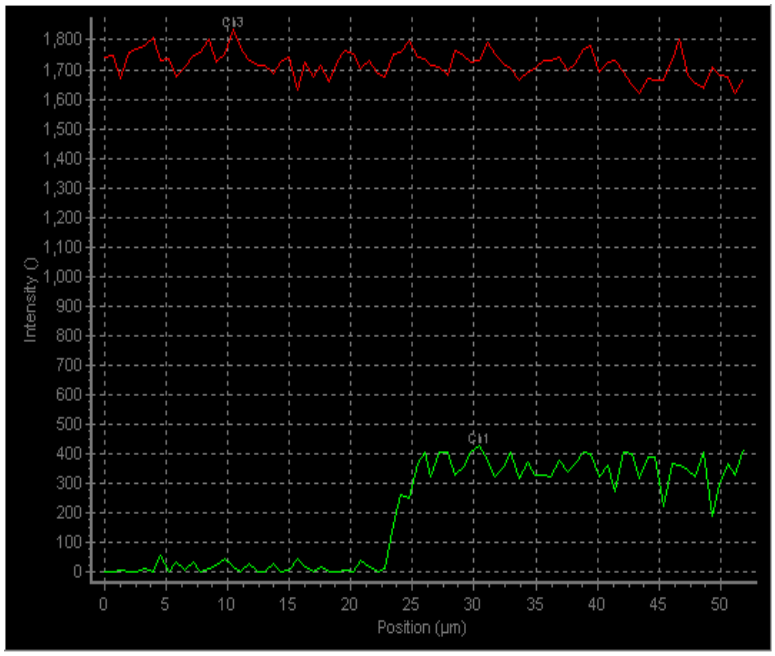

Figure 23. Linear fluorescent analysis of the representative molecular beacon attached to the molecular streptavidin coated onto a glass surface (Figure 22). X axis is position in micrometers and Y axis is measured fluorescence intensity. Green line – relative fluorescent intensity. Red line - relative intensity of the differential interference contrast (DIC).

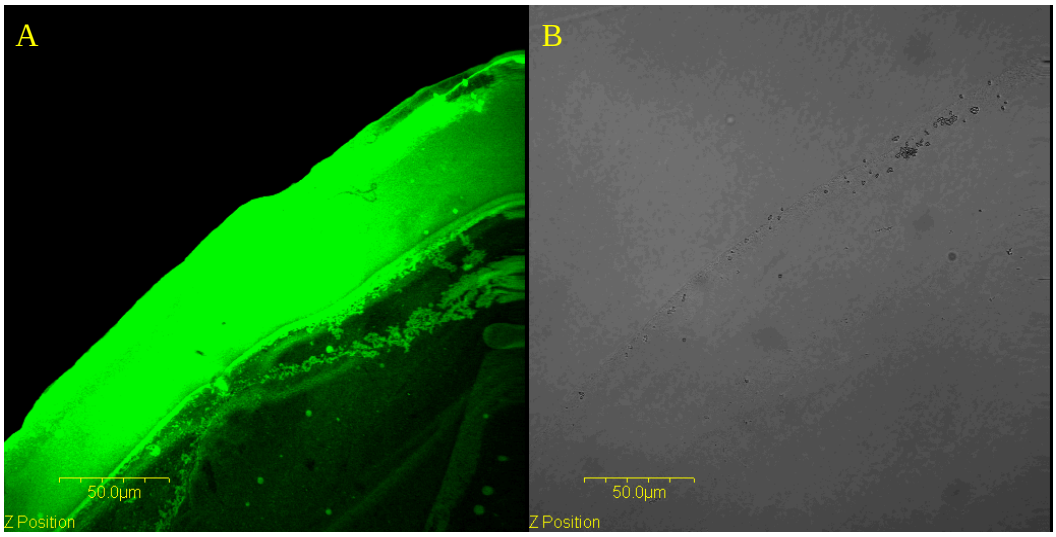

Figure 24. Representative digitized microscopy image of the MB (non-FRET) attached to the streptavidin bound to the glass surface. Fluorescent avidin coated polystyrene beads were used as a visual reference. (A) Fluorescent channel, (B) DIC channel. Magnification 60x, bead size 0.6µm

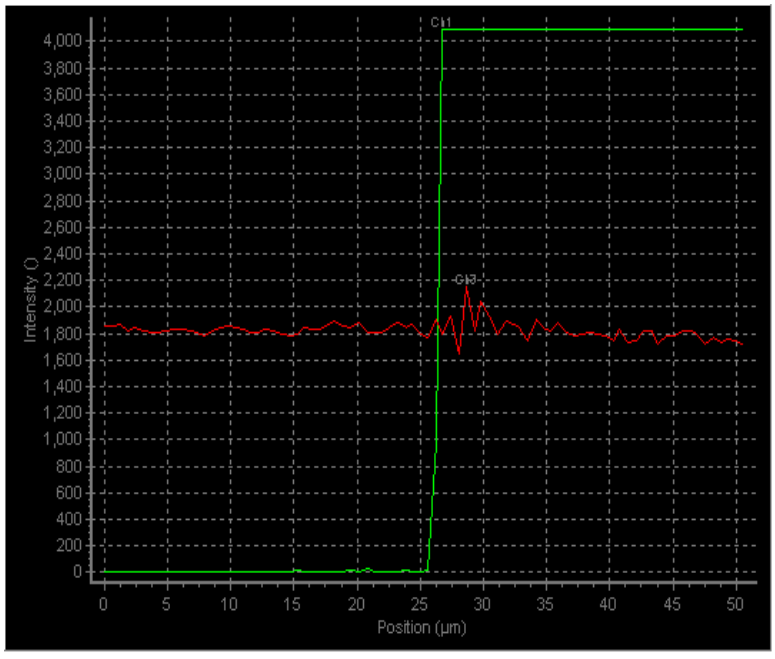

Figure 25. Linear fluorescent analysis of the representative molecular beacon attached to the molecular streptavidin coated on a glass surface (Figure 24). X axis is position in micrometers and Y axis is measured fluorescences intensity. Green line – relative fluorescent intensity. Red line - relative intensity of the differential interference contrast (DIC)

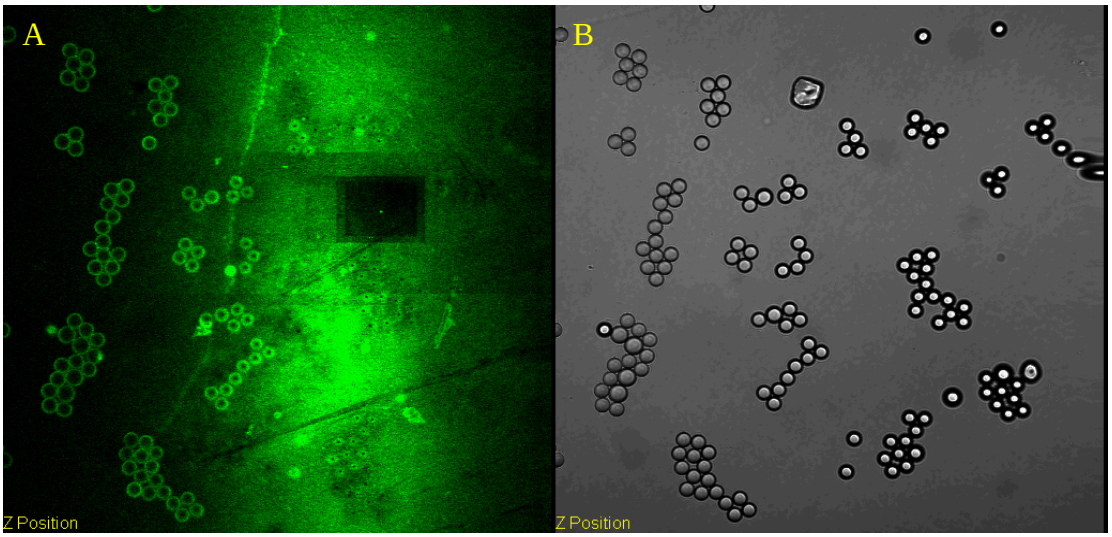

Figure 26. Photobleaching caused by an increased in laser intensity when focused on a consecutively smaller fields of view. (A) Fluorescent channel, (B) DIC channel

4.4 Plasmid Extraction and Transcription/ Translation Preparation

Plasmids were purified and extracted as discussed earlier (Reference section 3.1) and were analyzed using a NanoDrop® ND-1000 UV-Vis spectrophotometer to determine DNA purity and concentration (Table 1). Pure DNA has a 260/280 ratio of 1.8. The plasmids were run on a 1.2% agarose gel to determine proper extraction. Lane A of the gel contained the 1Kb DNA ladder which allowed for estimated measurements of each samples size in base pairs (Figure 27A). Lane B contained the pGRN83 (hTR) plasmid cut with Bstx 1 single restriction site linearizing the plasmid (Figure 27B, 3558 bp). Lane C contained the uncut pGRN83 (Figure 27C). The uncut plasmid was nicked and therefore migrated at a slower rate due the topology of the plasmid. If the plasmid was still in the cccDNA (covalently closed, circular DNA) configuration it would migrate at a faster rate than the digested plasmid (55). Lane D contained pcDNA 3.1/His C (hTERT) plasmid cut with EcoR I which has two restriction sites which produced two linear fragments (Figure 27D, 4065 bp and 5500 bp respectively). Lane E contained uncut pcDNA 3.1/His C. There are two significant bands in this lane. The first and most intense band which is above the 1kb ladder is the plasmid but the plasmid is in a nicked state. The topography of the plasmid slows the migration through the gel. The second band which is significantly less intense and is located about 9.5 Kb in relation to the 1kb ladder is the cccDNA

(covalently closed, circular DNA) form of this plasmid. The topography of this plasmid allows it to move slightly faster then the same size plasmid in the linear state (55).

Plasmids	Concentration	Purity
pGRN83	0.5511µg/µL	2.1
pcDNA 3.1/His C	0.6604 µg/µL	2.1

Table 1. Plasmid concentration and purity

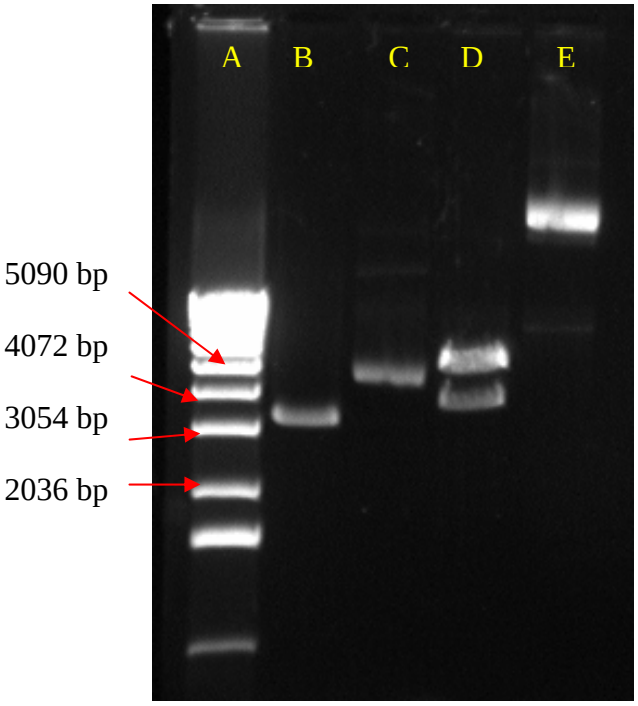

Figure 27. Gel electrophoresis results for Plasmid DNA extraction and restriction digests. (A) 1kb ladder, (B) Linear pGRN83 (3558bp), (C) Uncut pGRN83, (D) Linear pcDNA 3.1/ his C (4065bp and 5500bp respectively), (E) Uncut pcDNA 3.1/ his C which is present in two different topographic variations. 1.2% agarose gel run at 100v for 90 minutes. Picture generated by Eagle Eye® II

4.5 Telomerase Sample Analysis Using the TRAPeze Kit

The TRAPeze analysis is currently the molecular standard for analyzing telomerase activity. The results obtained from this analysis were used to compare with the MB assay results. The TRAPeze assay provides critical data which correlates to telomerase activity, and indirectly correlates to telomerase molecules. More telomerase activity in a sample is indicated by the number of bands produced, the intensity of those bands, and conversely to the reduction in signal intensity of the internal standard.

The digitized image of the dried gel is representative of the telomerase activity for the samples tested and reflected Dr. Gollahon's results from 1995 (Figure 28). Lane A is a negative control utilizing CHAPS lysis buffer. Lane B is a negative control utilizing DEPC treated water (diethyl pyrocarbonate). DEPC treated water is RNA, DNA, and protein free (PCR grade). Lane C is 2µL of protein extract from HME 32 (273) cell line (#104). Lane D is 2µL of protein extract from HME 31 E6/E7 cell line (56). Lane E is 2µL of protein extract from EC-2 32°C cell line (149). Lane F is 2µL of protein extract from HME 50 cell line (86). Lane G is 2µL of protein extract from HME 50-8 cell line (96). Lane H is 2µL of protein extract from HME 31 cell line (103). Lane I is 2µL of 1mM RRL. Lane J is 2µL of reconstituted telomerase. Lane K is 1µL of reconstituted telomerase. Lane L is 2µL of hTERT. Lane M is 2µL of hTR. Lane N is 2µL of

co-transcribed and translated telomerase. Lane O is 1µL of co-transcribed and translated telomerase. Lane P is the positive control (TSR8) included in the TRAPeze kit.

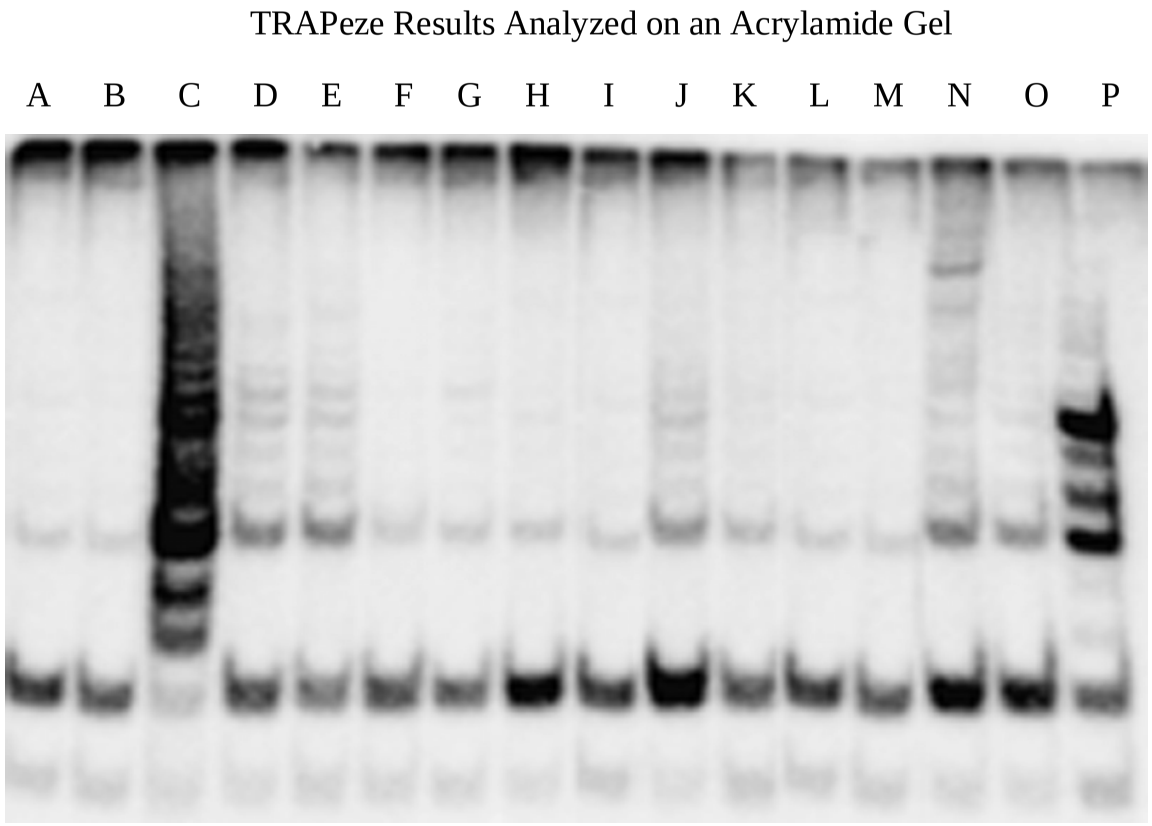

Figure 28. TRAPeze Results Analyzed on an Acrylamide Gel
Controls: (A) Negative control (Chaps lyses buffer), (B) Negative control (DECP treated water); telomerase positive samples: (C) Sample 104, (D) Sample 81, (E) Sample 149; telomerase negative samples: (F) Sample 86, (G) Sample 96, (I) Sample 103; TnT samples: (J) Reconstituted Telomerase (2µLs), (K) Reconstituted Telomerase (1µL), (L) hTERT translation, (M) hTR transcript, (N) Co transcription and translation telomerase (2µLs), (O) Co transcription and translation telomerase (1µLs), (P) Positive control (TSR8). The gel ran at 300v for two hours.

4.6 Molecular Beacon Bench-Top Assay Analysis of Reconstituted and Co-Transcribed and Translated Telomerase

The telomerase products produced by co-transcription/ translation reactions and the separate transcription and translation along with the individual components (hTERT, hTR) were tested with the MB bench-top assay. These samples provided several control components which were critical for further assay development and testing. Samples utilized were as follows: Solution, Blank, 4e10 oligos/µL, reconstituted telomerase (RC, separate transcription and translation), co-transcription and translation (Co), hTERT, hTR (See Reconstitution of Telomerase and Sample Preparation in Materials and Methods section), and 51mM RRL. The results are graphically presented in Figure 29. The hTR sample shows no increase in fluorescence compared to the blank. The hTERT sample had a strong increase in fluorescence as compared to the blank. The hTERT sample closely resembled the fluorescence in the 51mM RRL sample. The 51mM RRL sample had the highest fluorescence increase. The reconstituted telomerase and the co-transcribed samples both have very similar fluorescence, but the co-transcribed telomerase sample showed a slightly higher increase in fluorescence.

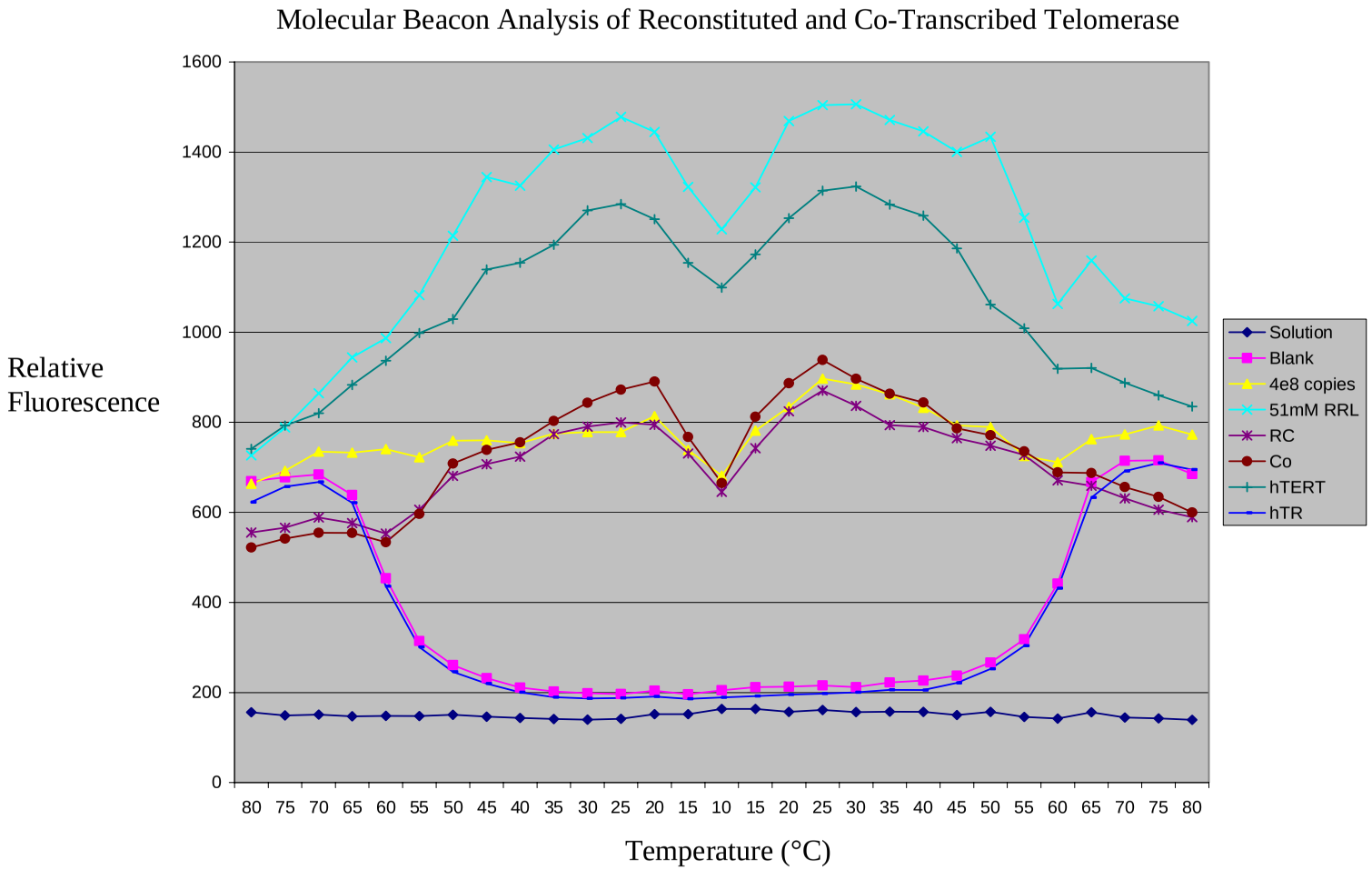

Figure 29. Molecular Beacon Analysis of Reconstituted and Co-Transcribed Telomerase.
The co-transcribed (Co) sample and the reconstituted (RC) sample demonstrated the same relative fluorescent intensity. The 51mM RRL sample and the hTERT sample also demonstrated very similar relative fluorescent intensities. The RRL and hTERT samples were significantly more intense than the two telomerase samples (Co and RC). The hTR sample had no increase in fluorescent intensity compared to the blank sample which is the base line MB signal.

4.7 Molecular Beacon Bench-Top Assay Analysis of Cell Protein Extracts for Telomerase

4.71 Assay Development

The development of this novel assay for molecular capture of telomerase went through several key steps: (1) fluorescently determining telomerase binding to the MB, (2) optimizing binding, and (3) minimizing background. These characteristics were explored through chemical variations to the assay components. These experiments were shortened to reduce overall run time. The temperature range reduction (to 80°C - 10°C - 30°C), insured that all critical experimental data was recorded because this temperature range showed all three thermodynamic states of the MB.

The initial experiment that included both a telomerase positive cell line and a telomerase negative cell line was the basis for assay refinement. Assay components for this experiment were as follows: 1.5mM $MgCl_2$, 20mM Tris-HCl pH 7.6, 63mM KCl, 125mM Rox, 29.4µM BSA, and 200nM MB. This experiment utilized cell protein extracts 144 and 100 (Reference section 3.16). When these samples were tested alone there was no increase in fluorescence in either sample, but when 51mM RRL was added to the samples *both* samples showed increased fluorescence. The 144 sample had a significantly higher fluorescence reading than the 100 sample, but the RRL background was higher

than the 100 sample and similar to the 144 sample (Figure 30). To validated the results, the background created by the addition of 51mM RRL needed to be decreased to a baseline level and more protein extracts needed to be tested.

The next set of experiments included a change in the assay components and the addition of two more protein extracts. The change in the assay components was the removal of the ultra pure BSA. The two new protein extracts were 147 (telomerase positive) and 103 (telomerase negative). The concentration of RRL remained 51mM. The relative fluorescence for the two telomerase positive cell lines were higher than the telomerase negative cell lines, but the high background created from the 51mM RRL did not yeild credible results for the fluorescent data observed (Figure 31).

The next experiment would directly address the background created by the RRL. Dilution experiments were performed with the RRL. The first experiment, RRL dilutions ranged from 65mM – 10mM (assay pH 7.6, Reference Appendix C). In the second dilution experiment, concentrations ranged form 5mM – 0.05mM (assay pH 8.3). The RRL dilutions of 5mM – 0.75mM were tested alone and in the presence of the telomerase positive protein extract 144. The only change to the assay components consisted of increasing the Tris-HCl pH from pH 7.6 to pH 8.3. The 5mM RRL sample showed an increase in fluorescence, but the sample with the 5mM RRL and 144 showed a greater increase in fluorescence.

The 1mM RRL sample showed no increase in fluorescence (equivalent to the blank), but again the 144 sample with 1mM RRL shows a significant increase in relative fluorescence. The sample with 144 and 0.75mM RRL showed increase in relative fluorescence, but the 0.75mM RRL also showed a marked increase in fluorescence (equivalent to the blank). Both the 1mM RRL and 0.75mM RRL showed no relative change in fluorescence but the 1mM RRL with the protein extract had a greater signal to noise ratio. Based on these results the 1mM RRL concentration was selected for continued assay development (Figure 32).

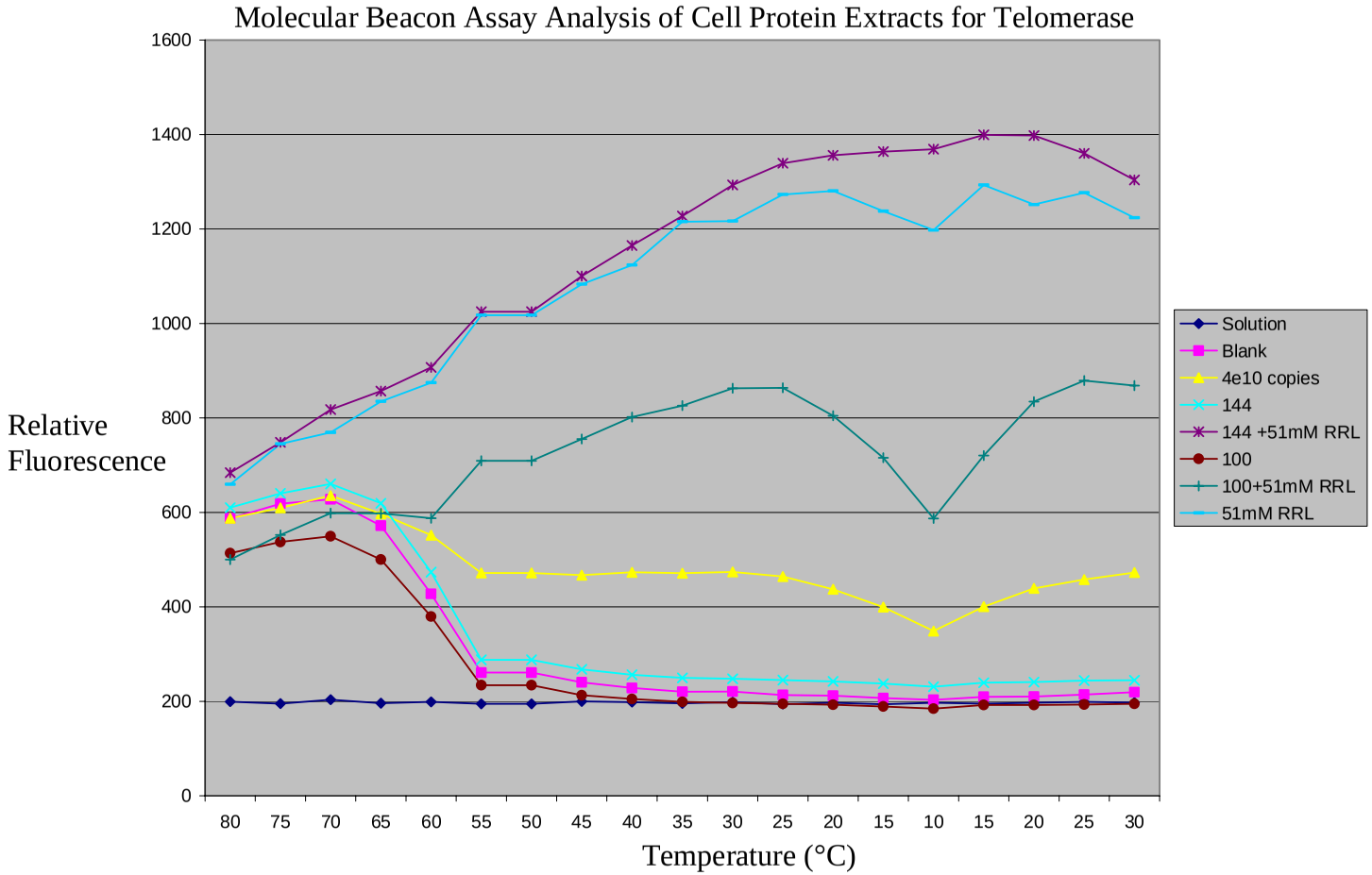

Figure 30. Molecular Beacon Assay Analysis of Cell Protein Extracts for Telomerase
The solution sample showed the background readings for FAM by the ABI prism. The blank solution shows the molecular beacon's natural thermodynamic stability through the temperature range. The 4e10 oligo copies/µL showed the molecular beacon's thermodynamic nature through the temperature range in the presence of target entity. The experimental samples showed an increased fluorescence beginning with the telomerase negative sample (100 + 51mM RRL) progressing to the 51mM RRL sample and then the highest fluorescent signal is the telomerase positive sample (144 + 51mM RRL).

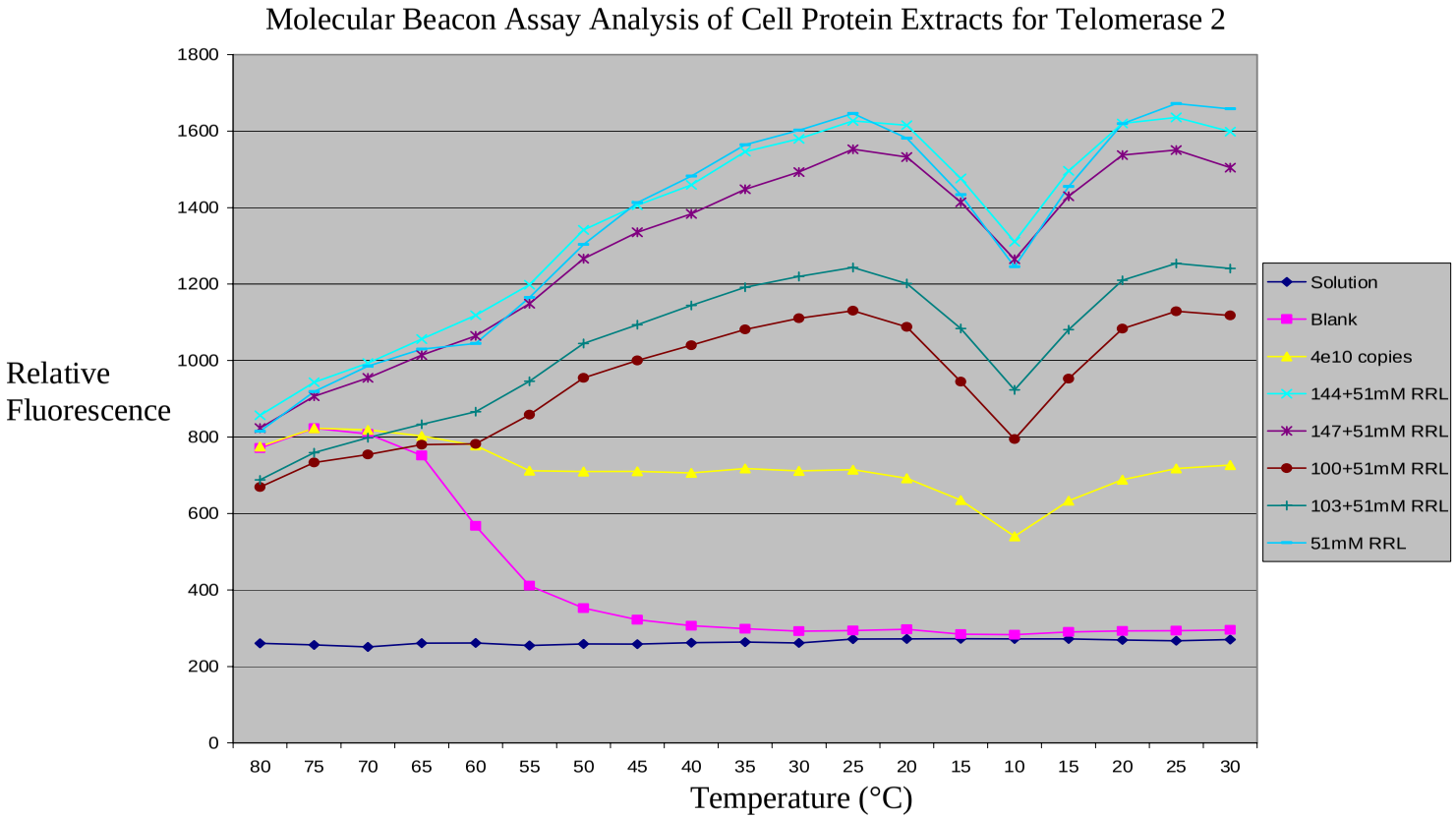

Figure 31. Molecular Beacon Assay Analysis of Cell Protein Extracts for Telomerase 2
The solution sample represented the background readings for FAM by the ABI prism. The blank solution represented the molecular beacon's natural thermodynamic stability through the temperature range. The 4e10 oligo copies/µL showed the molecular beacon's thermodynamic nature through the temperature range in the presence of target entity. The experimental samples demonstrated an increase in fluorescence beginning with the telomerase negative samples (100 + 51mM RRL, 103 + 51mM RRL) progressing to the 51mM RRL sample and the telomerase positive samples (147 + 51mM RRL, 144 + 51mM RRL).

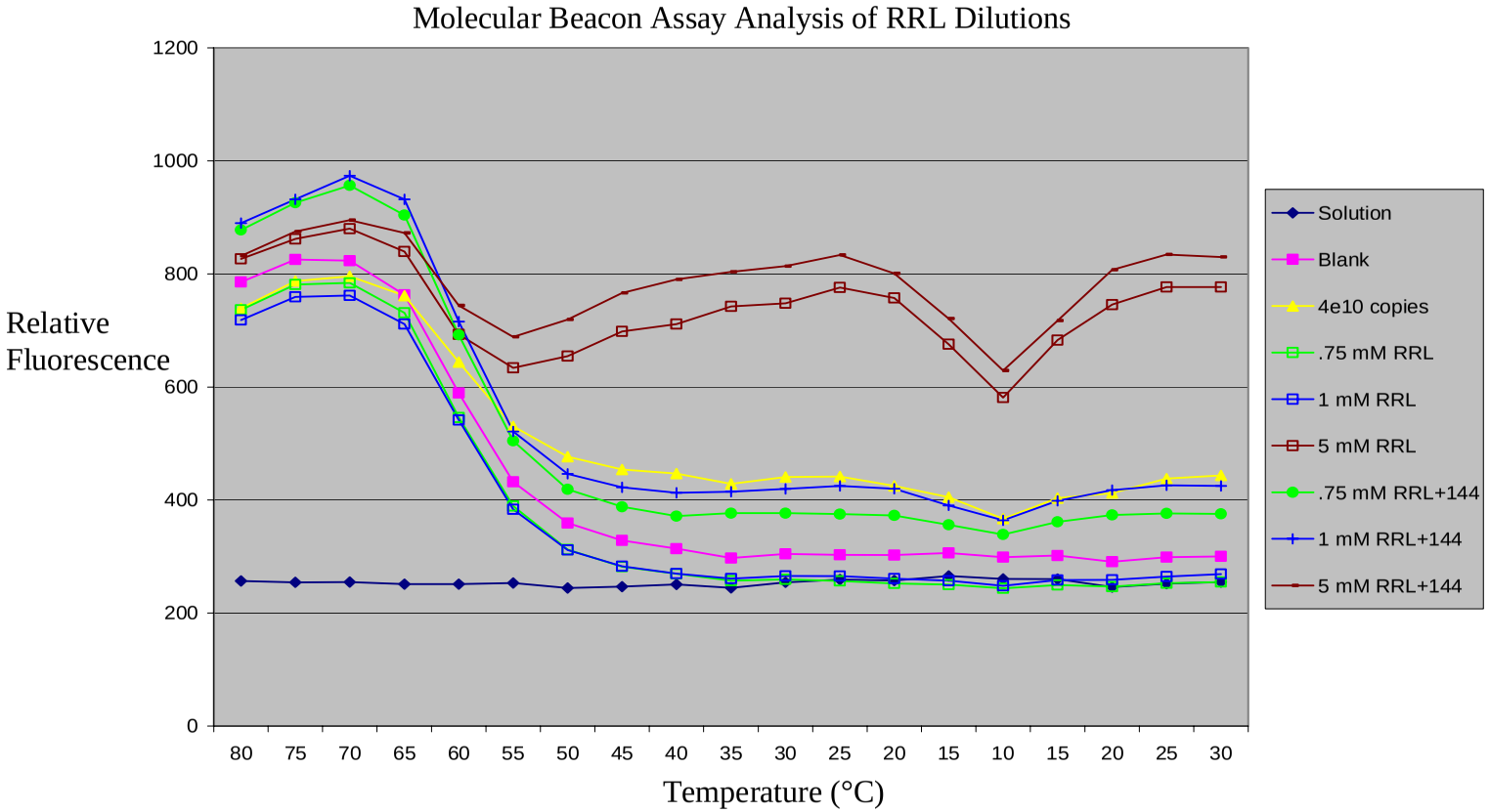

Figure 32. Molecular Beacon Assay Analysis of RRL Dilutions.
The solution sample represented the background readings for FAM by the ABI prism. The blank solution represented the molecular beacon's natural thermodynamic stability through the temperature range. The 4e10 oligo copies/µL represented the molecular beacon's thermodynamic nature through the temperature range in the presence of target entity. The experimental samples 1mM RRL and 0.75mM RRL showed no increase in fluorescence. The 5mM RRL show increased fluorescence, but the sample with the telomerase positive protein extract (144 + 5mM RRL) shows a greater increase in fluorescence. The 144 + 0.75mM RRL showed an increase in fluorescence well above the 0.75mM RRL, but the 144 + 1mM RRL demonstrated the greatest increase in fluorescence since both RRL only samples were compared to the solution alone and below the blank.

4.72 Molecular Beacon Bench-Top Assay Analysis of Cell Protein Extracts for Telomerase

The final assay compilation was used to access its efficacy on total cell extracts. To that end, three telomerase positive cell protein extracts and three telomerase negative cell protein extracts were analyzed. This experiment was run in triplicate to determine assay reproducibility. The error bars indicate the standard deviation between the three runs. The samples utilized in these experiments include: solution, blank, target oligo 4e8 copies/µL, 1mM RRL, telomerase positive cell protein extracts 104, 81, 149 and telomerase negative extracts 103, 86, and 96. The data from the above samples was represented by six representative data lines. The solution sample showed the baseline reading of the FAM fluorophore by the ABI Prism 7000. The Blank sample showed that the master mix was not contaminated as well as the baseline reading for the MB in the stem loop confirmation at lower temperatures. The 4e8 oligos/µL sample showed that the MB behaved throughout the experiment as predicted from the literature. The 1mM RRL sample showed the protein binding background. This concentration was added to all protein extract samples. The bottom portion of the graph also encompassed all the data collected from the telomerase negative cell protein extracts (103, 86, 96) and the 1mM RRL. This portion of the graph was represented by the 1mM RRL data set. The 104 + 1mM RRL data showed the

highest increase in fluorescence. The 81 + 1mM RRL and the 149 + 1mM RRL had very similar relative fluorescence and was represented by 149 + 1mM RRL (Figure 33). The graph illustrating total run results is figure 35. The overview data and the complete date set have been further manipulated so that the graphical representation would better reflect the thermodynamic states and their correlation to relative fluorescence. The blank solution in the revised graphs (Figure 34 and 36) were used to subtract baseline fluorescence of the MB during the temperature range. Therefore, the graph lines represented the fluorescence differential from the blank sample for each sample tested.

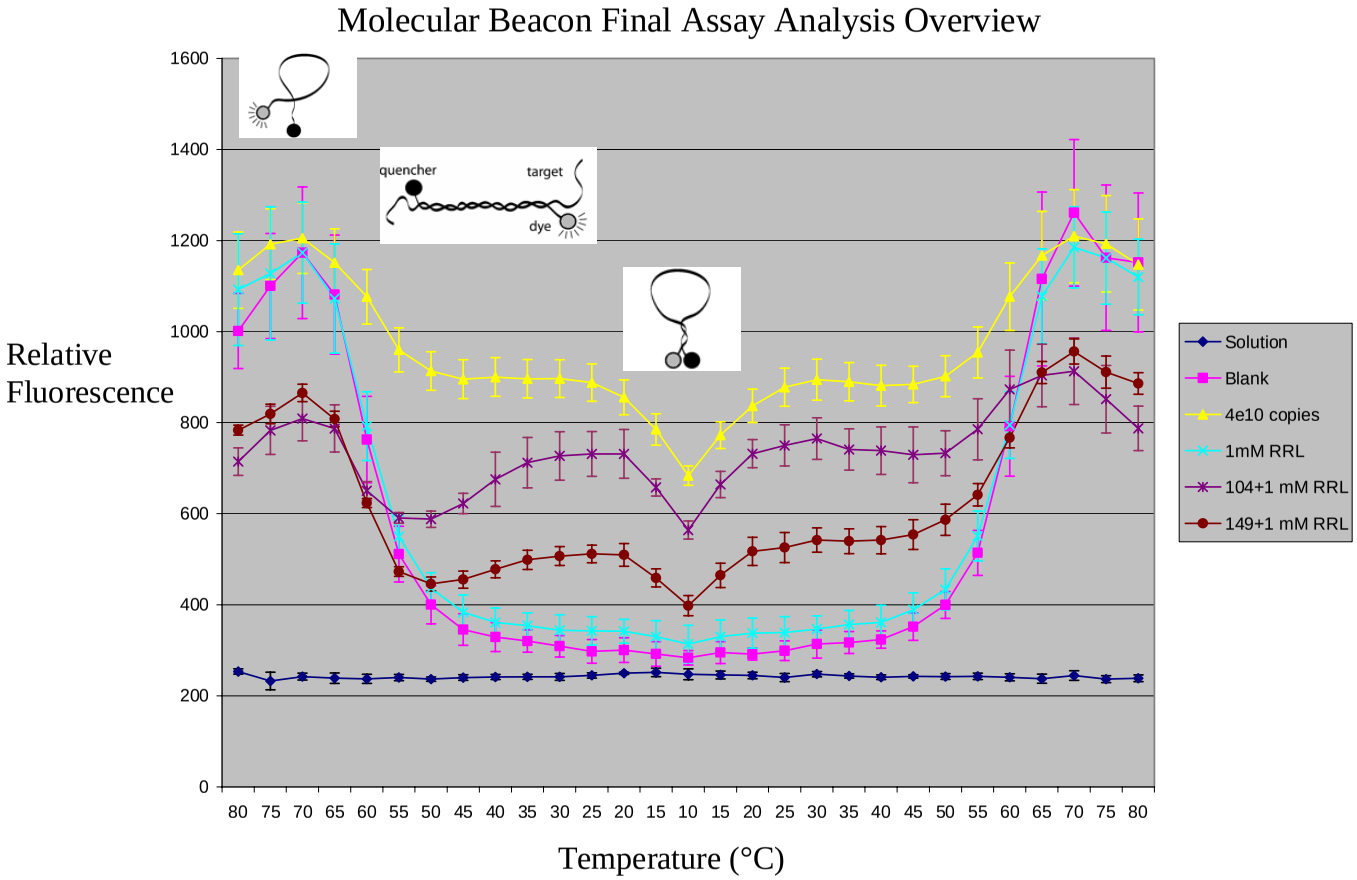

Figure 33. Molecular Beacon Final Assay Analysis Overview
The inserted picture above each portion of the fluorescent curve indicates the MB's thermodynamic state through that temperature range. The three samples of most interest are the two telomerase positive lines and the 1mM RRL. The 104 + 1mM RRL had the greatest fluorescent signal. The 149 + 1mM RRL represents 149 and 81. The third line of interest is the telomerase negative cell line sample which is represented by 1mM RRL.

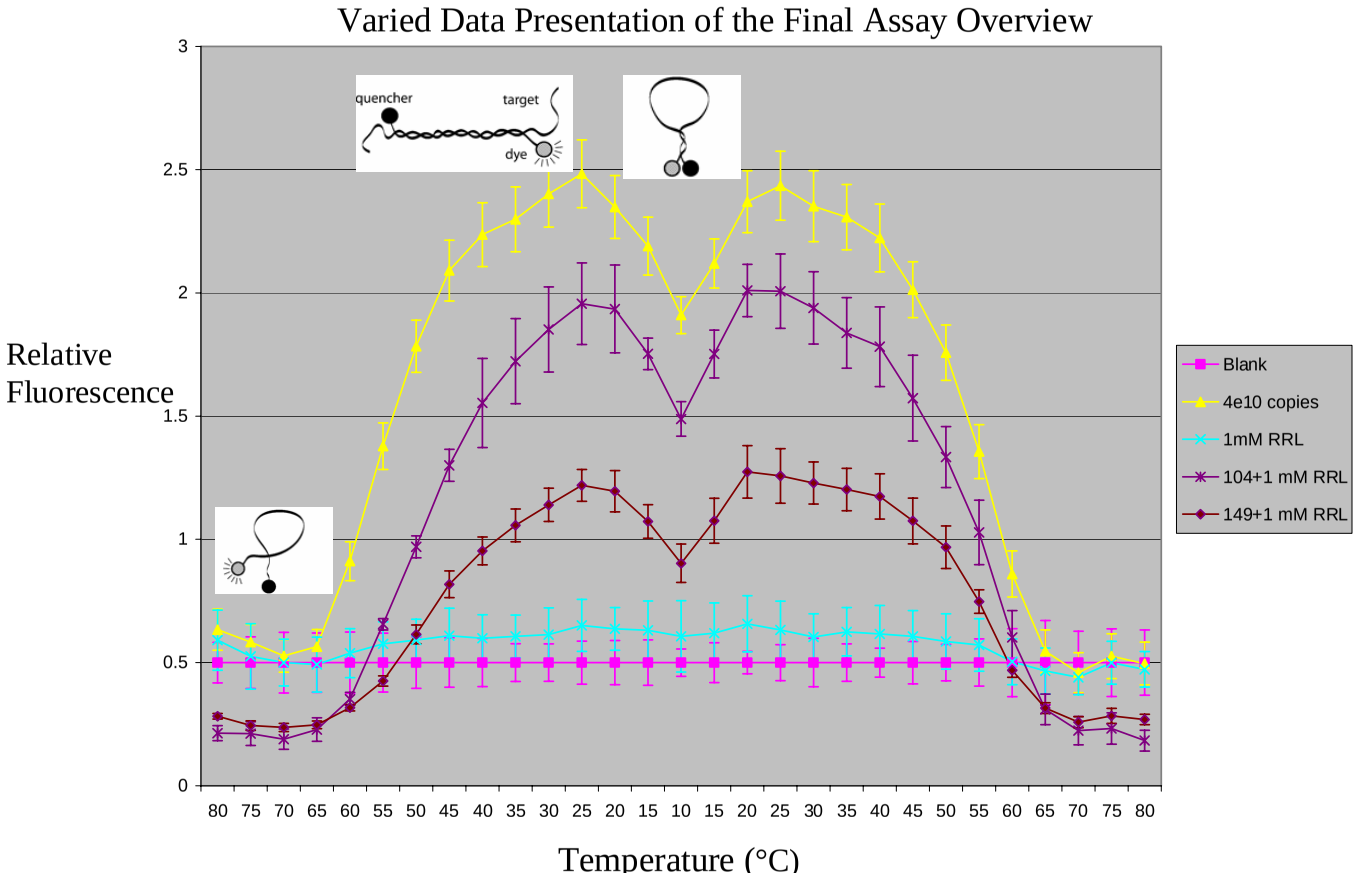

Figure 34. Varied Data Presentation of the Final Assay Overview. The figure above each portion of the fluorescent curve indicates the MB's thermodynamic state through that temperature range. This data represents relative fluorescence compared to the blank. The three sample lines of most interest are the two telomerase positive lines and the 1mMRRL. The 104 + 1mM RRL showed the greatest fluorescent signal. The 149 + 1mM RRL represents 149 and 81. The third line of interest is the telomerase negative cell line sample which is represented by 1mM RRL.

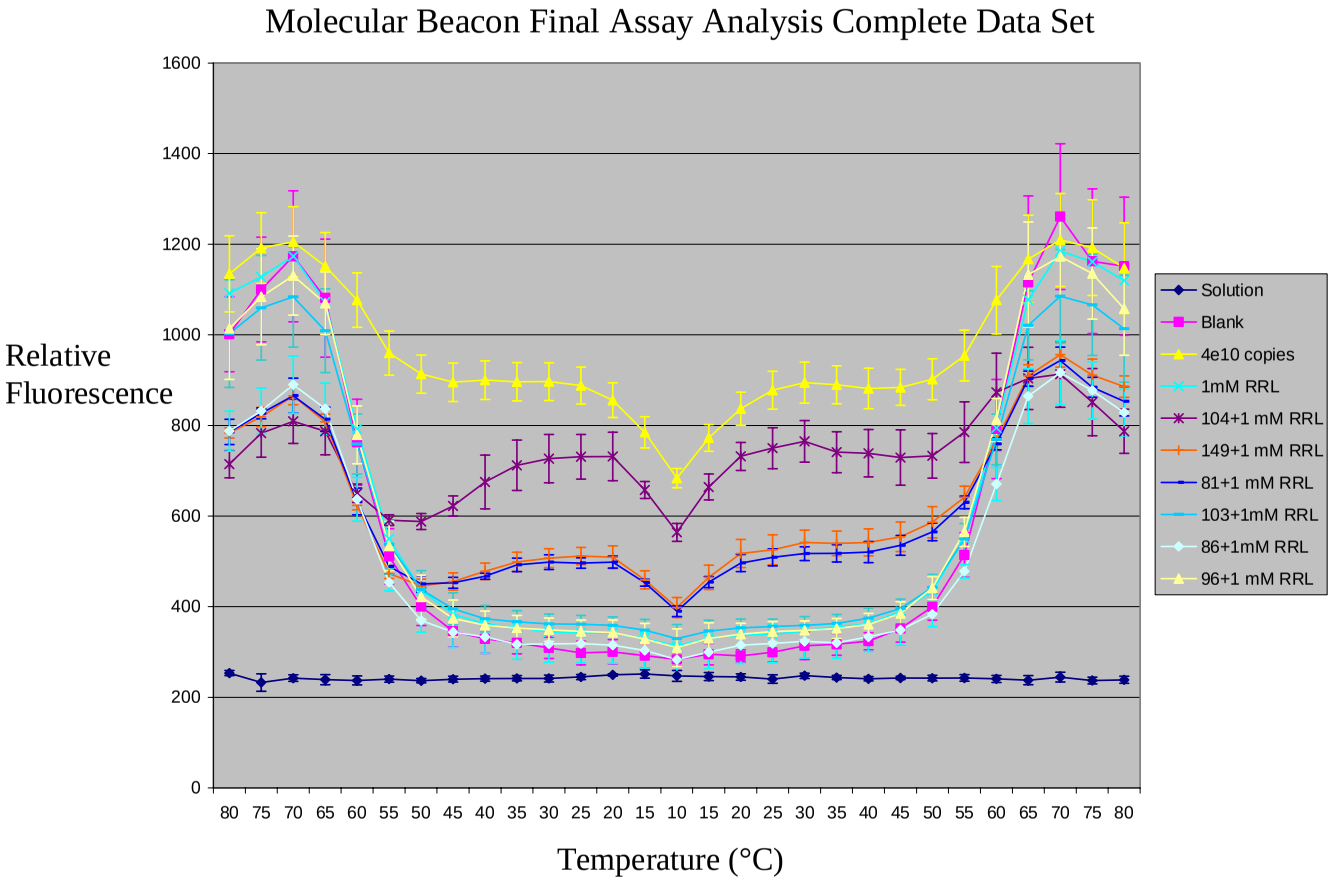

Figure 35. Molecular Beacon Final Assay Analysis Complete Data Set
This figure includes all cell extracts analyzed by this novel assay. The data showed the reproducibility of each sample when run in triplicate. Standard deviation is included. The telomerase positive samples (104, 81, 149) all have elevated fluorescence. The fluorescent intensity of the assay distinguishes between different telomerase positive cell lines. The telomerase negative samples (103, 86, 96), RRL, and blank have no significant fluorescence above background.

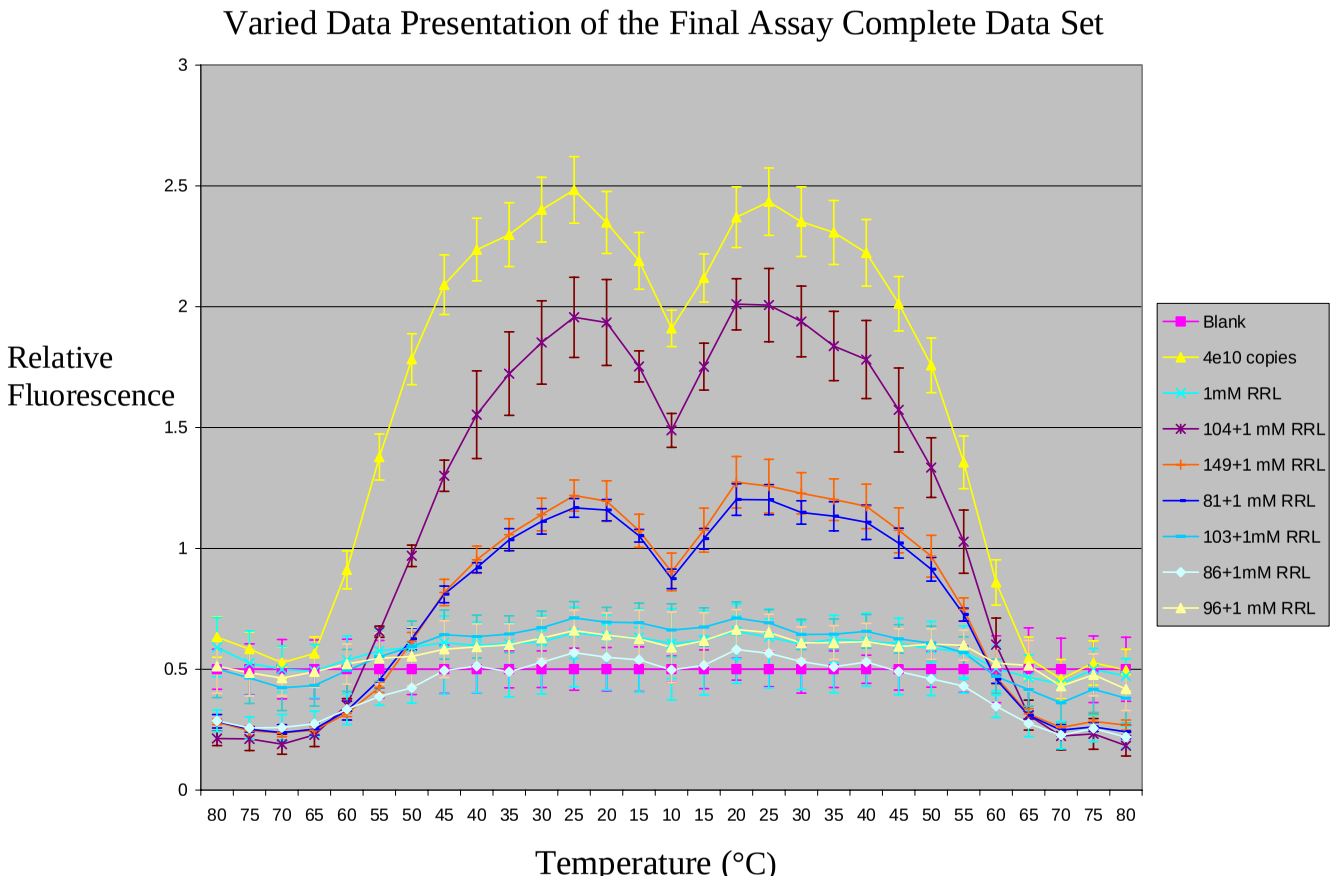

Figure 36. Varied Data Presentation of the Final Assay Complete Data Set
This figure includes all cell extracts analyzed by this novel assay. The data showed the reproducibility of each sample when run in triplicate. This data represents relative fluorescence compared to the blank. The telomerase positive samples (104, 81, 149) all have elevated fluorescence. The fluorescent intensity of the assay distinguishes between different telomerase positive cell lines. The telomerase negative samples (103, 86, 96), RRL, and blank have no significant fluorescence above background.

CHAPTER V

DISCUSSION

5.1 Overview

This is the first known experiment to directly assess the utility of a MB in capturing a targeted DNA binding protein. The successful implementation of this telomerase detection assay and the potential tailored modifications of this assay for other DNA binding proteins could have broad scientific impact. The ability to integrate this assay into a MEMS device with a unique optic detection scheme, would further constitute portability and allow field operations. Moreover, the ability to quantify molecules of telomerase and correlate it with cancer would give this assay high clinical relevance. Further, production of a MEMS device with this capability would give this assay scheme convenient and cost effective clinical significance.

5.2 Fluorescent Characterization of the FAM Labeled Molecular Beacon

Due to the novelty of this assay and its development, there was no "standard" mechanism for assay detection and quantitation. Therefore, the most accurate method of measuring and characterizing the thermodynamic binding behavior was to use a Real-Time PCR machine (Reference section 2.2 and Figure 5). The

characterization of the ABI Prism 7000 as a detection mechanism was perhaps the most valuable part of these experiments. Understanding how to use the software and manipulate components in the assay for reproducible, optimized results proved critical for successful assay development. The fluorescent data collected through the characterization of the MB with the ABI Prism 7000 were important not only for assay optimization, but also to understanding the thermodynamic behavior of the MB. In addition, the effectiveness of the ABI Prism 7000 as an initial detection mechanism could be assessed. However, differences would exist between the results from target oligo and the protein extracts because the DNA-DNA binding chemistry with a MB has been shown to be different than DNA-protein binding chemistry (11,28,29). The critical information extracted from these experiments included the machine characteristics, MB fluorescent characteristics, and data presentation. Ultimately, the assay development was best accomplished with the protein extract from telomerase negative and positive cell lines.

Experimental performance yielded a greater understanding of the MB behavior, which was critical in optimizing a working bench-top assay. The thermodynamic/fluorescent characteristics of the MB produced in these characterization experiments followed examples described in the literature (3,4,27,28,46,49,50). The MB data obtained during these experiments showed

the possible thermodynamic conformations that could occur: random coil, linear, and stem loop with their respective relative fluorescence (Reference section 2.12). The data also showed a direct relationship between target oligo concentrations and relative fluorescent readings (Figures 10-13). These results determined the optimum MB concentration for further assay development.

The data were compiled, analyzed in Microsoft EXCEL and presented so that the experimental results were accurately reflected. This process started out very simply (presenting raw data) and ended up being quite complex (normalizing all data). As the process evolved, the background was normalized between runs. Accomplishing this caused the data to become more revealing. This allowed for more in-depth analyses of the experimental runs.

5.3 Molecular Beacon Attachment

Two separate approaches to MB attachment provided information on several levels. First, familiarization with the attachment protocol and with confocal microscope operation was achieved. Second, these approaches produced comparative fluorescent results that allowed for data extrapolation and predictions for future experiments. The attachment protocol for the non-fluorescent avidin coated polystyrene beads preceded the attachment protocol for molecular streptavidin onto a glass substrate. Procedural and experimental results made this

methodology easily transferable to the glass substrate (Reference section 4.2 and Figures 14-19).

Understanding confocal microscopy theory and optimizing its intrinsic functions to best extract the data, yielded important results that would transfer to all successive experiments utilizing confocal microscopy for sample analysis (Reference section 2.3 and Figure 6).

The results produced by utilizing the confocal microscope for analysis of the non-fluorescent avidin coated beads protocol also carried over to succeeding experiments with molecular streptavidin. These data were important because they showed the most likely manner in which future data should be represented and yielded predictions of MB behavior in subsequent experiments.

The move from avidin coated polystyrene beads (6.7μm) to molecular streptavidin (~5nm) showed significantly different attachment efficiencies and properties. The attachment of the polystyrene beads appeared to be sporadic Figure 18). In contrast, molecular streptavidin showed a more uniform layer of particle coverage (Figure 22). The uniformity of the molecular streptavidin coverage suggested that the limiting factor in the process was the BSA-Biotin binding to the glass surface. By manipulating the BSA-Biotin concentration, binding the molecular streptavidin over a specific area could be accomplished to produce a homogeneous monolayer.

The ability to reproduce an even monolayer of streptavidin will be critical for further development of a functionalized liquid core waveguide (LCWG). The monolayer should produce several key qualities necessary for an optimized assay inside a liquid core waveguide. First, the monolayer will be applied to the entire inner lumen of the glass capillary. This monolayer should significantly reduce interaction or binding between the protein sample and the glass surface. Secondly, it would not limit the functionalization process to the number of molecular streptavidin bound to the surface. Surface modification could be regulated by the concentration of MB incubated. The ability to adjust the number of molecular beacons bound to the inner lumen would permit background fluorescence to increase the signal to noise ratio.

5.4 Plasmid Extraction and Transcription/ Translation Preparation

The extraction data indicated that the DH5α *E.coli* cells were properly transformed and the plasmid extractions were relatively pure. Each plasmid showed the proper fragment size when digested (Figure 27). The sizes of the undigested plasmids were somewhat distorted because of the physical characteristics of the plasmid. The plasmids were in a nicked state, i.e., they appeared much larger then they should when analyzed using electrophoresis.

These nicks in the plasmids were most likely due to mechanical shearing that occurred during the extraction protocol.

5.5 Molecular Beacon Bench-Top Assay Development, Validation and Comparison

The development of this assay passed through several key milestones. First, fluorescent determination of telomerase binding to MB occurred. Second, identifying the proper concentration of RRL was critical for delineating the telomerase positive cell line extracts from the RRL background. Third, testing key components of the assay master mix was critical in optimizing the assay for telomerase detection. Fourth, evaluation and elimination of as many known proteins or RNA molecules that might bind the MB (and show a false positive) was done. Fifth, reproducibility as a bench-top assay was evaluated. The major points of these five milestones are discussed in detail below. For further details please reference Trouble Shooting (Appendix C- F).

The initial experiments to validate the utility of the bench-top assay employed telomerase positive and negative cell protein extracts. The sample cell protein extracts initially results showed no binding to the MB (Appendix D). Plausible explanations were that either telomerase was not binding, or telomerase was binding and did not provide enough energy to separate the stem of the MB. Due

to observations made by multiple sources (3,4,27,28,46,49,50) and the well documented characteristics of telomerase (14,41), the latter explanation was the premise upon which my future experiments were based. The concentration of RRL was calculated based on the master RRL provided (assumed to be 1M) in the Promega PROTEINscripII kit.

The RRL behaved differently alone and when mixed with cell extracts. By itself, RRL showed significant increase in fluorescence (Figure 30-31). The entire loop of the MB was free for binding from any protein present in the RRL solution. Consequently, fluorescent intensity was high. In contrast, in the presence of the protein extracts, a decreased fluorescence was observed. The protein extract samples plus RRL showed different *magnitudes* of fluorescence which correlated with telomerase positive or negative. Not surprisingly, the telomerase positive protein extracts had higher fluorescence values than did the telomerase negative protein extracts. Interestingly, while the RRL concentration continued to show this high fluorescence value, the protein extract data showed a specific, reproducible, hierarchy of signal. This hierarchy from lowest fluorescent signal to highest always followed this order: blank, telomerase negative, oligo, telomerase positive and RRL (Figure 25). The important point in this reproducible hierarchy is the fact that even with the addition of RRL, both the telomerase positive and negative cell extracts demonstrated differences in MB

interactions. However, while interesting and perhaps biologically important, with high RRL background, the results showed no definitive conclusions. The RRL fluorescence (protein binding background) needed to be eliminated while increasing the signal to noise ratio of the telomerase positive cell lines. A serial dilution experiment for RRL concentration was performed to determine a "threshold" level for RRL. This experiment produced the minimum concentration of RRL required for successful telomerase binding without biasing the results. Figure 32 shows that at 1mM RRL, the RRL control protein binding background was negligible (effectively zero). In contrast, the telomerase positive protein extract's signal with 1mM RRL was significantly higher. Although it was not as high as the 51mM RRL, I felt it was valid because at a baseline 1mM, RRL signal was effectively eliminated. After eliminating the RRL protein binding background, the assay components were optimized for telomerase binding and sample differentiation. The initial composition of the assay was based on the TRAPeze kit buffer. The utilization of the TRAPeze buffer showed no results (Reference Appendix E). One of the TRAPeze components was apparently inhibiting binding of all proteins and DNA. After sequential elimination of each component, the inhibiting element was ultimately determined to be EGTA (Appendix F). The final assay was composed of 63mM KCl, 1.5mM $MgCl_2$, 125nM Rox, 20mM Tris-HCl pH 8.3, and 200mM MB.

After determining the optimal assay conditions, the two telomerase components (hTERT and hTR) were eliminated. The reconstituted telomerase and co-transcribed/translated telomerase would no longer be utilized for further comparisons because of the inability to separate them from the high concentration of the RRL needed to produce the telomerase protein *in vitro*. I felt this inability to separate telomerase products from the RRL left no means for valid comparison. At this point, the assay was developed enough to start testing its reproducibility with total protein extracts from cell lines. Experimental replicates showed results varying by +/- 10% at each data point through the MB's non-FRET configuration (Figure 29). No correlation between the standard oligo concentration and the unknown protein concentrations of the telomerase molecules could be made, due to the vastly different binding kinetics for the two species.

The connection between the MB bench-top assay and the TRAPeze analysis was strong however. The telomerase positive cell lines' protein extracts showed telomerase activity in the TRAPeze assay and corresponding fluorescence with the MB bench-top assay. Samples that showed highly intense telomerase activity in the TRAPeze analysis, also showed a correspondingly significant increase in fluorescence when compared to the other telomerase positive protein extracts in the MB bench-top assay. The telomerase negative cell lines' protein extracts showed no telomerase activity in either the TRAPeze assay or their respective

fluorescence in the MB bench-top assay. The two major components conferring telomerase activity, hTERT and hTR, when assayed individually, showed no telomerase activity in either the TRAPeze assay or the MB bench-top assay. Both the reconstituted and co-transcribed/translated telomerase samples showed telomerase activity and showed a fluorescent signal for the MB bench-top assay. However this result was deemed inconclusive due to the high protein binding background of the RRL.

5.6 Interpretation of MB – Telomerase Binding Results

The results from the cell extracts with no RRL were surprising (Appendix). One possibility for lack of MB of fluorescence could be the specific thermodynamic characteristics of the MB. The present MB configuration of 24 bps in the hairpin loop may be too large and the binding of telomerase alone may not be enough to split the stem structure (Figure 35). For the stem structure of the MB to separate the bases contained in the hairpin loop must fully interact with another molecule or molecules that will decrease the free energy of the MB so that the linear configuration becomes stable. The addition of the RRL to the protein cell extracts may provide "helper" proteins (single stranded DNA binding proteins) in the solution so that the combined energy of the telomerase and

"helper" proteins binding the hairpin loop splits the stem and allows fluorescence (Figure 36).

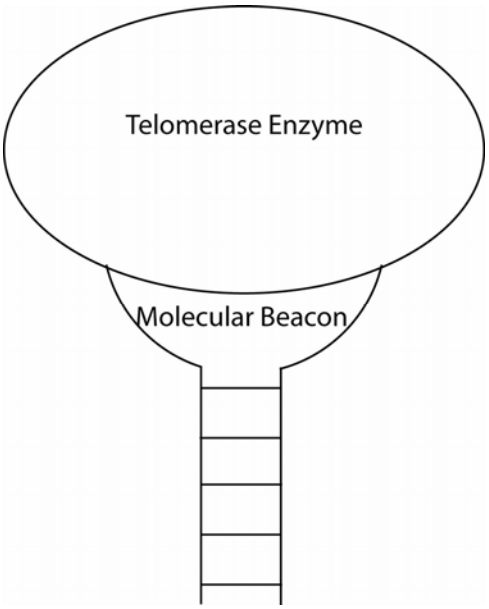

Figure 37. Possible Interactions Between Telomerase and the Molecular Beacon. In this scenario, telomerase does not provide enough thermodynamic energy to split the stem structure. As a result, the MB remains in the stem-loop conformation (FRET).

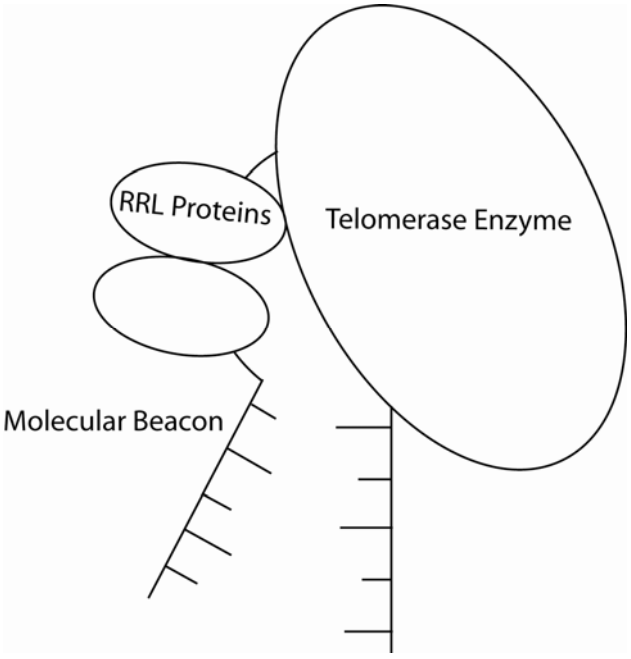

Figure 38. Possible Interactions Between Telomerase, Molecular Beacon and RRL. The addition of RRL to the solutions provided "helper" proteins that bind the hairpin loop fulfilling the thermodynamic energy necessary to split the stem structure (non-FRET) and allow the fluorophore to fluoresce.

Alternatively, the binding of telomerase to the hairpin loop may play another role in regulating other protein binding species. Since the hairpin loop is 24bps in length a telomerase molecule may conceivably bind in several different places on the loop. If telomerase binds in the center of the hairpin loop other proteins may not be able to bind the loop (Figure 37). However, if telomerase binds the 3' or 5' end of the hairpin loop there may be room for other protein binding (Figure 38). The transition of the molecular beacon's hairpin loop from 24bp to a size larger than 6bp may redefine the capabilities of this assay. The ability of telomerase to separate the stem without the presence of RRL would increase reliability and reproducibility considerably.

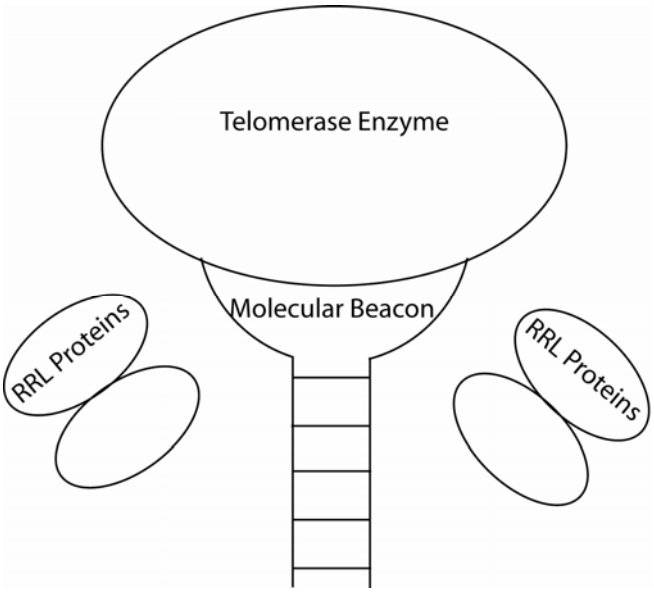

Figure 39. Telomerase Binds to the Middle of the Hairpin Loop. Telomerase binds to the middle of the hairpin loop which does not allow room for other proteins to interact with the molecular beacon. This preferential binding would inhibit the utilization of this specific molecular beacon.

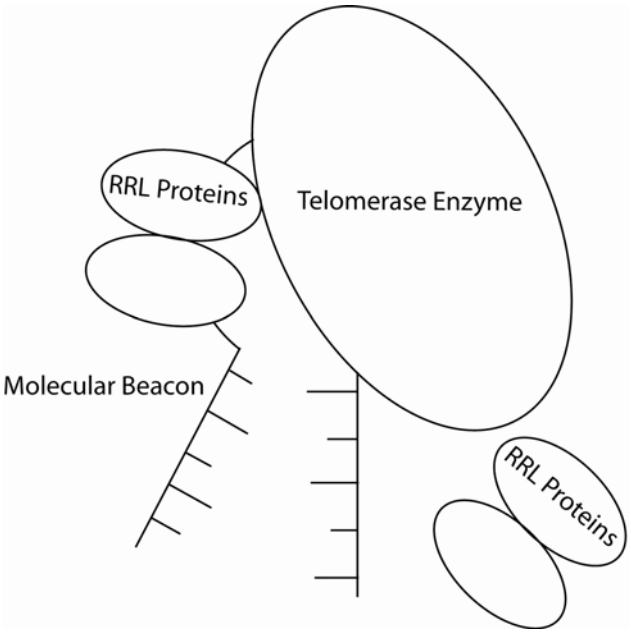

Figure 40. Telomerase Binds to the 3' or 5' end of the Hairpin Loop. When telomerase binds to the 3' or 5' end of the molecular beacon a significant portion of the hairpin loop is available for other protein DNA interactions.

One very important observation was that even in the presence of RRL, telomerase negative cell lines showed no binding or (at least) greatly reduced binding compared to the RRL alone. These results suggested that there was no accessibility to hairpin loop. Alternatively, the opening of the loop was being inhibited by some as yet unknown mechanism. Therefore, there appears to be a protective mechanism inherent in the telomerase negative cell extracts, because even at 51mM RRL, the telomerase negative cell lines were significantly lower than the RRL sample. Possibilities include a protein like p53 recognizing the accessible DNA of the loop as "damaged" and binding to it. However if this is the case, other proteins need to be involved, otherwise the MB should open. Another possibility is that the whole loop is encased in a series of interconnected

proteins therefore alleviating any binding. Finally, the stem structure could be targeted in telomerase negative cell lines. Double stranded DNA binding proteins such as TRF_1 and TRF_2 may detect the stem structure as subtelomeric. They may be binding to the stem structure and effectively increasing the energy needed to split the stem so high that no binding to the loop would have enough energy to break the stem structure.

The MB – cell extract results obtained in this project have led to a number of important questions concerning protein-DNA interactions. It is evident that besides telomerase, there are other important distinctions between telomerase positive and negative cell lines with respect to DNA interactions. Although there is still much work to be done with cell lines at various stages of immortalization as well as tissue extracts, the MB may have great utility in addressing these questions.

CHAPER VI

CONCLUSION

Cancer is a debilitating and deadly disease that takes its toll on society. The ability to screen for cancer on a regular basis in a cost effective and time efficient manner would increase survival rates of cancer patients. The goal of this project was to develop a preliminary assay utilizing a MB to detect telomerase molecules in a cell protein extract, with an ultimate goal of developing a screening technique that is based on detection of telomerase molecules. This would allow establishment of numbers of telomerase molecules that directly correspond to cancer stage, and possibly even type. This test could also help with prognosis and evaluate treatment effectiveness.

The data collected during the duration of this research suggest that telomerase is binding to the MB. The fluorescent intensity of the MB assay correlates with the telomerase activity (measured by the TRAP assay) for both the telomerase positive and negative cell protein extracts. This preliminary assay needs further characterization and development to better understand the variables involved with assay performance and further correlation to specific cell lines.

The correlations between the TRAPeze assay for enzyme activity and the MB bench-top assay were very promising, but further testing is needed. The protein

or proteins causing the MB to linearize must be confirmed by other means outside the scope of this research project. Once confirmation is complete, determining the minimum number of bases that telomerase will bind will allow for further optimization of the MB. This optimized MB with a shortened hairpin loop should be specific for detecting telomerase binding without the necessity of any "helper" proteins provided by the RRL. Once the effects of RRL have been eliminated, further analysis can be performed on hTERT, hTR and the cell extracts.

Integration of this assay into a MEMS device or a bionanotechnology platform would enhance its utility and effectiveness. This integration would utilize engineering principles to produce a small scale, portable device with functionalized disposable capillaries. The fabrication and development of such an integrated device that would contain a biologically modified glass capillary, specifically engineered for LCWG based detection, would be very convenient. This device could be used in a clinical setting or in the field.

This research project has accomplished the first documented binding of a target DNA-binding protein to a MB. This assay will hopefully facilitate development of similar assays to capture other DNA binding proteins. However to make this assay truly versatile a detection scheme specific for MB binding will also need to be developed.

LITERATURE CITED

1. 2004. Cancer Facts & Figures. *In* D.o.t.A.C. Society (Ed.),Amercian Cancer Society.

2. Abravaya, K., J. Huff, R. Marshall, B. Merchant, C. Mullen, G. Schneider and J. Robinson. 2003. Molecular beacons as diagnostic tools: technology and applications. Clin Chem Lab Med *41*:468-474.

3. Bonnet, G., O. Krichevsky and A. Libchaber. 1998. Kinetics of conformational fluctuations in DNA hairpin-loops. Proc Natl Acad Sci U S A *95*:8602-8606.

4. Bonnet, G., S. Tyagi, A. Libchaber and F.R. Kramer. 1999. Thermodynamic basis of the enhanced specificity of structured DNA probes. Proc Natl Acad Sci U S A *96*:6171-6176.

5. Breslow, R.A., J.W. Shay, A.F. Gazdar and S. Srivastava. 1997. Telomerase and early detection of cancer: a National Cancer Institute workshop. J Natl Cancer Inst *89*:618-623.

6. Chan, S.R.W.L., Blackburn, E.H. 2003. Telomeres and telomerase. Phil. Trans. R. Soc. Lond. *359*:109-121.

7. Chang, J.Y. 2004. Telomerase: A potential molecular marker and therapeutic target for cancer. Journal of Surgical Oncology *87*:1-3.

8. Cong, Y.S., W.E. Wright and J.W. Shay. 2002. Human telomerase and its regulation. Microbiol Mol Biol Rev *66*:407-425, table of contents.

9. Coursen, J.D., W.P. Bennett, L. Gollahon, J.W. Shay and C.C. Harris. 1997. Genomic instability and telomerase activity in human bronchial epithelial cells during immortalization by human papillomavirus-16 E6 and E7 genes. Exp Cell Res *235*:245-253.

10. Dhaene, K., E. Van Marck and R. Parwaresch. 2000. Telomeres, telomerase and cancer: an up-date. Virchows Arch *437*:1-16.

11. Fang, X., J.J. Li, J. Perlette, W. Tan and K. Wang. 2000. Molecular beacons: novel fluorescent probes. Anal Chem *72*:747A-753A.

12. Feng, J., W.D. Funk, S.S. Wang, S.L. Weinrich, A.A. Avilion, C.P. Chiu, R.R. Adams, E. Chang, R.C. Allsopp, J. Yu and et al. 1995. The RNA component of human telomerase. Science *269*:1236-1241.

13. Gollahon, L.S. and J.W. Shay. 1996. Immortalization of human mammary epithelial cells transfected with mutant p53 (273his). Oncogene *12*:715-725.

14. Granger, M.P., W.E. Wright and J.W. Shay. 2002. Telomerase in cancer and aging. Crit Rev Oncol Hematol *41*:29-40.

15. Greider, C.W. 1999. Telomeres Do D-Loop-T-Loop. Cell *97*:419-422.

16. Greider, C.W., Blackburn, E.H. 1996. Telomeres, Telomerase and Cancer. Scientific American:92-97.

17. Harley, C.B. 1991. Telomere loss: mitotic clock or genetic time bomb? Mutat Res *256*:271-282.

18. Hecht, E. 2001. Schaum's Outline of Optics. Addison Wesley.

19. Hiyama, E. and K. Hiyama. 2002. Clinical utility of telomerase in cancer. Oncogene *21*:643-649.

20. Hiyama, E. and K. Hiyama. 2003. Telomerase as tumor marker. Cancer Lett *194*:221-233.

21. Holt, S.E., D.L. Aisner, J. Baur, V.M. Tesmer, M. Dy, M. Ouellette, J.B. Trager, G.B. Morin, D.O. Toft, J.W. Shay, W.E. Wright and M.A. White. 1999. Functional requirement of p23 and Hsp90 in telomerase complexes. Genes Dev *13*:817-826.

22. Huffman, K.E., S.D. Levene, V.M. Tesmer, J.W. Shay and W.E. Wright. 2000. Telomere shortening is proportional to the size of the G-rich telomeric 3'-overhang. J Biol Chem *275*:19719-19722.

23. Ishikawa, F. 1996. [Telomere and telomerase]. Hum Cell *9*:287-294.

24. Janknecht, R. 2004. On the road to immortality: hTERT upregulation in cancer cells. FEBS Lett *564*:9-13.

25. Kim, N.W., M.A. Piatyszek, K.R. Prowse, C.B. Harley, M.D. West, P.L. Ho, G.M. Coviello, W.E. Wright, S.L. Weinrich and J.W. Shay. 1994. Specific association of human telomerase activity with immortal cells and cancer. Science *266*:2011-2015.

26. Lavranos, T.C., J.M. Mathis, S.E. Latham, B. Kalionis, J.W. Shay and R.J. Rodgers. 1999. Evidence for ovarian granulosa stem cells: telomerase activity and localization of the telomerase ribonucleic acid component in bovine ovarian follicles. Biol Reprod *61*:358-366.

27. Li, J., W. Tan, K. Wang, D. Xiao, X. Yang, X. He and Z. Tang. 2001. Ultrasensitive optical DNA biosensor based on surface immobilization of molecular beacon by a bridge structure. Anal Sci *17*:1149-1153.

28. Li, J.J., X. Fang, S.M. Schuster and W. Tan. 2000. Molecular Beacons: A Novel Approach to Detect Protein - DNA Interactions This work was partially supported by a U.S. NSF Career Award (CHE-9733650) and by a U.S. Office of Naval Research Young Investigator Award (N00014-98-1-0621). Angew Chem Int Ed Engl *39*:1049-1052.

29. Liu, X., W. Farmerie, S. Schuster and W. Tan. 2000. Molecular beacons for DNA biosensors with micrometer to submicrometer dimensions. Anal Biochem *283*:56-63.

30. Madou, M.J. 1997. Fundamentals of Microfabrication. CRC Press.

31. Makamba, H., J.H. Kim, K. Lim, N. Park and J.H. Hahn. 2003. Surface modification of poly(dimethylsiloxane) microchannels. Electrophoresis *24*:3607-3619.

32. Marras, S.A., F.R. Kramer and S. Tyagi. 2002. Efficiencies of fluorescence resonance energy transfer and contact-mediated quenching in oligonucleotide probes. Nucleic Acids Res *30*:e122.

33. Mathieu, N., L. Pirzio, M.A. Freulet-Marriere, C. Desmaze and L. Sabatier. 2004. Telomeres and chromosomal instability. Cell Mol Life Sci *61*:641-656.

34. McDonald, J.C., D.C. Duffy, J.R. Anderson, D.T. Chiu, H. Wu, O.J. Schueller and G.M. Whitesides. 2000. Fabrication of microfluidic systems in poly(dimethylsiloxane). Electrophoresis *21*:27-40.

35. Nazarenko, I.A., S.K. Bhatnagar and R.J. Hohman. 1997. A closed tube format for amplification and detection of DNA based on energy transfer. Nucleic Acids Res *25*:2516-2521.

36. Olovnikov, A.M. 1973. A theory of marginotomy. The incomplete copying of template margin in enzymic synthesis of polynucleotides and biological significance of the phenomenon. J Theor Biol *41*:181-190.

37. Park, S.H., Yan, H., Reif, J. H., LaBean, T. H. 2004. Electronic nanostructures templated on self-assembled DNA scaffolds. Nanotechnology *15*:S525-S527.

38. Schrader, M., A.M. Burger, M. Muller, H. Krause, B. Straub, G.L. Smith, E.S. Newlands and K. Miller. 2002. Quantification of human telomerase reverse transcriptase mRNA in testicular germ cell tumors by quantitative fluorescence real-time RT-PCR. Oncol Rep *9*:1097-1105.

39. Selvin, P.R. 1995. Fluorescence resonance energy transfer. Methods Enzymol *246*:300-334.

40. Selvin, P.R. 2000. The renaissance of fluorescence resonance energy transfer. Nat Struct Biol *7*:730-734.

41. Shay, J.W. 1998. Telomerase in cancer: diagnostic, prognostic, and therapeutic implications. Cancer J Sci Am *4 Suppl 1*:S26-34.

42. Shay, J.W. and W.E. Wright. 1996. Telomerase activity in human cancer. Curr Opin Oncol *8*:66-71.

43. Shay, J.W., Y. Zou, E. Hiyama and W.E. Wright. 2001. Telomerase and cancer. Hum Mol Genet *10*:677-685.

44. Sia, S.K., Whiteside, G.M. 2003. Microfluidc Devices Fabricated in Poly(dimethylsiloxane) for Biological Studies. Electrophoresis *24*:3563-3576.

45. Sun, C., J. Yang, L. Li, X. Wu, Y. Liu and S. Liu. 2004. Advances in the study of luminescence probes for proteins. J Chromatogr B Analyt Technol Biomed Life Sci *803*:173-190.

46. Tan, W., X. Fang, J. Li and X. Liu. 2000. Molecular beacons: a novel DNA probe for nucleic acid and protein studies. Chemistry *6*:1107-1111.

47. Tan, W., K. Wang and T.J. Drake. 2004. Molecular beacons. Curr Opin Chem Biol *8*:547-553.

48. Tesmer, V.M., L.P. Ford, S.E. Holt, B.C. Frank, X. Yi, D.L. Aisner, M. Ouellette, J.W. Shay and W.E. Wright. 1999. Two inactive fragments of the integral RNA cooperate to assemble active telomerase with the human protein catalytic subunit (hTERT) in vitro. Mol Cell Biol *19*:6207-6216.

49. Tsourkas, A., M.A. Behlke and G. Bao. 2002. Structure-function relationships of shared-stem and conventional molecular beacons. Nucleic Acids Res *30*:4208-4215.

50. Tsourkas, A., M.A. Behlke, S.D. Rose and G. Bao. 2003. Hybridization kinetics and thermodynamics of molecular beacons. Nucleic Acids Res *31*:1319-1330.

51. Tsourkas, A., M.A. Behlke, Y. Xu and G. Bao. 2003. Spectroscopic features of dual fluorescence/luminescence resonance energy-transfer molecular beacons. Anal Chem *75*:3697-3703.

52. Tyagi, S. and F.R. Kramer. 1996. Molecular beacons: probes that fluoresce upon hybridization. Nat Biotechnol *14*:303-308.

53. Unger, M.A., Chou, H., Throsen, T., Scherer, A., and Quake, S.R. 2000. Monolithic Microfabricated Valves and Pumps by Multilayer Soft Lithography. Science Magizine *288*:113-116.

54. Watson, J.D. 1972. Origin of concatemeric T7 DNA. Nat New Biol *239*:197-201.

55. Watson, J.D., Baker, T. A., Bell, S. P., Gann, A., Levine, M., Losick, R. 204. Molecular Biology of the Gene. Benjamin Commings.

56. Weinrich, S.L., R. Pruzan, L. Ma, M. Ouellette, V.M. Tesmer, S.E. Holt, A.G. Bodnar, S. Lichtsteiner, N.W. Kim, J.B. Trager, R.D. Taylor, R. Carlos, W.H. Andrews, W.E. Wright, J.W. Shay, C.B. Harley and G.B. Morin. 1997. Reconstitution of human telomerase with the template RNA component hTR and the catalytic protein subunit hTRT. Nat Genet *17*:498-502.

57. Wright, W.E., M.A. Piatyszek, W.E. Rainey, W. Byrd and J.W. Shay. 1996. Telomerase activity in human germline and embryonic tissues and cells. Dev Genet *18*:173-179.

58. Yeung, E.S. 1994. Acc. Chem. Res. *27*:409.

59. Zhang, H., B. Zhang, J. Wang, C. Liu, J. Han, S. Yang and L. Hou. 2002. Single domain antibody to human telomerase catalytic subunit: preparation and characterization. Zhonghua Bing Li Xue Za Zhi *31*:143-147.

Appendix A

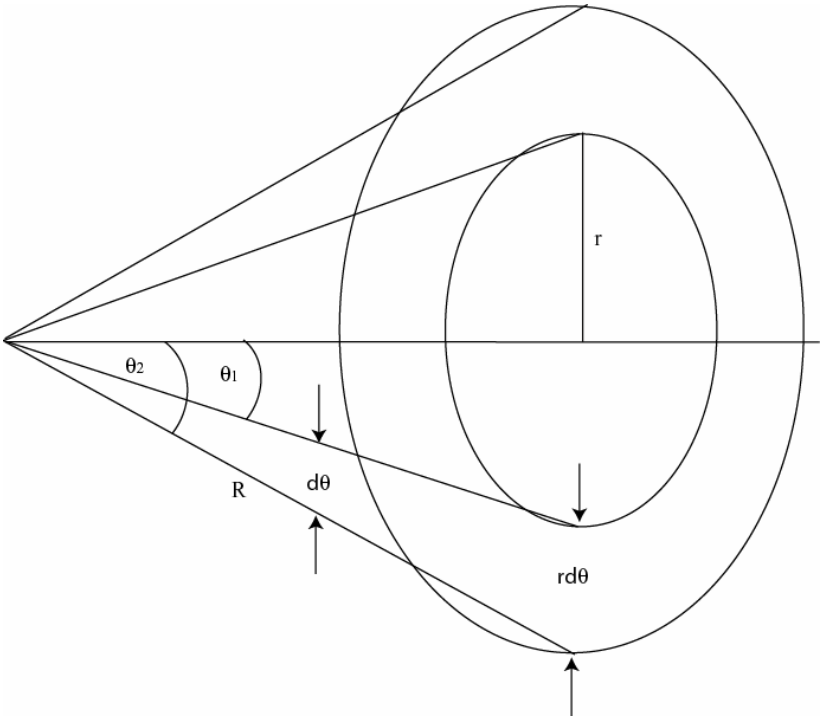

Figure 41. Solid Angle Derivation Defined by the Cone Angles.

$r = R \sin\theta$

$dA = 2\pi r\,(R\,d\theta)$

$= 2\pi\,(R \sin\theta)(R\,d\theta)$

$= 2\pi R^2 (\sin\theta\, d\theta)$

$d(\sin\theta) = \cos\theta\, d\theta$

$d(\cos\theta) = \sin\theta\, d\theta$

$-d(\cos\theta) = \sin\theta\, d\theta$

$A = \int dA = \int_{\theta 1}^{\theta 2} 2\pi R^2 (\sin\theta\, d\theta)$

$= 2\pi R^2 \int_{\theta 1}^{\theta 2} \sin\theta\, d\theta$

$= 2\pi R^2 \int_{\theta 1}^{\theta 2} - d\cos\theta$

$= -2\pi R^2 \int_{\theta 1}^{\theta 2} d\cos\theta$

$= -2\pi R^2 \cos\theta\,{}_{\theta 1}^{\theta 2}$

$= -2\pi R^2 (\cos\theta_2 - \cos\theta_1)$

$= 2\pi R^2 (\cos\theta_1 - \cos\theta_2)$

$\Omega = 2\pi R^2 (\cos\theta_1 - \cos\theta_2)$ (**1**)

Appendix B

Water – Glass – Air LCWG Configuration

Water – Glass Interface

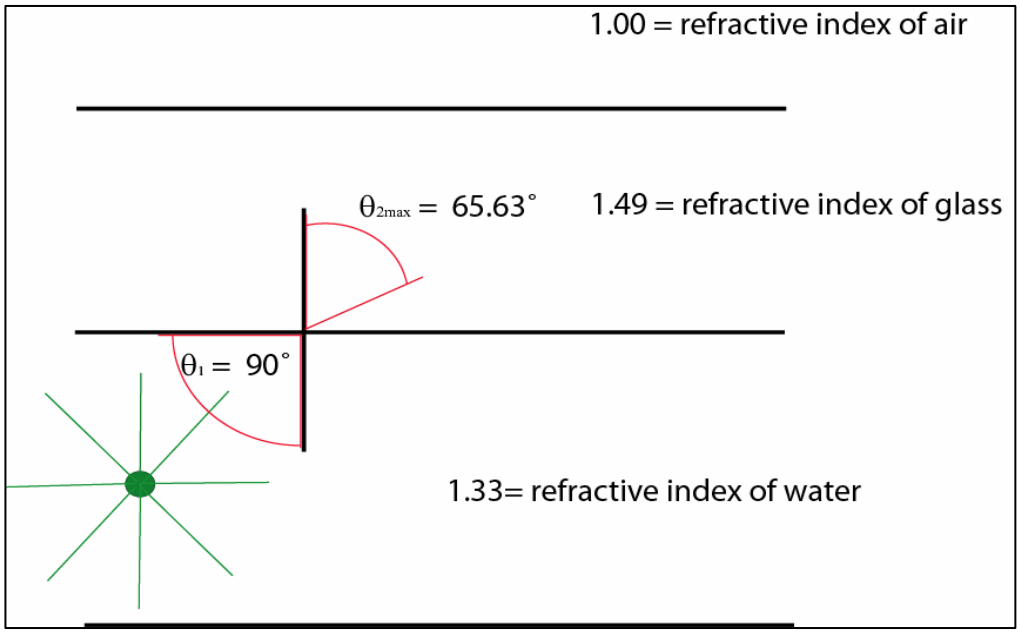

Figure 42. Water – Glass Interface

$n_1 = 1.33$ (index of water)
$\theta_1 = 90°$
$n_2 = 1.49$ (index of glass)
$\theta_2 = \theta_{2max}$ (maximum refraction angle in glass)
$1.33 (\sin 90°) = 1.49 (\sin \theta_{2max})$
$\sin \theta_{2max} = [1.33 (\sin 90°)]/1.46$
$\theta_2 = 0.9109/\sin$
$\theta_{2max} = 65.63°$ (Figure 40)

No fluorescent signal will be TIR at the water glass interface. The fluorescence signal will be concentrated in the glass between 0° and 65.63° from normal.

Glass – Air Interface

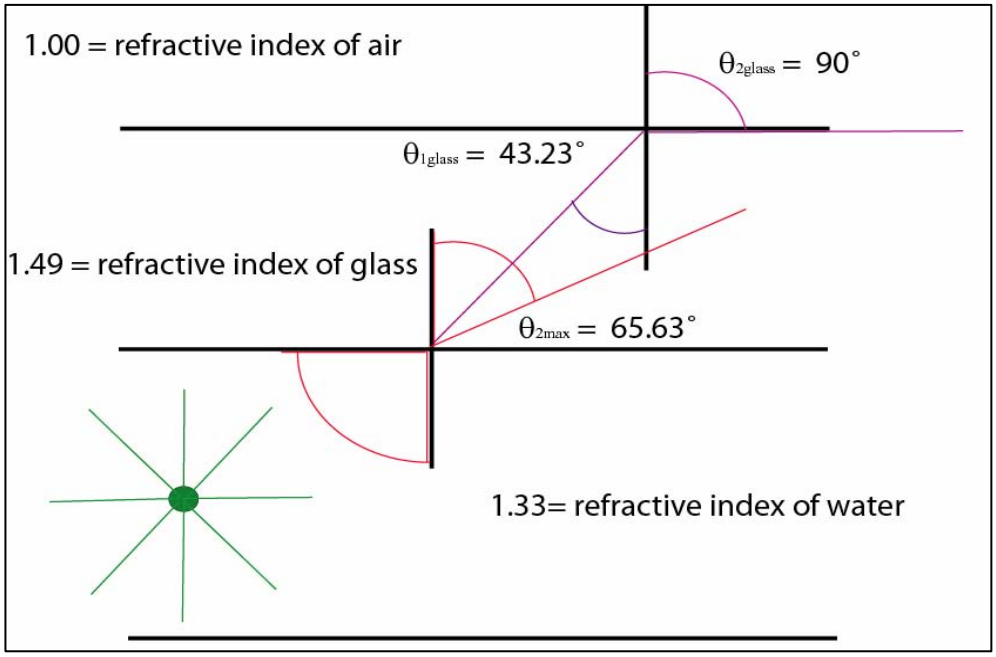

Figure 43. Glass – Air interface

$n_1 = 1.49$ (index of glass)
$\theta_1 = \theta_{1glass}$ (Critical angle)
$n_2 = 1.0$ (index of Air)
$\theta_2 = 90°$
$1.49 (\sin \theta_{1glass}) = 1.00 (\sin 90°)$
$\sin \theta_{1glass} = [1.00 (\sin 90°)]/1.46$
$\theta_{1glass} = 0.6849/\sin$
$\theta_{1glass} = 43.23°$ (Figure 41)

Fluorescence with an angle of incidences smaller than the critical angle will not be TIR.

The percentage of fluorescence TIR in the glass cladding is calculated as follows:

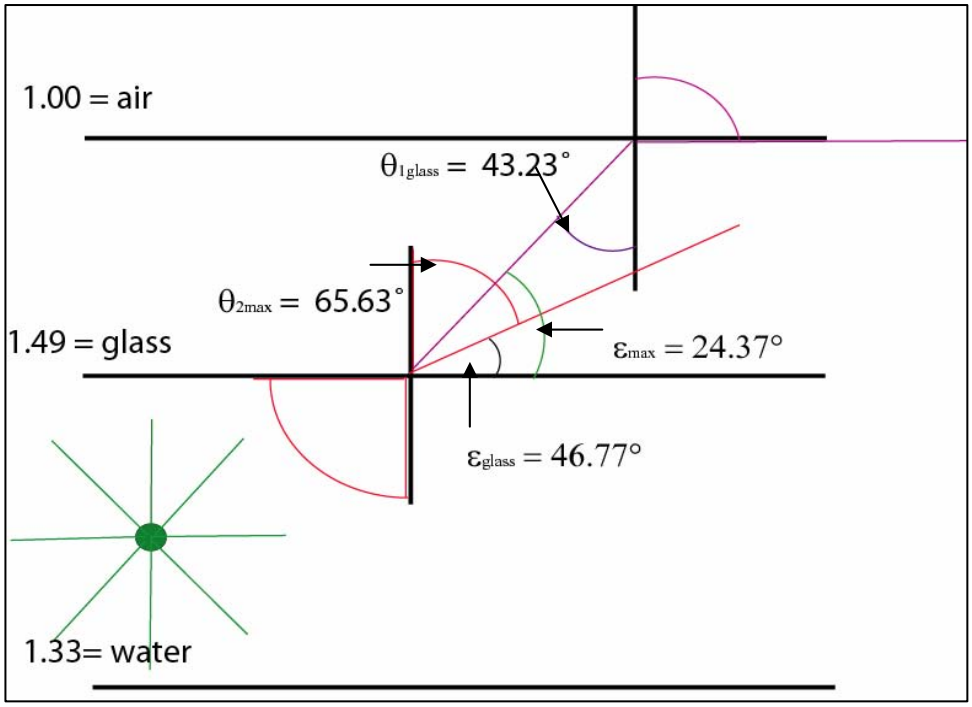

Figure 44. Solid Angle of TIR Fluorescence

R = 1
$\varepsilon_{max} = 90° - \theta_{2max}$
$\varepsilon_{glass} = 90° - \theta_{1glass}$
$\Omega = 2\pi R^2 (\cos \varepsilon_{max} - \cos \varepsilon_{glass})$ (Appendix A)
% captured = $2(\Omega/4\pi)$ x 100
$\varepsilon_{max} = 24.37°$ (figure 8)
$\varepsilon_{glass} = 46.77°$ (figure 8)
$\Omega_{capture} = 2\pi (\cos 24.37° - \cos 46.77°)$
$\Omega_{capture} = 1.4198$

Since all the light is between 0° and 65.63° the area represented by the light must be found to determine the correct percentage captured.

$\theta_1 = 0°$
$\theta_2 = 65.63°$
$\varepsilon_{\theta 1} = 0°$
$\varepsilon_{\theta 2} = 24.37°$
$\Omega_{total} = 2\pi (\cos 24.37°)$
$\Omega_{total} = 5.7233$
% captured = $(\Omega_{capture} / \Omega_{total})$ x 100
% captured = (1.4198/5.7233) x 100
% captured = 24.807

Appendix C

The premise behind these dilution experiments was to determine the optimal concentration of RRL for the greatest signal to noise ratio. The individual components of the reaction mix were: 20mM Tris-HCl pH 7.6, 63mM KCl, 1.5mM $MgCl_2$, 150nM ROX, 200nM MB, and water. RRL was tested in varying concentrations (10mM – 60mM) and the same concentrations of RRL were tested in solution with a telomerase positive protein extract. The individual concentrations of RRL were compared to their counter parts which were tested in the presences of telomerase positive protein extracts. The difference in relative fluorescence and signal to noise ratio was observed.

The data is broken up into several graphs for viewing purposes. Figures 45-47 have the sample solution, blank, and 4e10 oligo copies/µL sample results, because the entire data set was collected at the same time. Figure 45 shows RRL dilutions from 10-20mM and their counter parts with the telomerase protein extract. This graph represents the samples with the greatest signal to noise ratios. The signal to noise ratio is the degree of separation between the sample containing the RRL and the protein extract and the sample containing only the RRL concentration. Figure 46 shows dilutions from 25-45mM RRL and their corresponding samples with telomerase positive protein extracts. Figure 47 shows dilutions from 45-60mM RRL and their corresponding samples with telomerase positive protein extracts.

The data shows that there is a range of RRL concentrations that allows for optimal signal to noise ratio. Increasing or decreasing of the RRL concentration relative to the optimal range (15-25mM) decreases the signal to noise ratio. This data was used to optimize the assay when the pH of the assay was changed to pH 8.3.

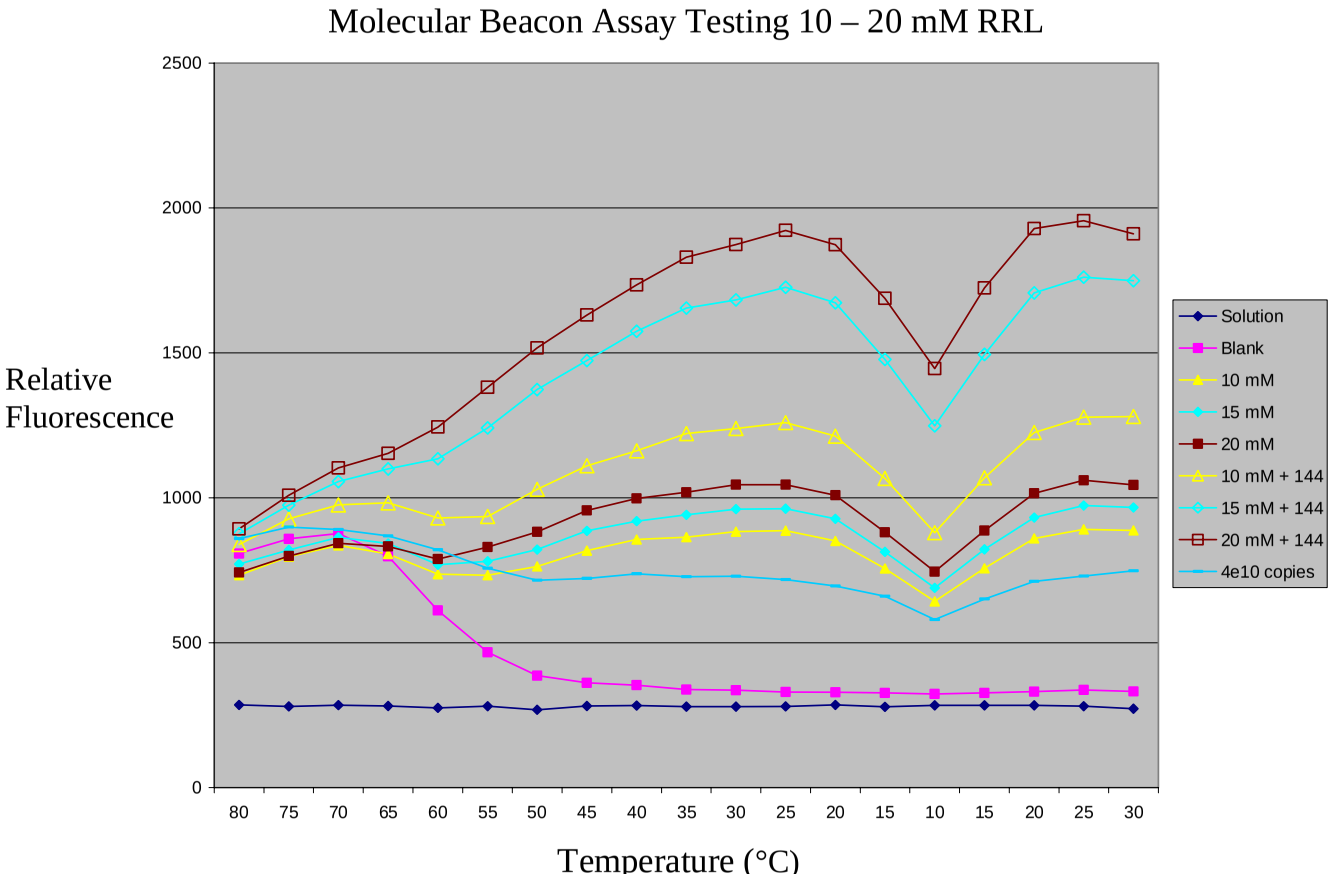

Figure 45. Molecular Beacon Assay Testing 10 – 20 mM RRL

The solution sample showed the baseline reading for FAM when utilizing the ABI Prism 7000. The blank sample showed the thermodynamic characteristics of the molecular beacon throw the temperature range when no target is present. The experimental samples of RRL and the corresponding RRL plus the telomerase positive protein extract showed the specific signal to noise ratio for that RRL concentration.

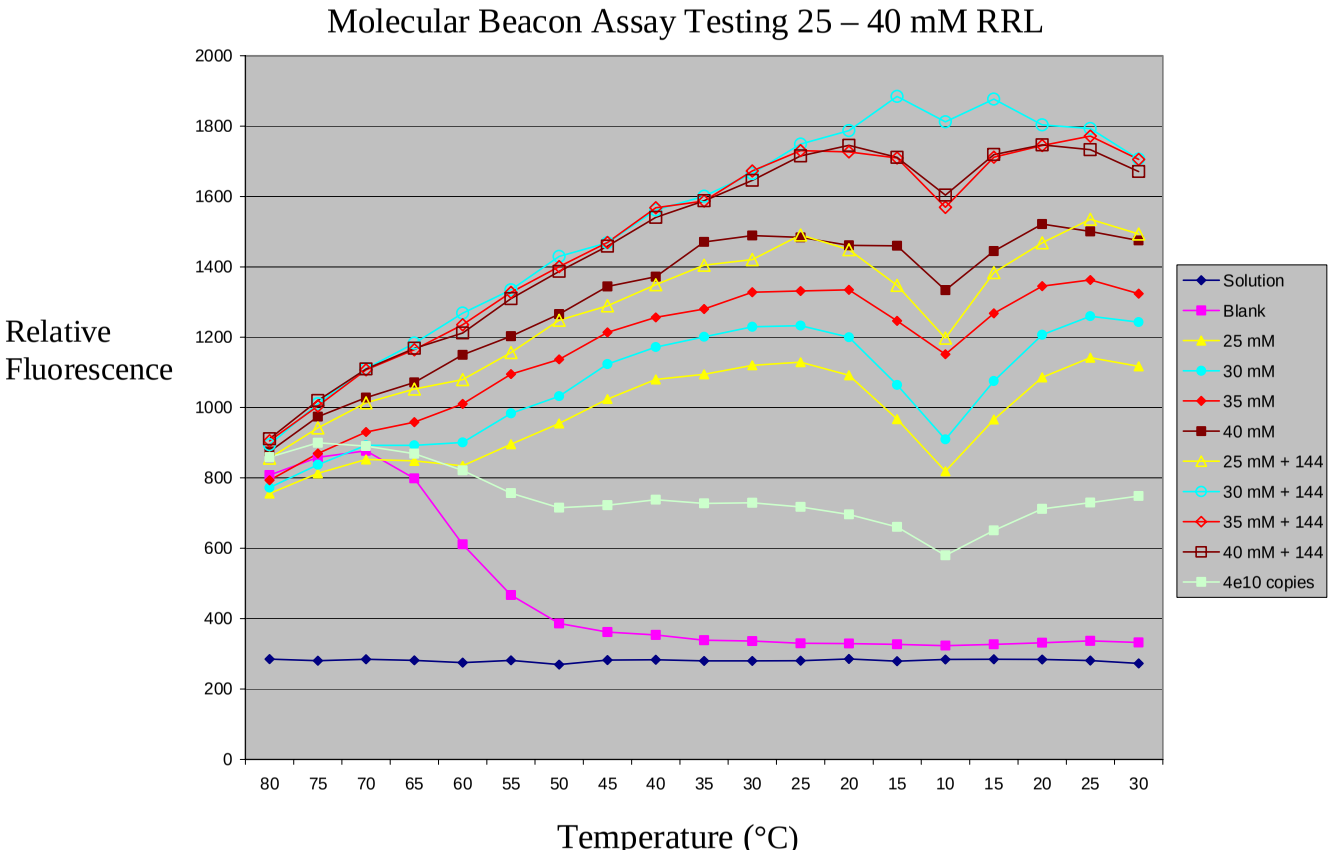

Figure 46. Molecular Beacon Assay Testing 25 – 40 mM RRL

The solution sample showed the baseline reading for FAM when utilizing the ABI Prism 7000. The blank sample showed the thermodynamic characteristics of the molecular beacon throw the temperature range when no target is present. The experimental samples of RRL and the corresponding RRL plus the telomerase positive protein extract showed the specific signal to noise ratio for that RRL concentration.

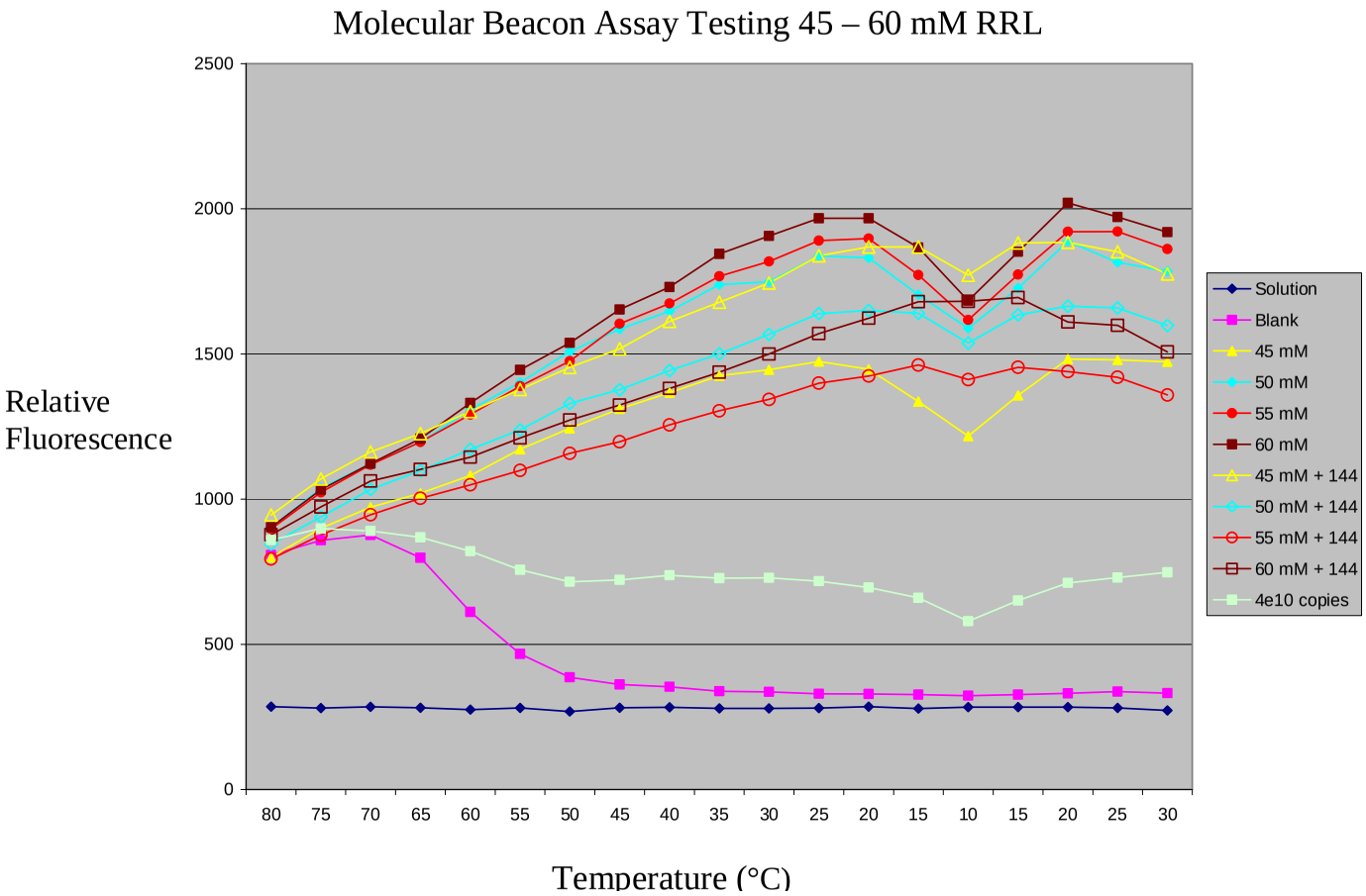

Figure 47. Molecular Beacon Assay Testing 45 – 60 mM RRL
The solution sample showed the baseline reading for FAM when utilizing the ABI Prism 7000. The blank sample showed the thermodynamic characteristics of the molecular beacon throw the temperature range when no target is present. The experimental samples of RRL and the corresponding RRL plus the telomerase positive protein extract showed the specific signal to noise ratio for that RRL concentration.

Appendix D

The initial assay experiments utilizing telomerase positive and negative protein extracts showed no detectable increase in fluorescence. The assay components were: 200nM MB, 50mM KCl, 20mM Tris-HCl pH 7.6, and 10mM MgCl2, 125nM ROX, and water. The data represented in the graph contain three controls and two experimental samples. The solution sample shows the back ground of the system because the sample contains no FAM fluorophore. The blank sample contains all components of the assay but water was added instead of an experimental sample. The data obtained from the blank sample shows the MB's thermodynamic characteristics (through the tested temperature range) when there is no target in solution. The last control was the DNA control. This sample had 2e12 target oligos added to the assay components (4e10 oligos/µL). The data obtained from this sample showed that the MB was functioning as expected throughout the temperature range tested. The two experimental samples were telomerase positive (144) and telomerase negative (100) protein extracts (Figure 48).

There were several possibilities that could explain this data. The first is that telomerase was not binding to the molecular beacon; therefore no fluorescence would be detected. The second was that a small number of telomerase molecules were binding and changing the conformation of the MB but the fluorescence was

beneath the minimal detection limits of the detection system. The third explanation was that telomerase was binding the MB but the binding event did not have enough energy to break the stem structure of the MB allowing for fluorescence.

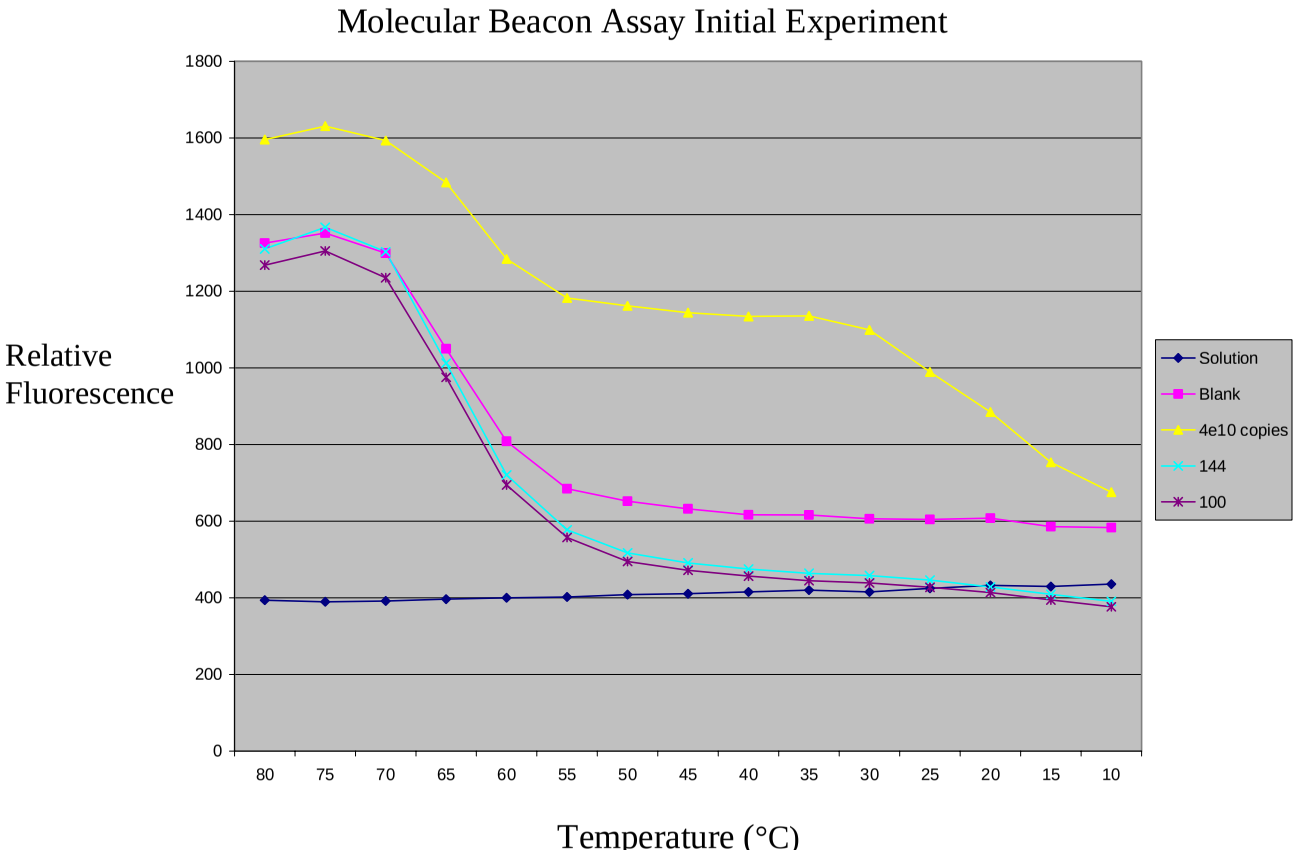

Figure 48. Molecular Beacon Assay Initial Experiment

The blank sample shows the MB's thermodynamic characteristics through the tested temperature range when no target is present. The solution sample shows the baseline fluorescent detection for FAM. The 4e10 oligos/µL shows that the MB is properly functioning. Sample 144 which is telomerase positive shows no fluorescent increase and the same is true for sample 100 which is telomerase negeative.

Appendix E

The process of assay development is an intricate method of optimizing individual components of an assay to produce the best reproducible results. The simplest method of development would be to utilize an assay buffer that functions to produce some of the same results. The TRAPeze buffer is utilized to optimize telomerase binding to a G-rich oligo in solution, telomerase elongation of that oligo, and PCR amplification of that oligo. The function of the TRAPeze buffer that was significant to my assay development was telomerase binding. The TRAPeze buffer was utilized for the MB assay. The components of the TRAPeze buffer are: 20mM Tris-HCl, pH 8.3, 1.5mM $MgCl_2$, 63mM KCl, 0.05% Tween 20, and 1mM EGTA. The buffer was added to water and the samples were added to a final volume of 50µL.

The initial experiment utilizing the TRAPeze contained four control samples and four experimental samples. The controls samples were: solution, blank, 4e10 oligo/µL, and RRL. The experimental samples were: 144 (telomerase positive), 144 + RRL, 100 (telomerase negative), and 100 + RRL. The results from this experiment are contained in figure 49. The results show no increase in fluorescence of any of the experimental samples. The RRL control should have showed an increase in fluorescence, but it did not. The analysis of these results shows that a component of the assay was inhibiting protein binding.

There were two components of the TRAPeze buffer that have not been used in previous experiments. These components are Tween 20 and EGTA. Experiments were performed to determine which element was inhibiting the protein binding. EGTA was found to be the protein binding inhibitor (Figure 50). The data shows elevated fluorescence of all the samples containing RRL and the DNA control. The protein extracts alone show no increase in fluorescence while the protein extracts in the presences of RRL showed varied fluorescence. The telomerase positive extract (144+RRL) with RRL shows a significant increase in fluorescence compared to the telomerase negative (100+RRL) with RRL. The RRL sample has a relative fluorescence which is equal to or greater then that of the telomerase positive extract with RRL. The high back ground created by the large concentration of RRL did not allow for a definitive analysis of the results.

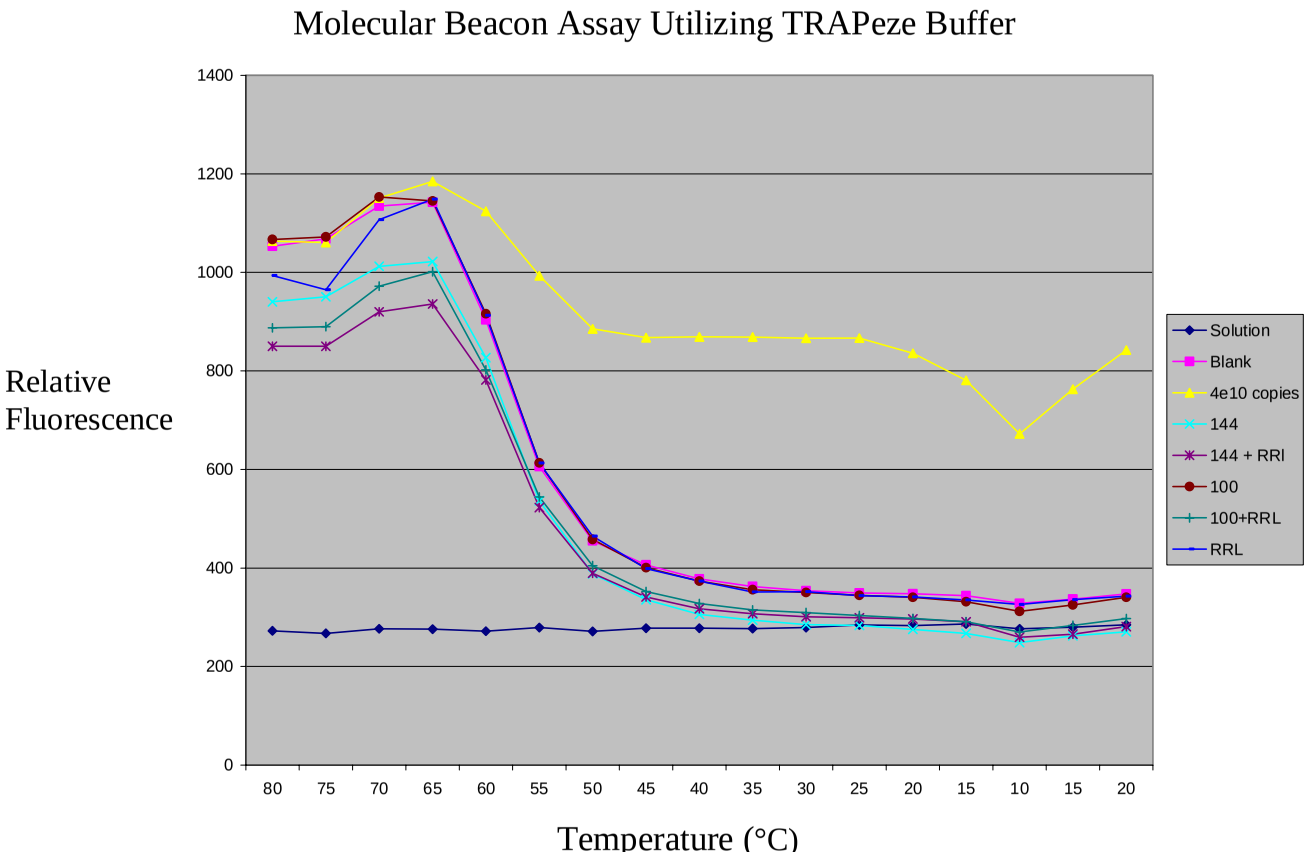

Figure 49. Molecular Beacon Assay Utilizing TRAPeze Buffer

The solution sample shows the baseline fluorescence of the detection system. The blank sample shows the MB's thermodynamic characteristics when not in the presences of a target (through the tested temperature range). The 4e10 oligos/µL shows that the MB is functioning properly. All the experimental samples show no increase in fluorescence in comparison to the blank. There must be a component in the assay that is inhibiting the protein from binding to the MB.

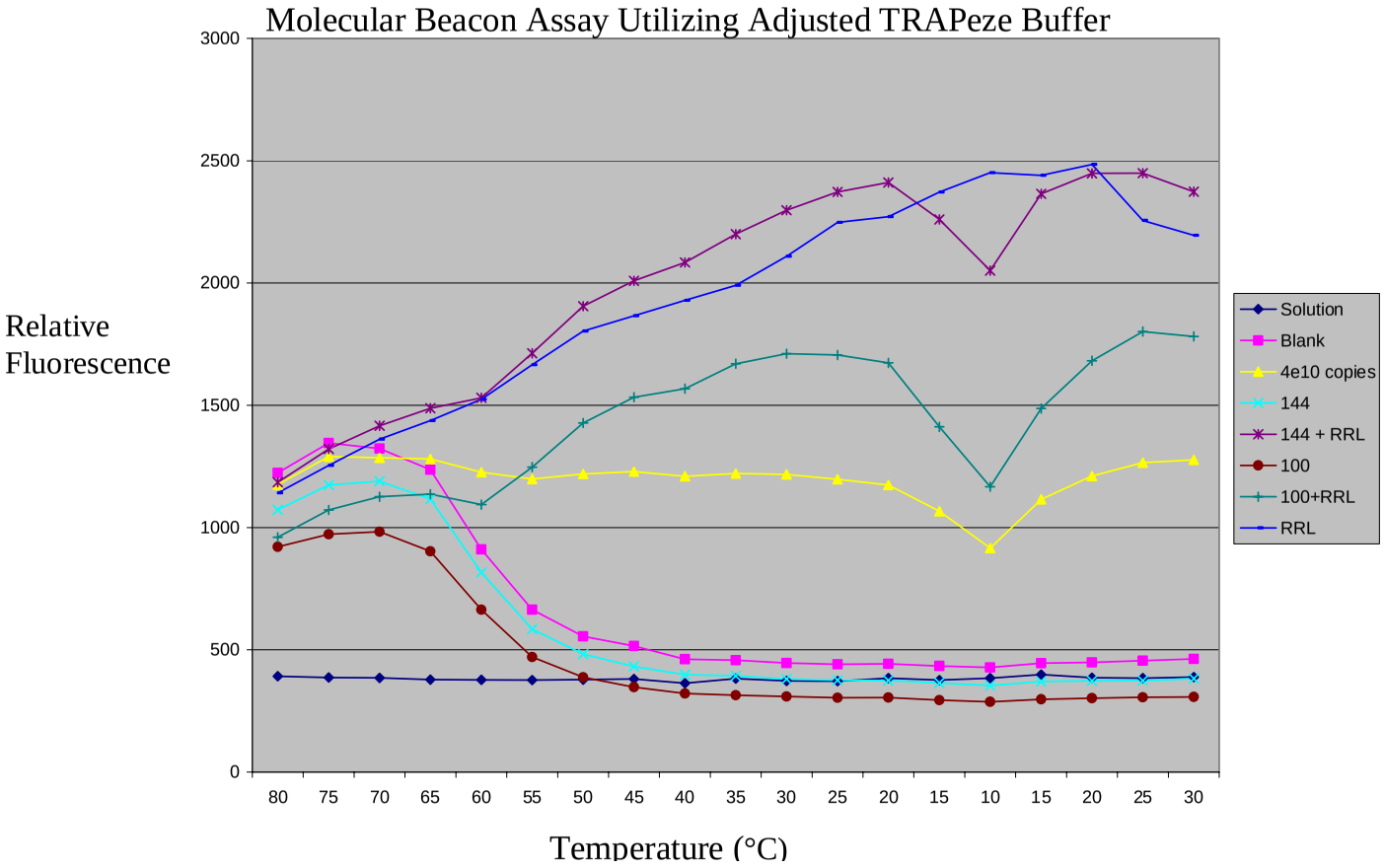

Figure 50. Molecular Beacon Assay Utilizing Adjusted TRAPeze Buffer
The solution sample shows the baseline fluorescence of the detection system. The blank sample shows the MB's thermodynamic characteristics when not in the presences of a target (through the tested temperature range). The 4e10 oligos/µL shows that the MB is functioning properly. The RRL sample shows a large increase in fluorescence. The telomerase positive protein extract with RRL shows a much greater fluorescent increase than the telomerase negative protein extract with RRL. Both of the protein extract sample that do not have any RRL added to them show no increase in fluorescence.